Extreme Deformation and Failure of Metals by Pulsed Lasers

Marc A. Meyers

Y.Z. Tang, C.-H. Lu, T. Remington, S. Zhao, E. Hahn UCSD

E. M. Bringa, C. Ruestes, U. N. Cuyo, Argentina

B. A. Remington, B. Maddox, H. S. Park, R. Rudd, LLNL

Funding: UCOP, DOE-NNSA

Laboratory for Laser Energetics (LLE), University of Rochester

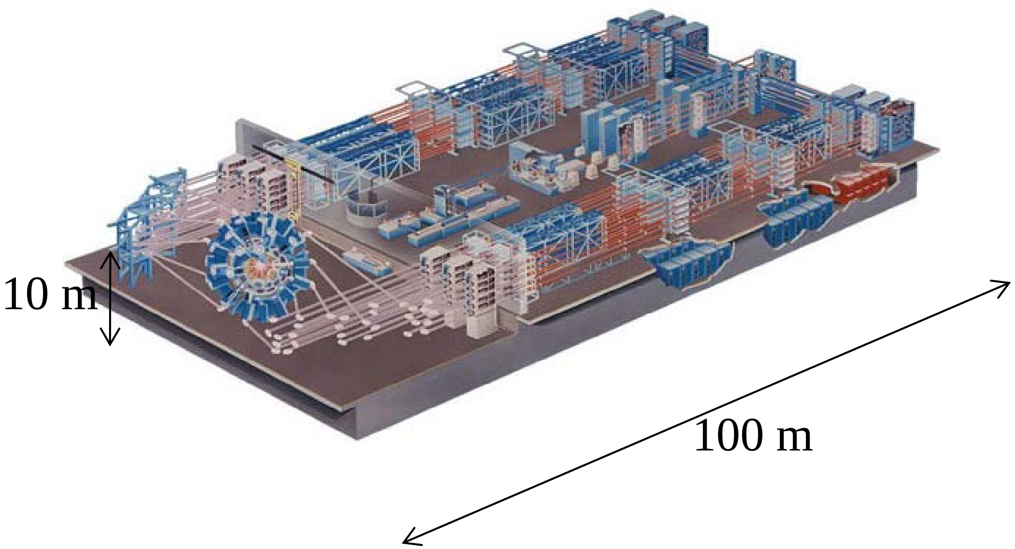

- 60 laser beams
- Energy up to 40,000 J
- 351 nm wavelength

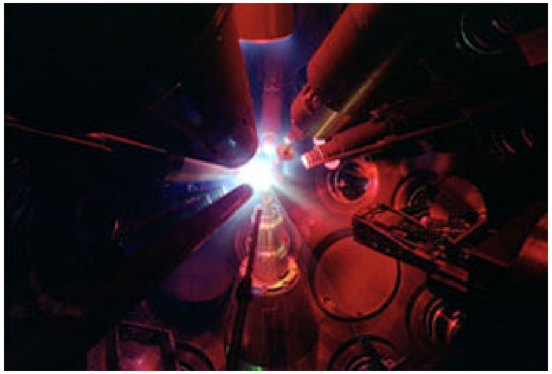

http://www.lle.rochester.edu/

THE OMEGA TARGET CHAMBER

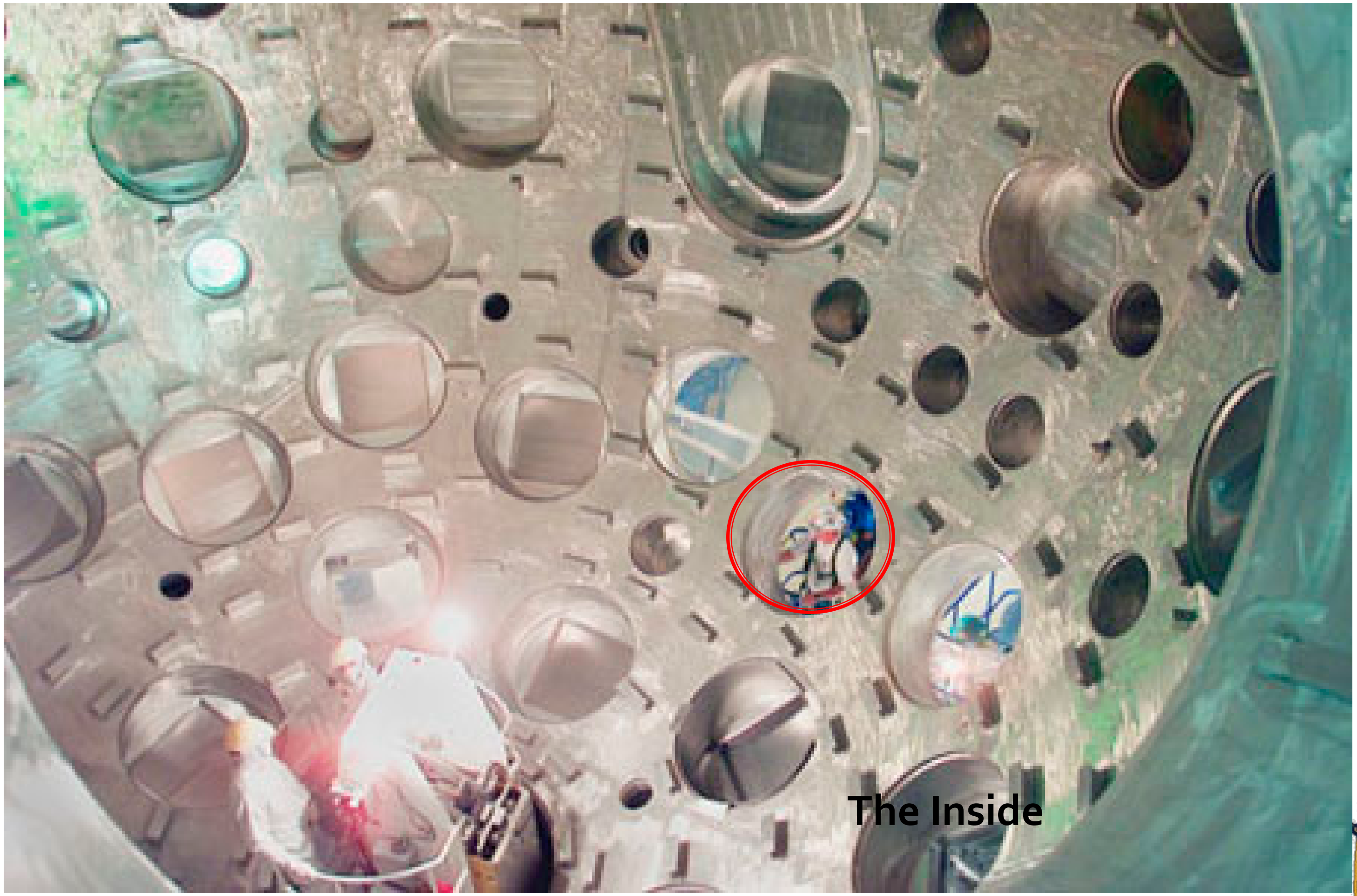

Source: http://www.llnl.gov/nif/project/lib_construction.html

Recovery Fixture and Diagnostics for High Amplitude Lasers

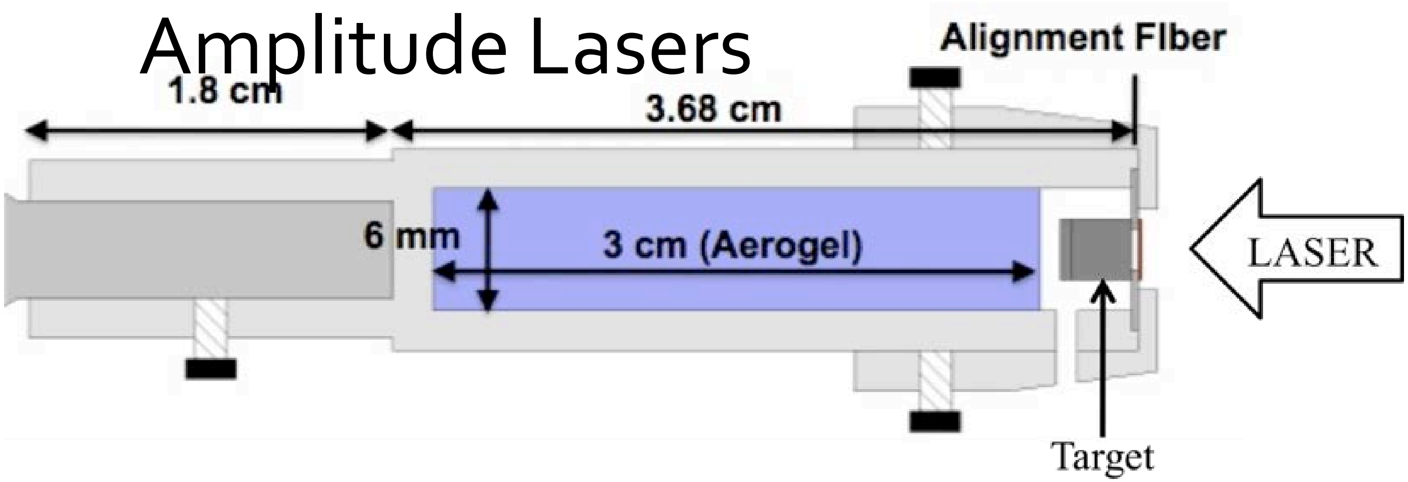

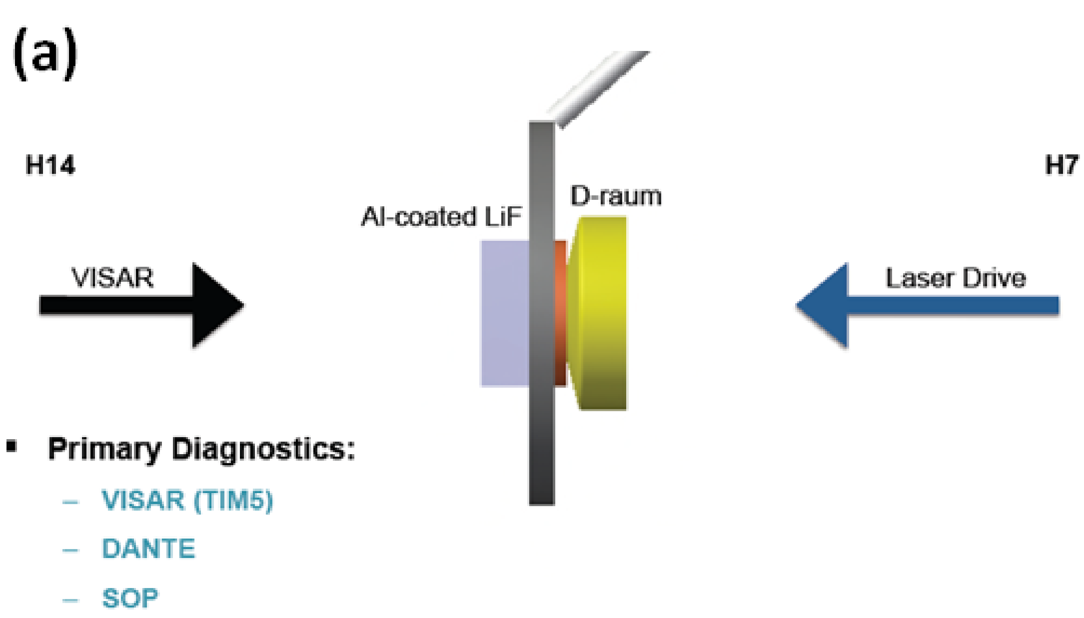

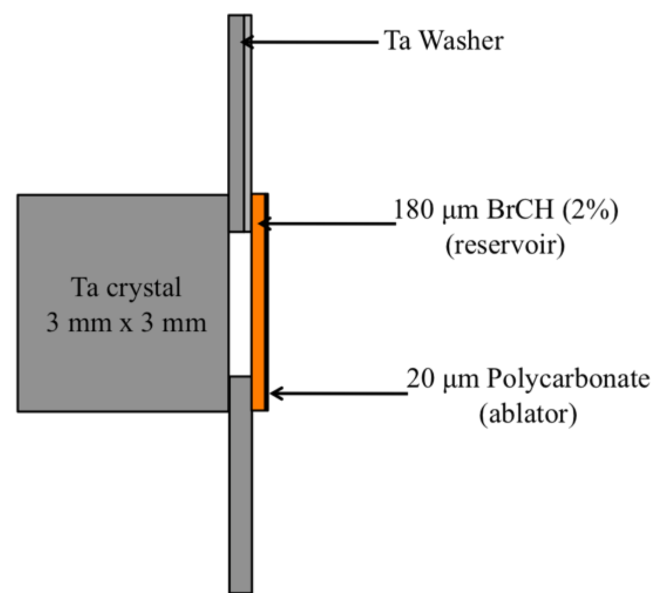

Fundamental Questions

- Strength under extreme strain rates and pressures

- Dislocations in shock compression: homogeneous generation v. multiplication
- The slip/twinning transition
- Void nucleation and growth: defects and kinetics
- The search for the elusive supersonic dislocation

Lasers: time: ~1 ns strain rate: ~10^9 s^{-1}

Molecular dynamics: time : ps strain rate: 10^9 s^{-1}

Strength under Extreme Compression

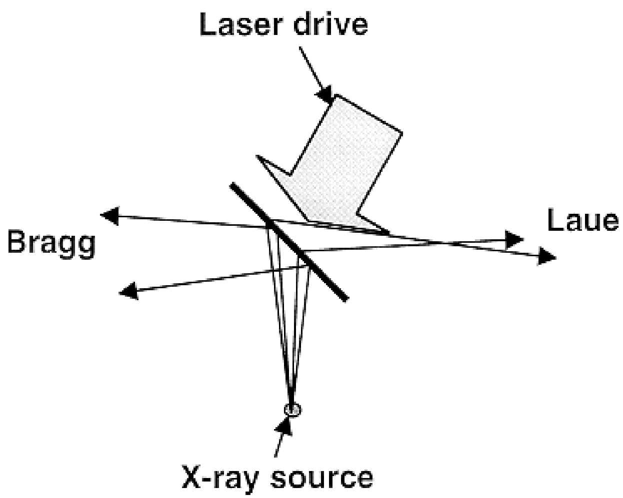

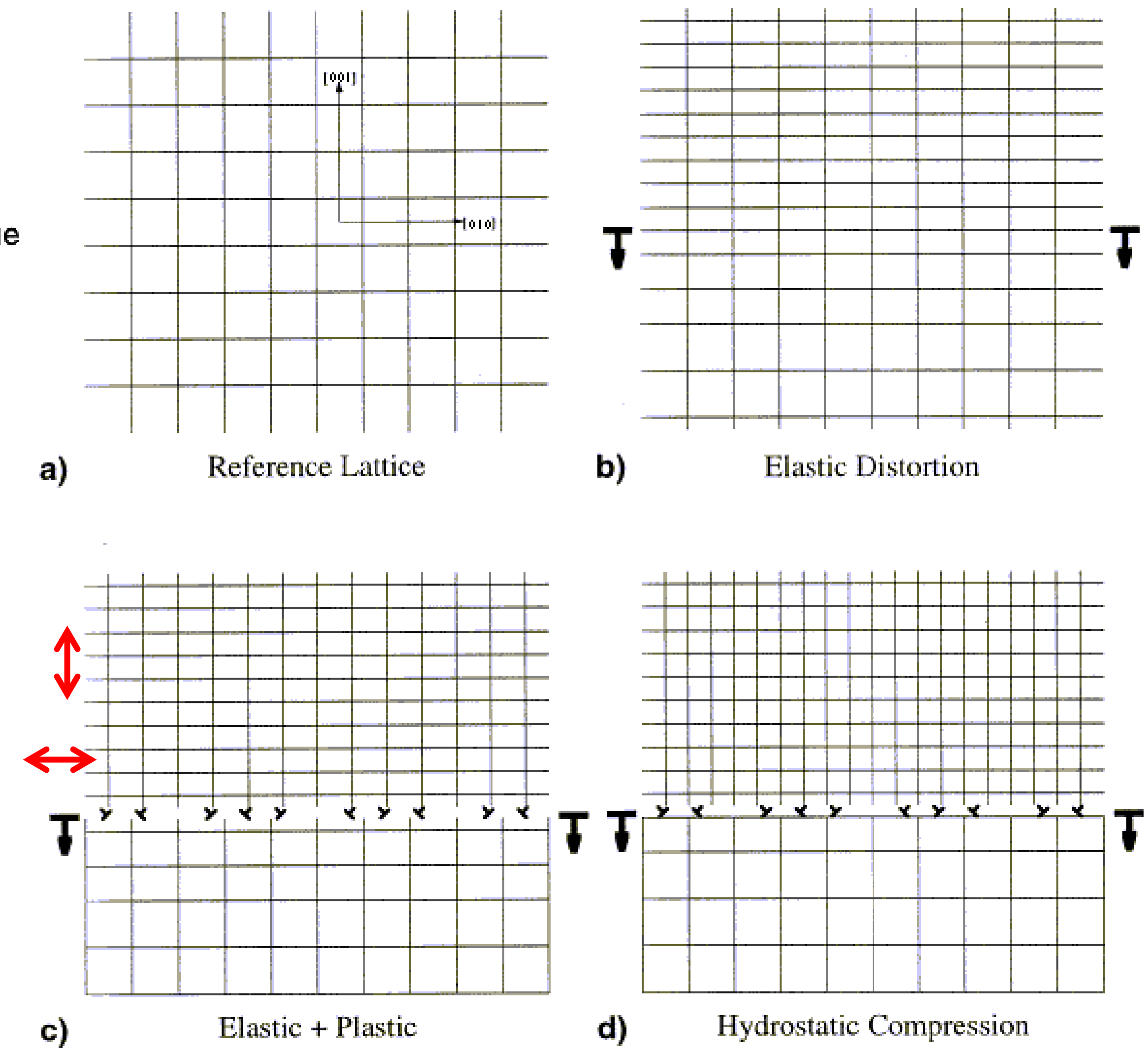

Bragg $\varepsilon_2 = -0.030$

Laue $\varepsilon_1 = -0.025$

Pressure = 18 GPa

X Ray Diffraction: Bragg(reflection) and Laue (transmission)

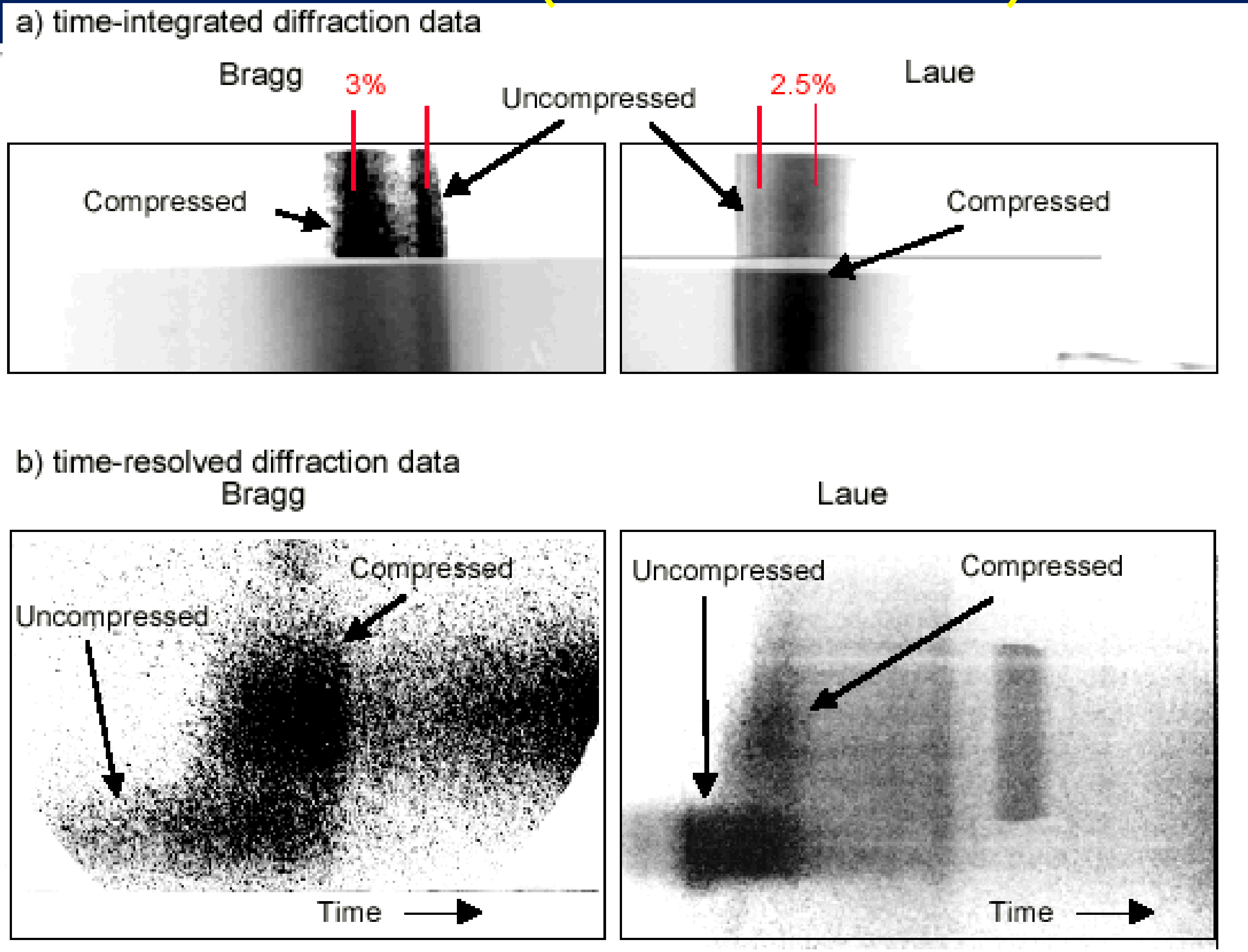

Meyers, Wark, Remington, Ravichandran et al., Acta Mat, 2001

$(\sigma_{12})_f = (\varepsilon_1 - \varepsilon_2)\, G = 435$ MPa

Strength through Diffraction during Shock Compression

$$\gamma = \frac{\pi}{2} - \tan^{-1}\left(\frac{1+\varepsilon_1}{1+\varepsilon_2}\right)$$

$$\dot{\varepsilon} = \frac{\varepsilon}{t_f} = \frac{\frac{2}{3}\ln\left(\frac{V}{V_o}\right)}{t_f}$$

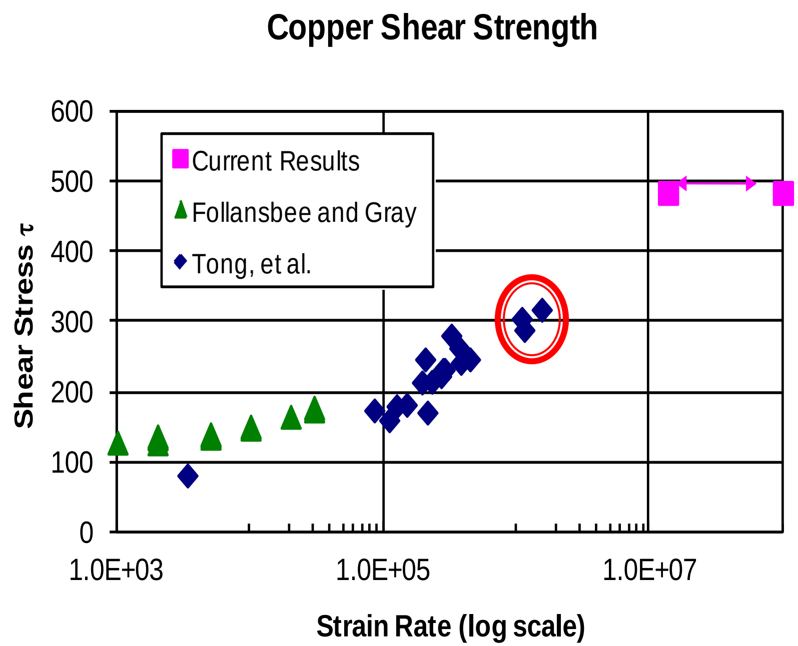

$(\sigma_{12})_f = \gamma G = (\varepsilon_1 - \varepsilon_2)\, G = 435$ MPa

Pressure = 18 GPa

Meyers, Wark, Remington, Ravichandran et al., Acta Mat, 2001

Highest Strain Rate for [001] Cu; P~100 GPa

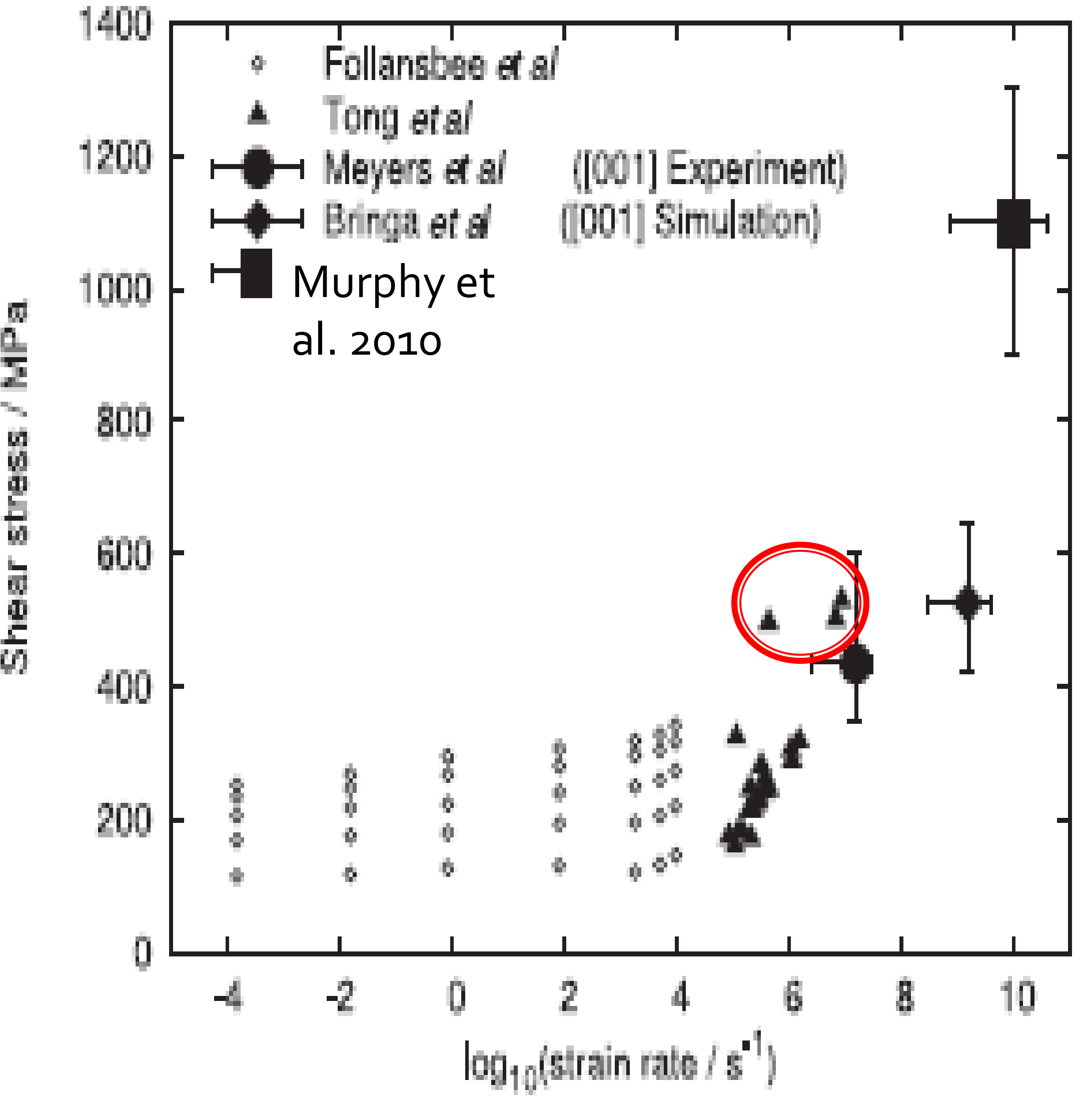

W.J. Murphy, A. Higginbotham, G. Kimminau, B. Barbrel, E.M. Bringa, J. Hawreliak, R. Kodama, M. Koenig, W. McBarron, M.A. Meyers, B. Nagler, N. Ozaki, N. Park, B. Remington, S. Rothman, S. M. Vinko, T. Whitcher and J.S. Wark, J Phys : Condens. Matter, 22 (2010), 065404.

Dislocation Generation

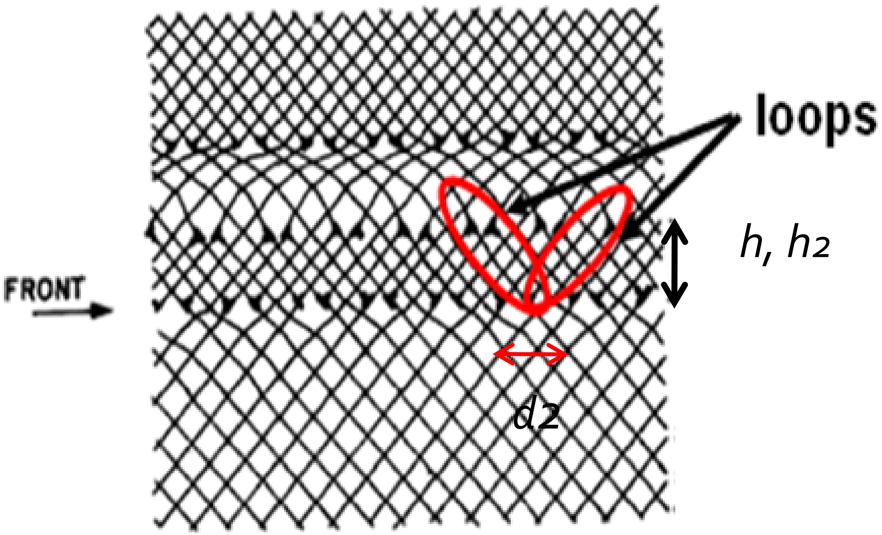

$$P = \frac{C_0^{\ 2}\left\{1-\left\{1-\sqrt{2}\left[\frac{0.8\, b_0^{\ 2}(1-\nu)\rho}{2\pi^2}\right]^{1/3}\right\}^3\right\}}{V_0\left\{1-S\left\{1-\sqrt{2}\left[\frac{0.8\, b_0^{\ 2}(1-\nu)\rho}{2\pi^2}\right]^{1/3}\right\}^3\right\}^2}$$

$$\sigma_{11} \approx \frac{Gb}{2\pi(1-\upsilon)}\frac{2\sqrt{2}}{nd_2^2} \rightarrow \sum_{-\infty}^{=\infty}\frac{1}{n} = 0$$

$$\sigma_{22} \approx \frac{Gb}{2\pi(1-\upsilon)}\left(-2h^2\right)\frac{2\sqrt{2}}{nd_2^2} \rightarrow \sum_{-\infty}^{=\infty}\frac{1}{n^3} = 0$$

$$\sigma_{12} \approx \frac{Gb}{2\pi(1-\upsilon)}\frac{2\sqrt{2}}{n^2 d_2^2}h \rightarrow \sum_{-\infty}^{=\infty}\frac{1}{n^2} = \frac{\pi^4}{90}$$

$$h = \frac{0.8(1-\upsilon)}{\pi^2 b}d_2^2$$

$$\rho = \frac{2}{d_2 h}$$

Moving dislocations

$$h_2 = h\left[1+\frac{k\upsilon_s}{U_s}\right]$$

Meyers, Remington, Wark, Ravichandran, et al. Acta mat. 2001
Meyers, Remington, Bringa, Jarmakani, in 'Dislocations in Solids,' Ed. J. P. Hirth, Vol. 15, 2010

FCC Metals: Generation of Partial Dislocation Loops

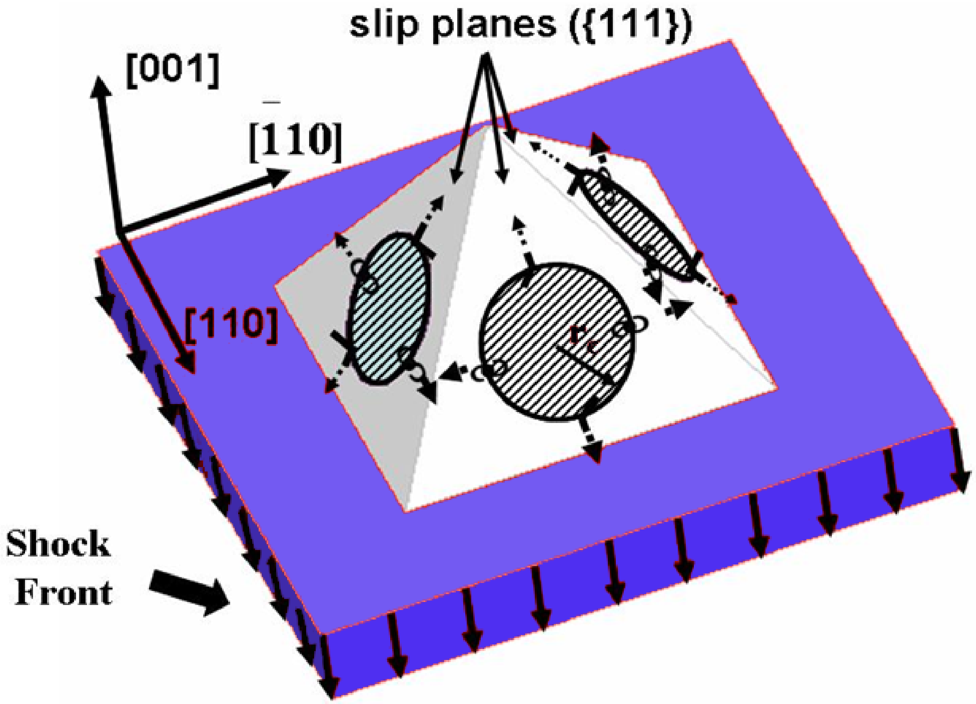

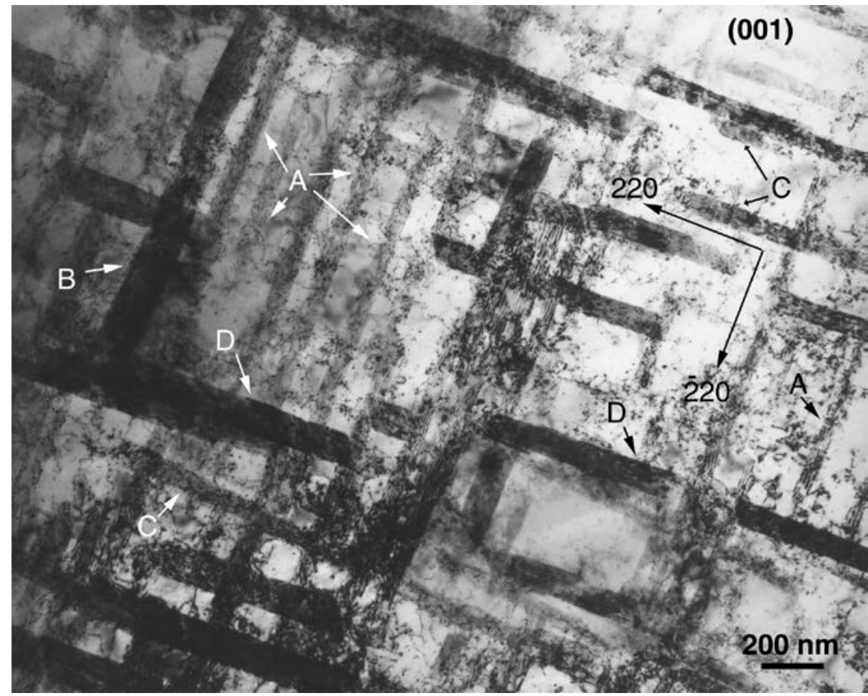

Predicted and Observed Dislocation Densities: FCC Ni

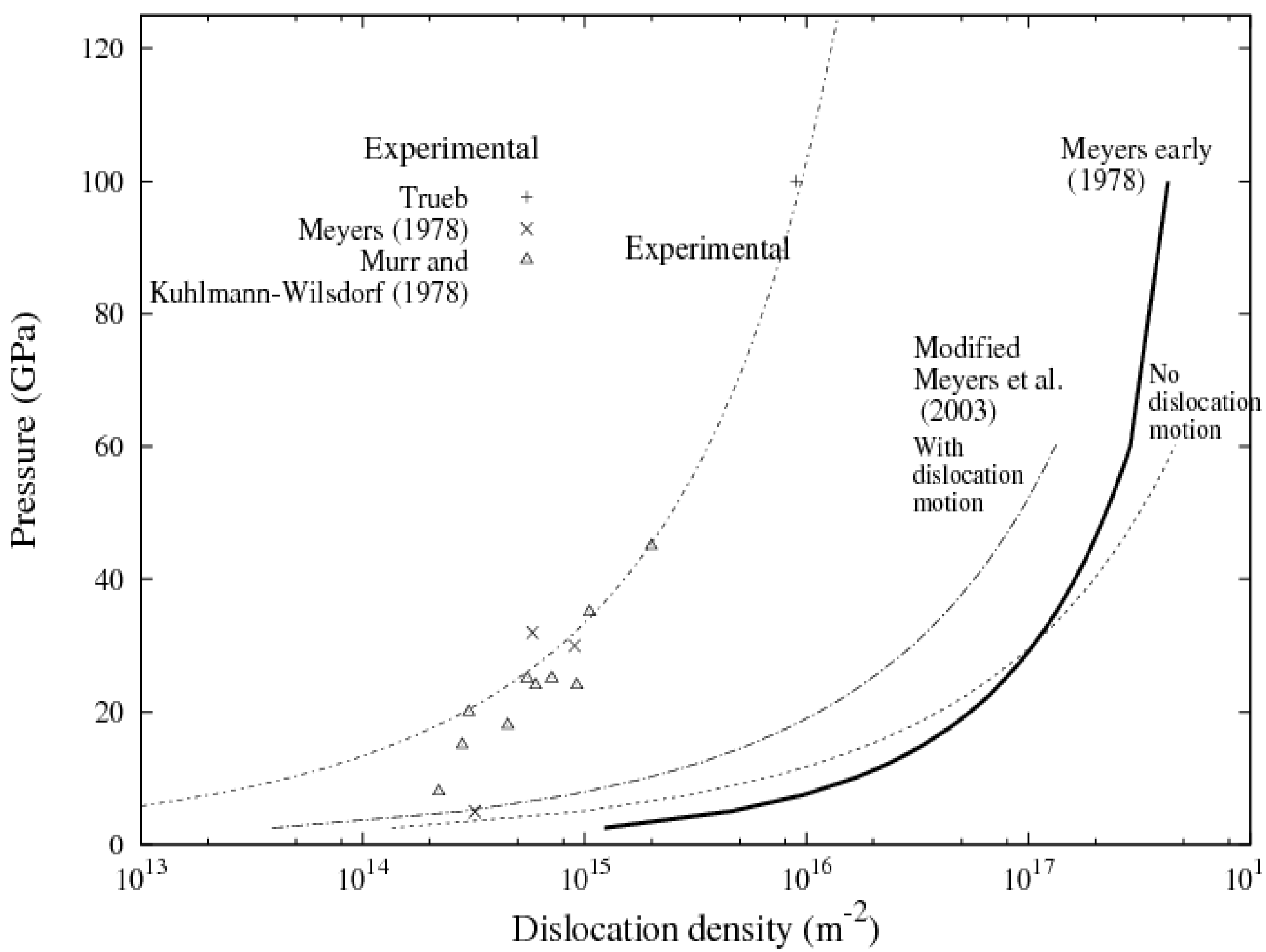

Stacking-Fault Formation above HEL: FCC Ni and Cu

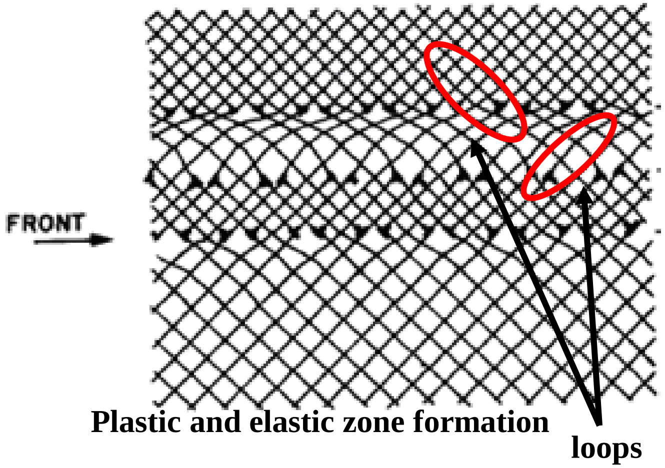

Plastic and elastic zone formation

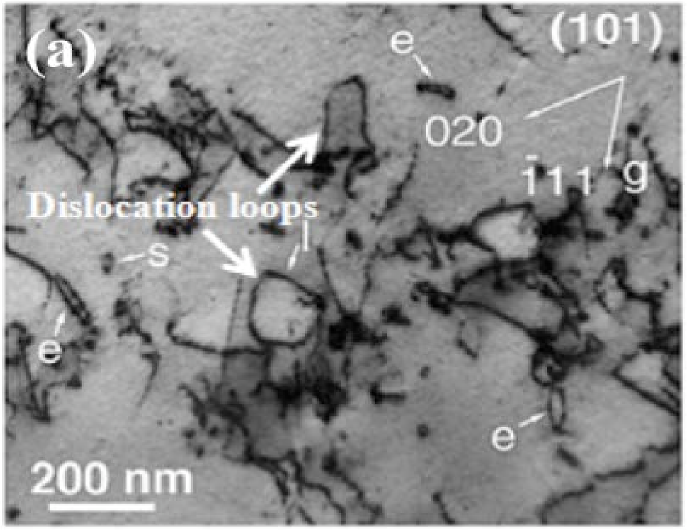

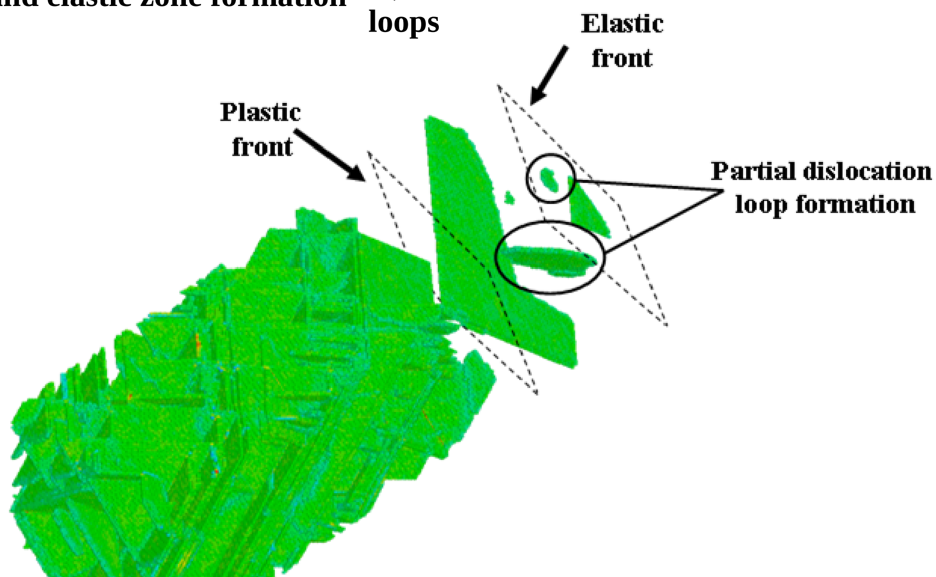

Shock compression along [001]

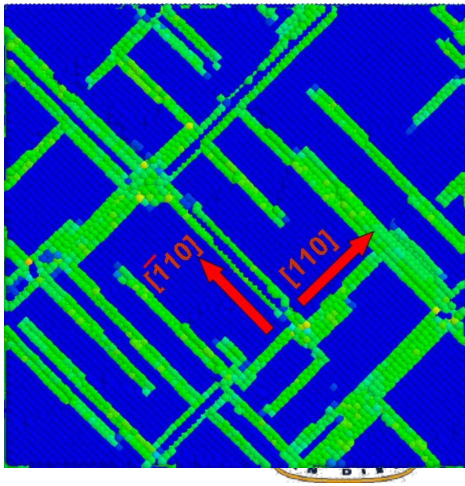

Shock Compression and Unloading: FCC

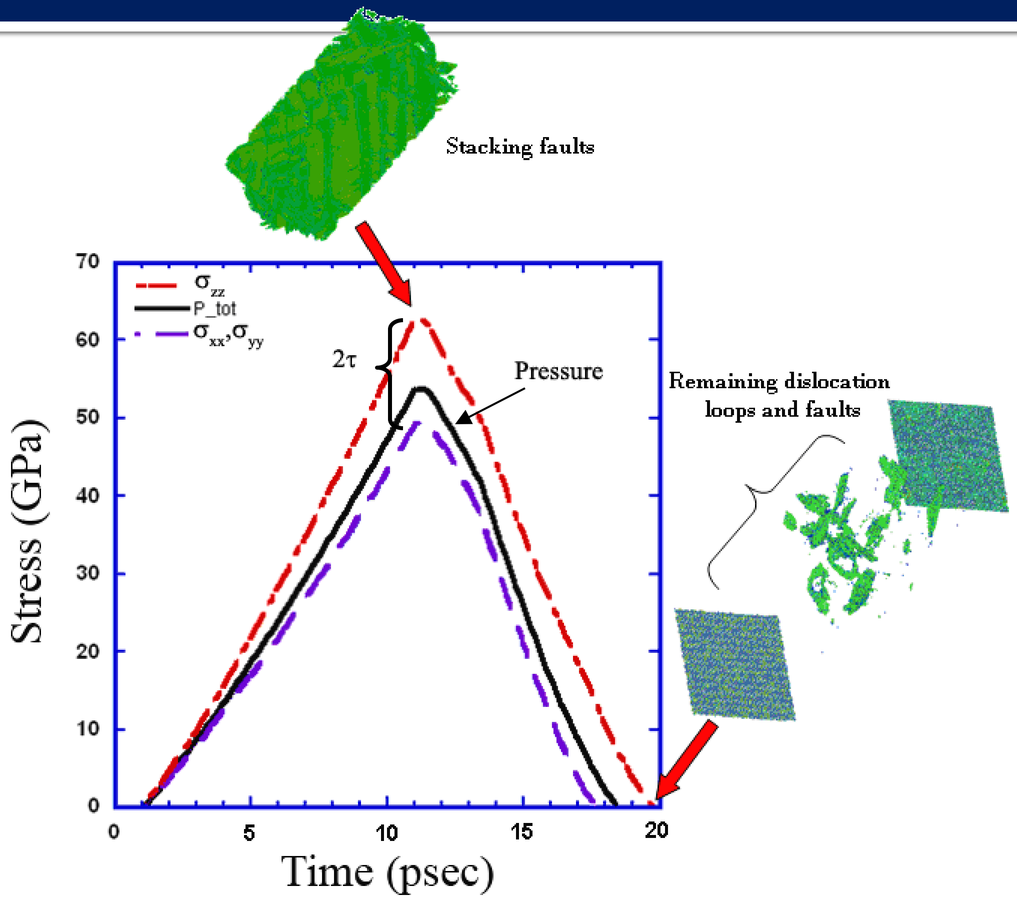

P_{tot}, σ_{xx}, σ_{yy}, σ_{zz} vs. time step, U_p=1.094 km/s

Holian-Lomdahl plot

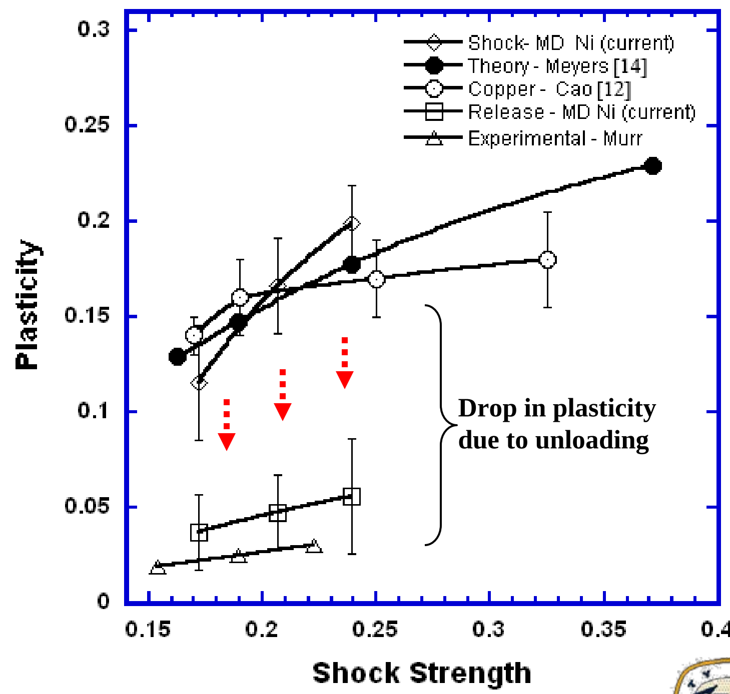

Plasticity: a_o/l

shock strength: U_p/C_o

Jarmakani et al. Acta mat 2008

BCC: Generation of Perfect Dislocations

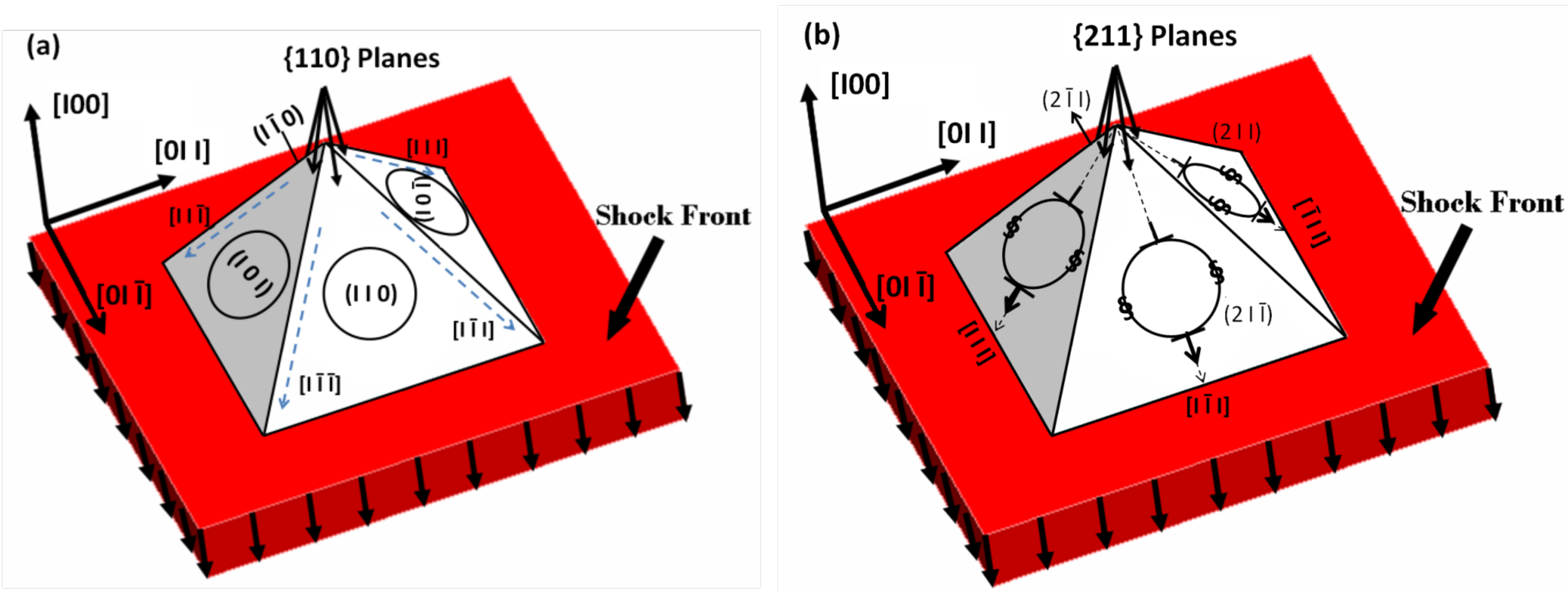

MD predictions:
Threshold for Dislocation nucleation: very high

Dislocation Multiplication: from Orowan to Kocks to Arsenlis/Barton

Orowan

$$\dot{\gamma} = \frac{d\gamma}{dt} = Mb\rho\frac{\partial \ell}{\partial t} + Mb\ell\frac{\partial \rho}{\partial t} = Mb\left(\rho\upsilon_d + \ell\dot{\rho}\right)$$

Kocks

$$\dot{\rho} = \dot{\rho}_{gen} + \dot{\rho}_{ann}$$

$$\dot{\rho} = \left(k_1\rho^{1/2} - k_2\rho\right)\dot{\gamma}$$

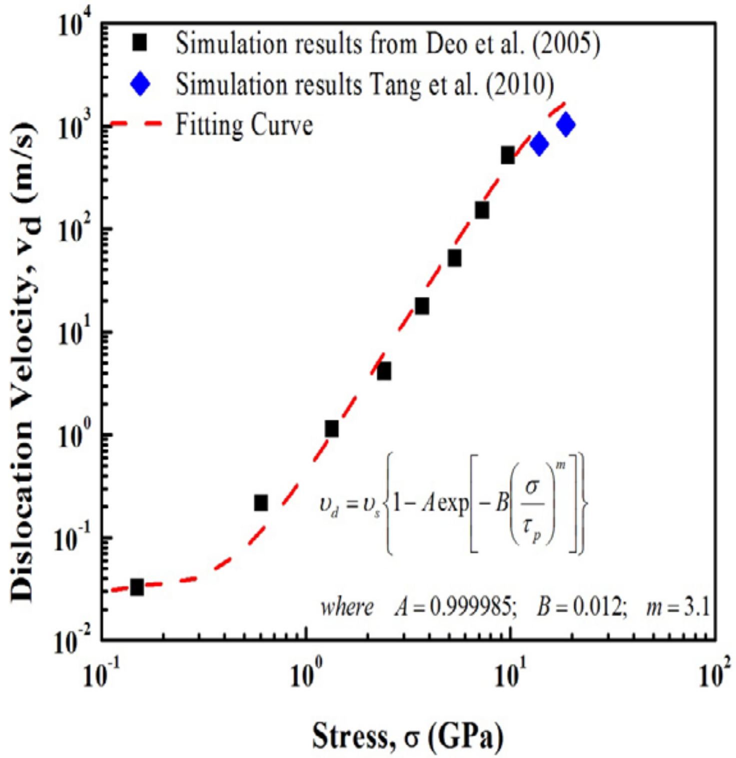

Arsenlis/Barton

$$\rho = \rho\left(\dot{\varepsilon}_p, \upsilon_d\right) = \rho(P) = \frac{\dot{\varepsilon}_p - Mb\upsilon_d tR\dot{\varepsilon}_p}{\left(Mb\upsilon_d - \dfrac{Mb\upsilon_d tR\dot{\varepsilon}_p}{\rho_{sat}\left(\dot{\varepsilon}_p\right)}\right)}$$

Grady-Kipp

$$\dot{\varepsilon} = 27.34\times 10^{-36}\times P_{shock}^4$$

Lu et al. Acta 2012

Homogeneous Dislocation Generation vs. Dislocation Multiplication: Tantalum (BCC)

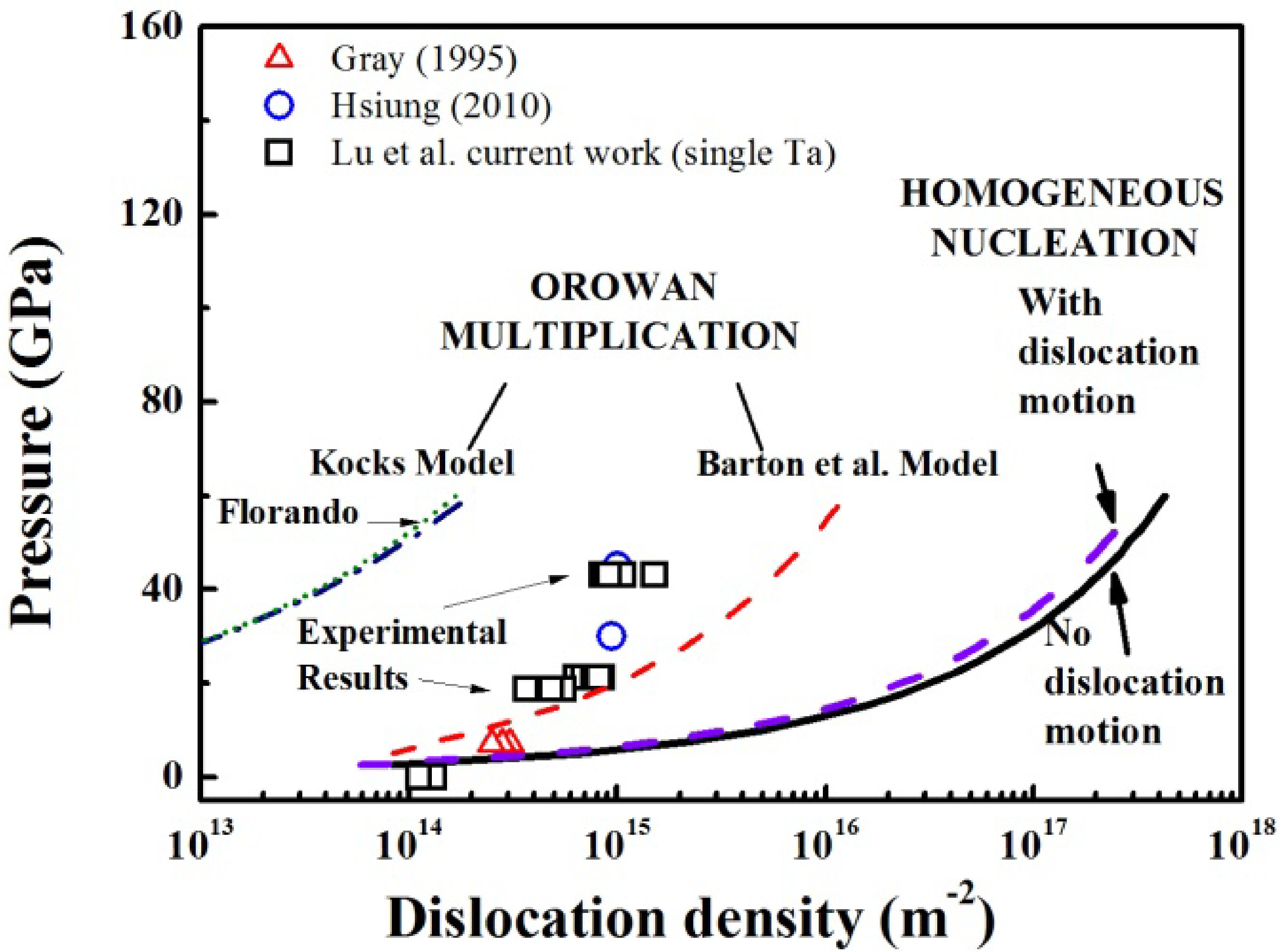

Lu et al., Acta Mat. 2012

Slip-Twinning Transition

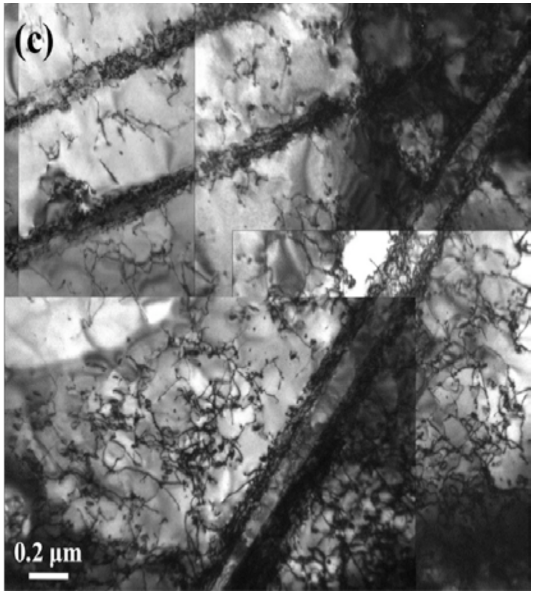

$$\sigma_S = \sigma_S^* + C_2 e^{-C_3 T} \dot{\varepsilon}^{C_4 T} + k_S d^{-1/2}$$

$$\sigma_T = \sigma_0 + m\left(\frac{Gb}{C_1}\right)^{1/2}\left[\frac{U^*}{RT}\ln\frac{\dot{\varepsilon}}{\dot{\varepsilon}_0}\right]^{1/q} d^{-1/2}$$

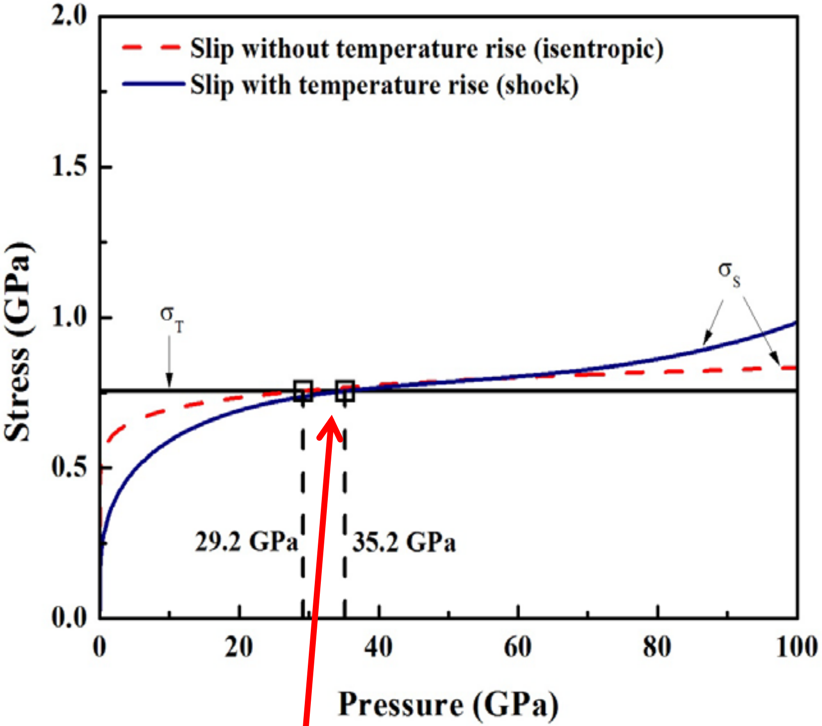

$$\sigma_S = \sigma_T$$

Slip-Twinning transition

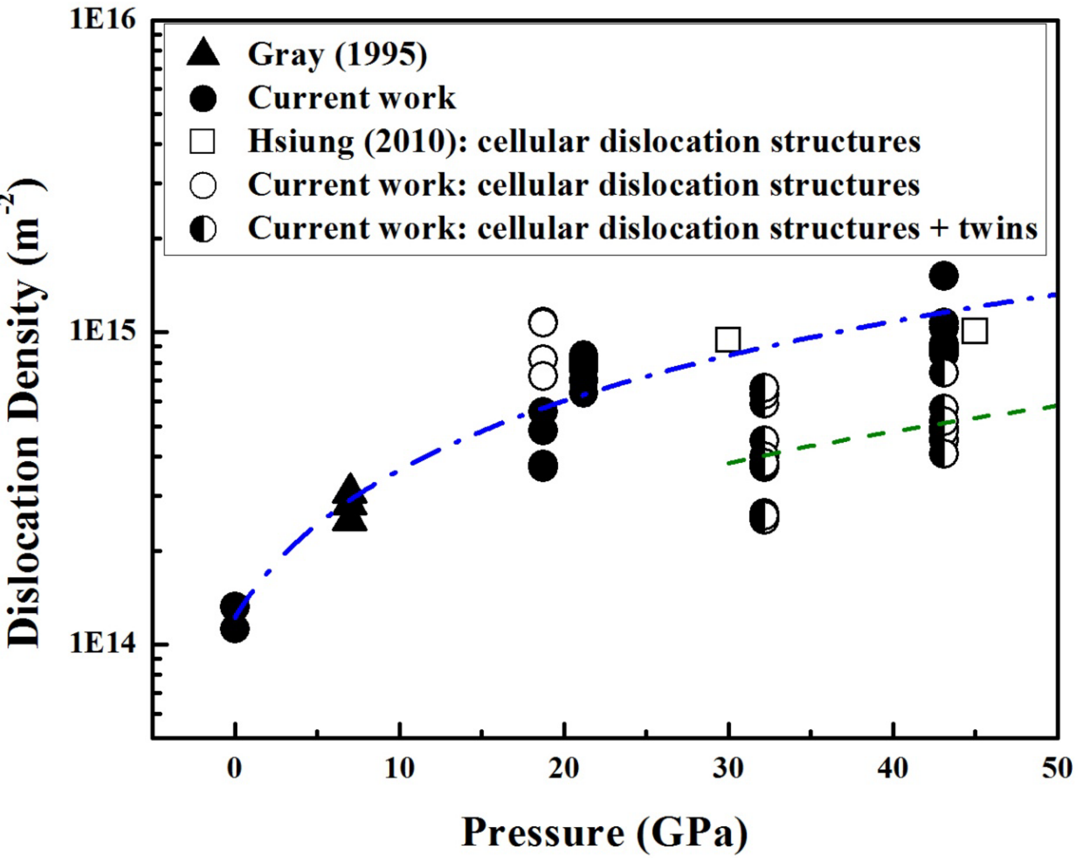

$$\gamma = \begin{cases} Mb\rho_{\perp} l & \text{if } \quad \dot{\gamma} < \dot{\gamma}_{threshold} \\ Mb\rho_{\perp} l + f_T \gamma_T & \quad\quad \dot{\gamma} > \dot{\gamma}_{threshold} \end{cases}$$

Lu et al. Acta 2012

Strength in Tension

- **Void growth in FCC (Cu) and BCC (Ta) metals**

Spall Strength: Effect of Time

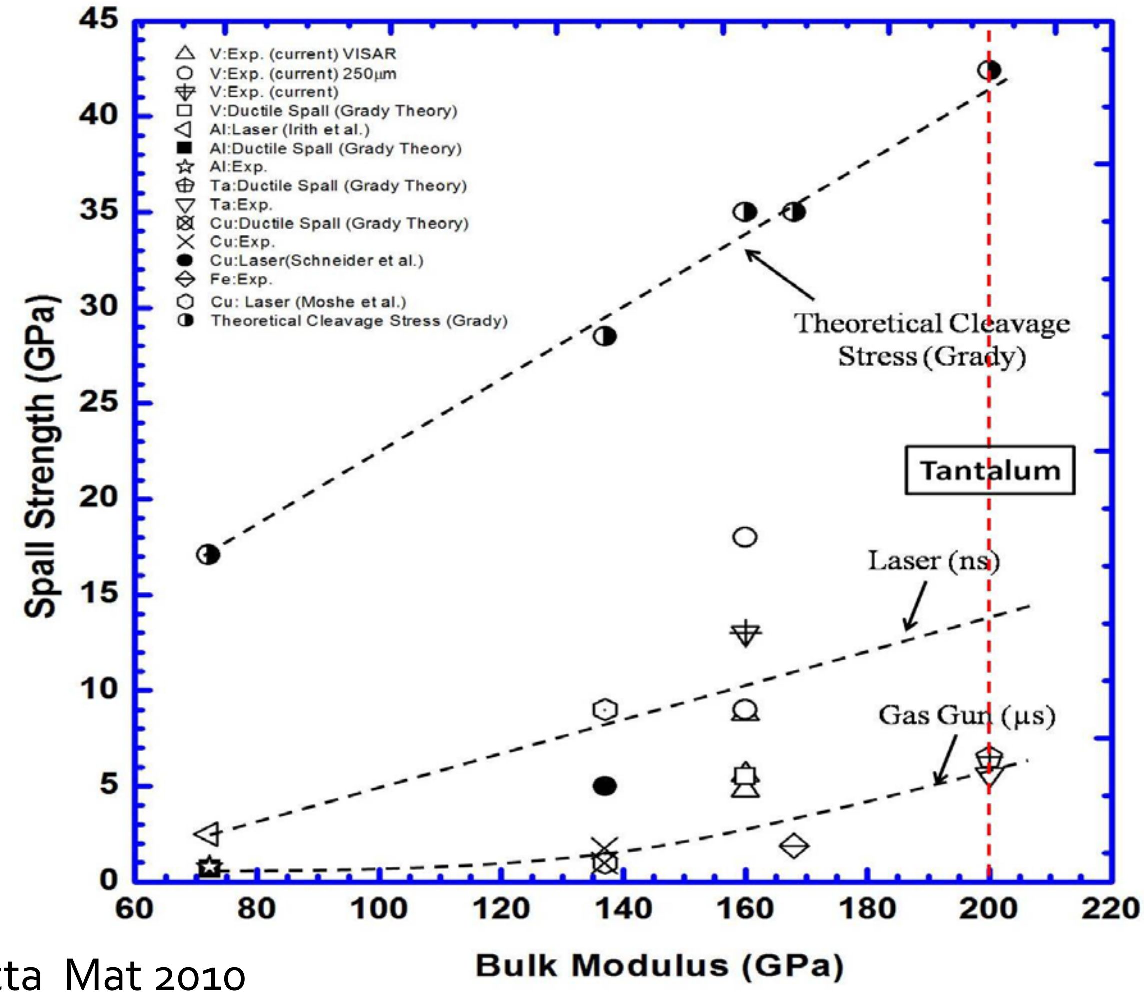

Meyers et al. Acta Mat 2010

Void Seen in High Voltage TEM: KRATOS, **NCEM 1 MeV**

Christy, Pak, Meyers , Explomet Proc., 1986

Experimental Observation

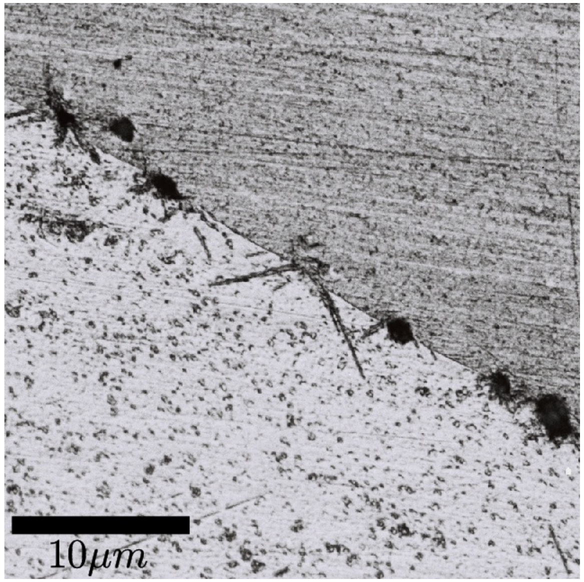

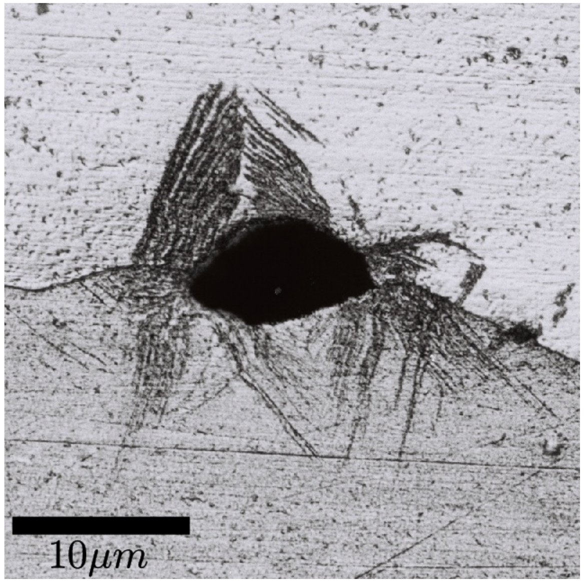

- Dislocation activity (slip) around growing voids

Meyers MA, Aimone CT. Prog in Matls Sci 1983;
Christy et al. Metallurgical Applications of Shock Wave and High-Strain-Rate Phenomena, Dekker 1986

Loading on [110] (z-axis)

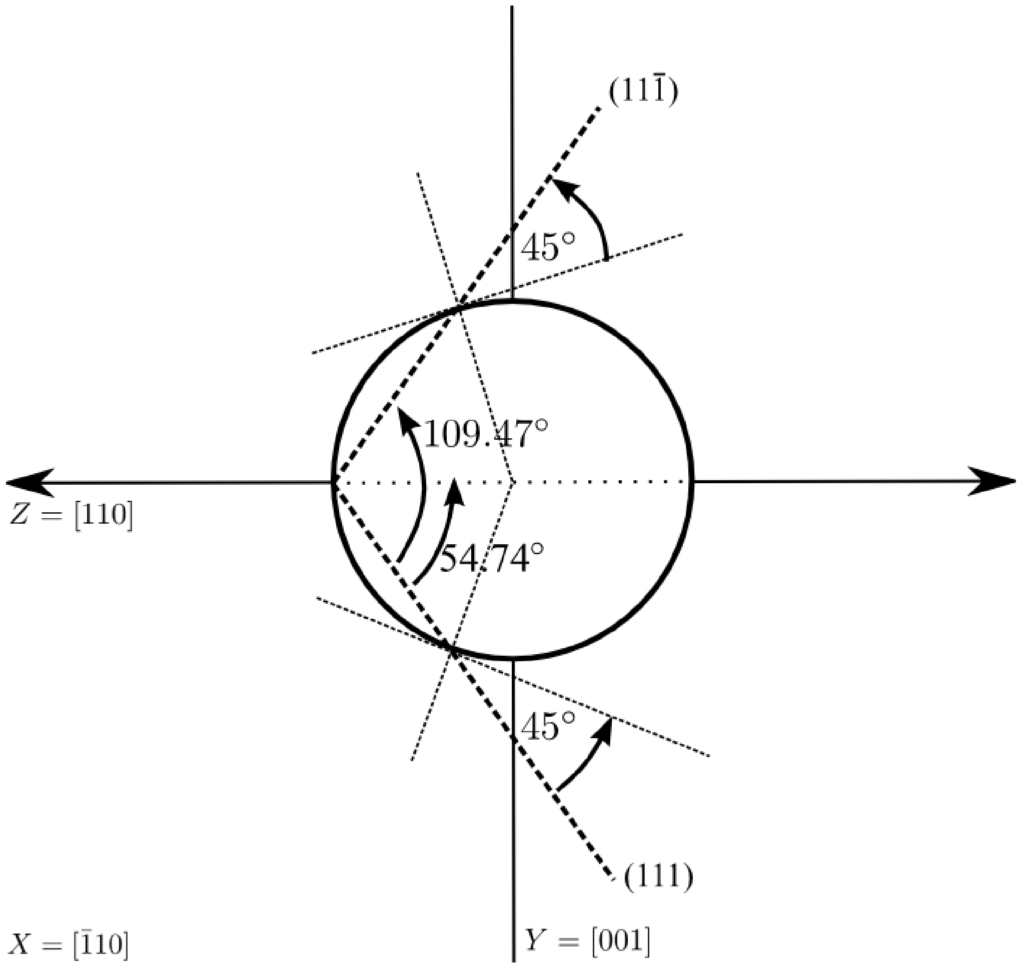

Traiviratana et al. Acta Mater 2008;

Nanovoid growth:Marian, Knap, Ortiz

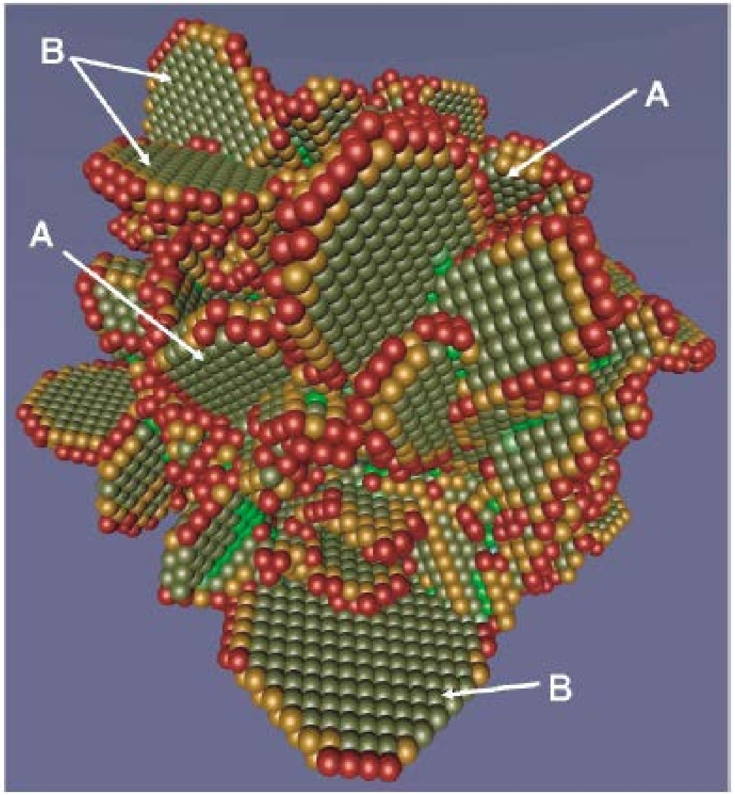

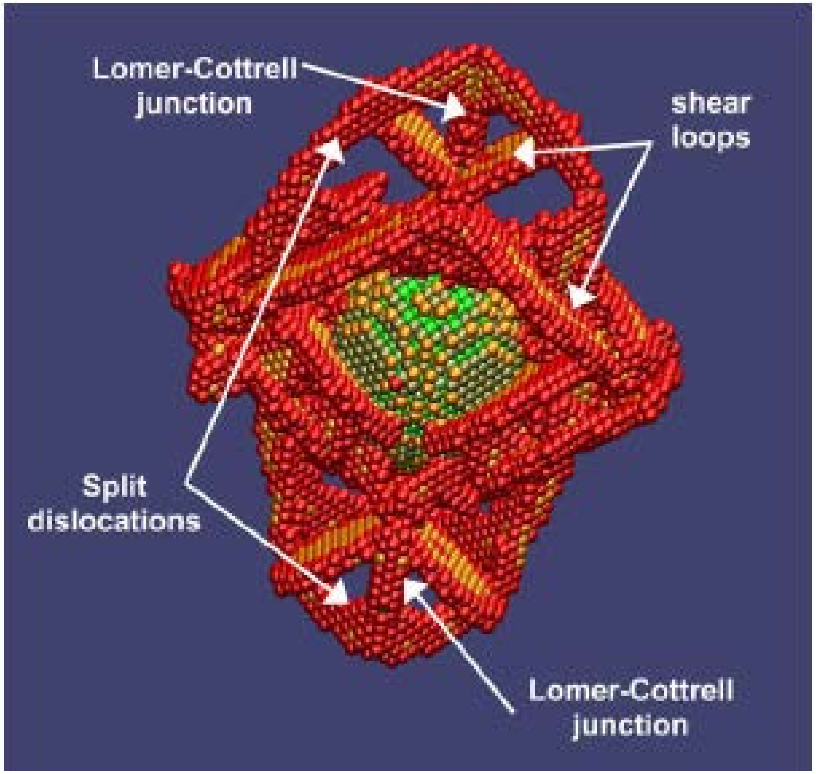

Marian, Knap, Ortiz, PRL, 93(2004)165503 Marian, Knap, Ortiz, Acta mat., 53(2005)2893

Void Growth Simulation-loading [110]

[110] strain direction along z-axis

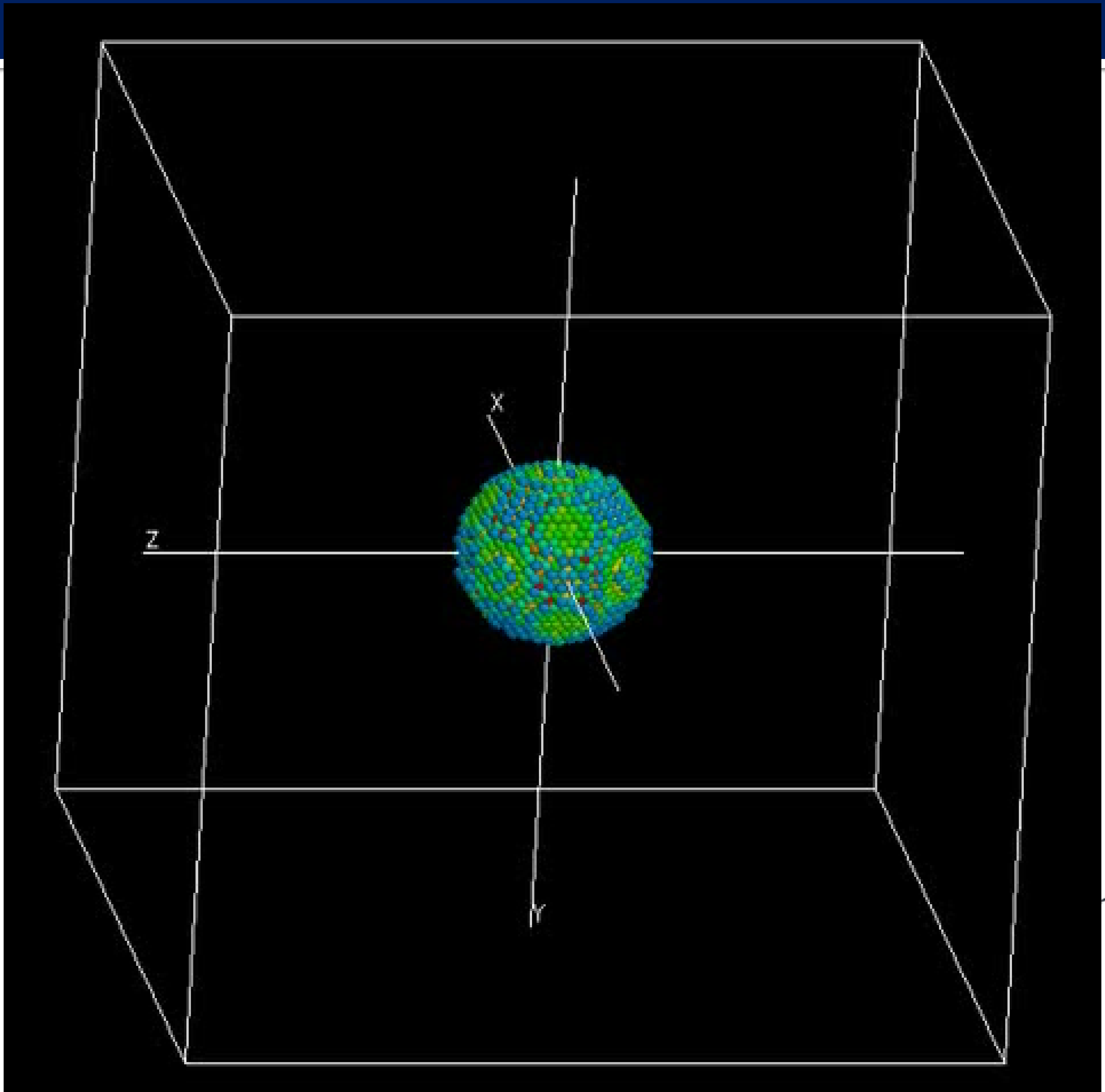

Void Growth Simulation-loading [111]

[111] strain direction along z-axis

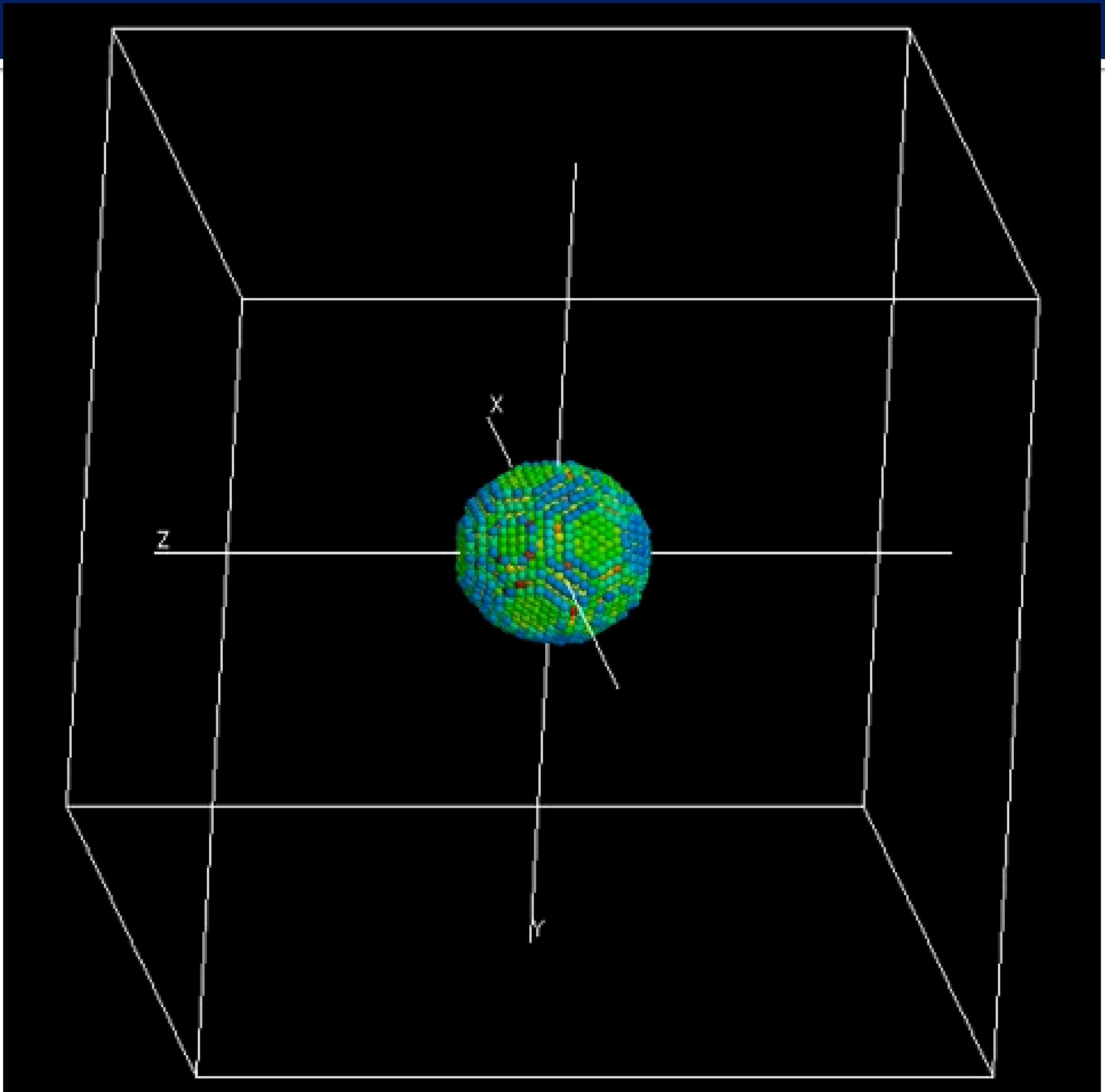

Loading on [111] Triplanar Loops

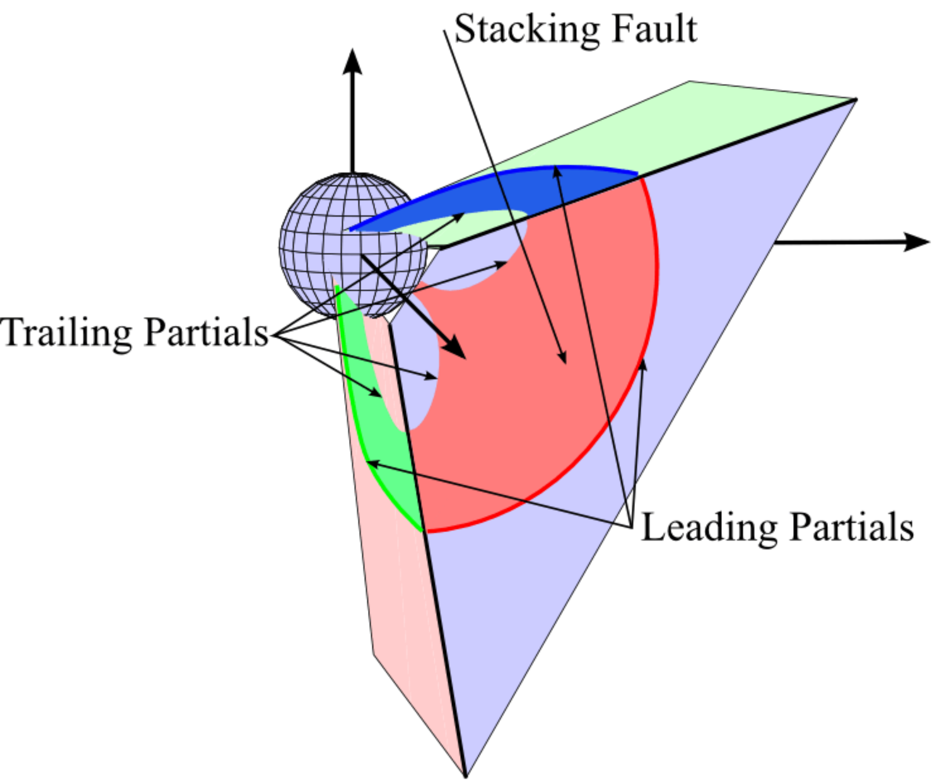

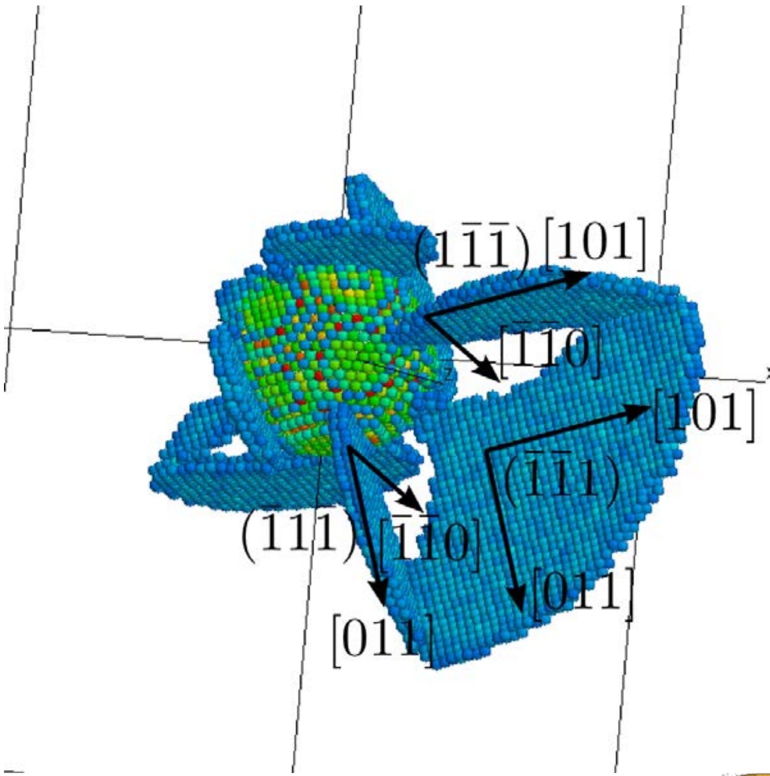

Hydrostatic tension-Tantalum Prismatic Loop Formation

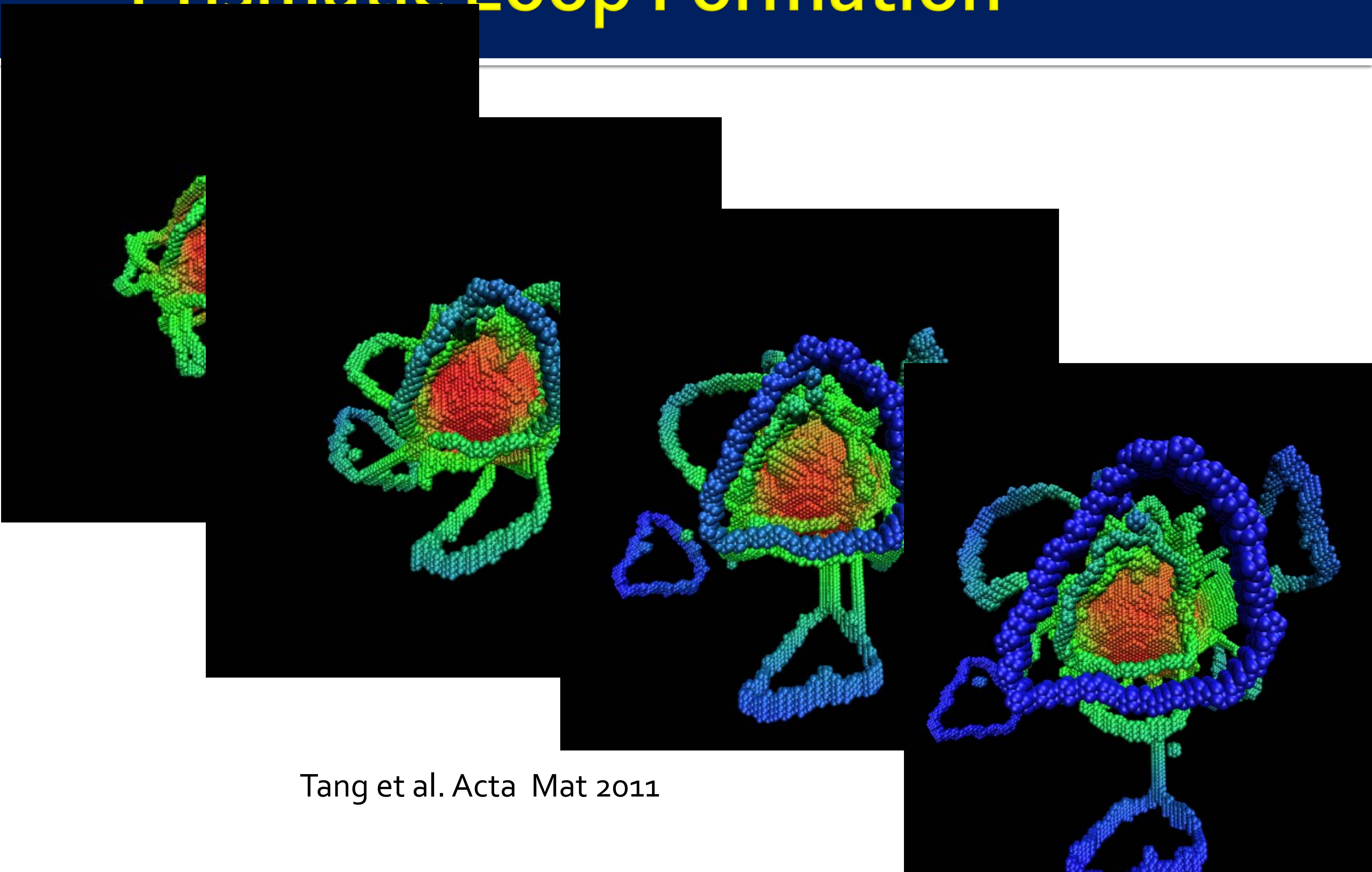

Tang et al. Acta Mat 2011

Sequence of Shear Loop Emission in Ta

3.3 nm radius void, uniaxial compressive strain, strain rate $10^8\ s^{-1}$

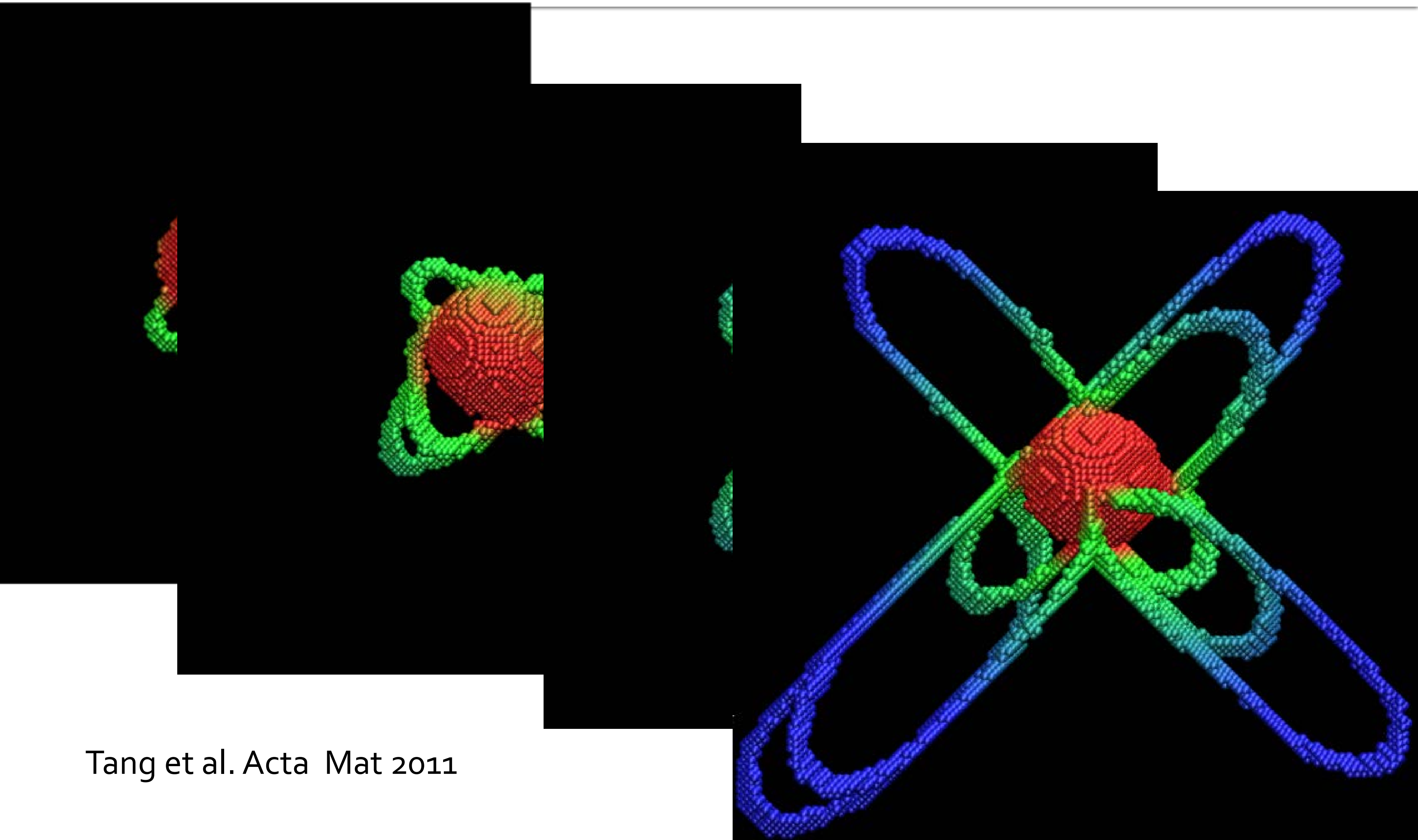

Tang et al. Acta Mat 2011

Stress for Dislocation Loop Emission

1. Creation of a new surface step during the emission process.

$$\tau_1 = \frac{2\gamma\rho b}{\pi[(\rho b)^2 + r^2]}$$

2. Stress required to generate and bow a dislocation loop to a radius R1 that is a fraction of the void radius *R*.

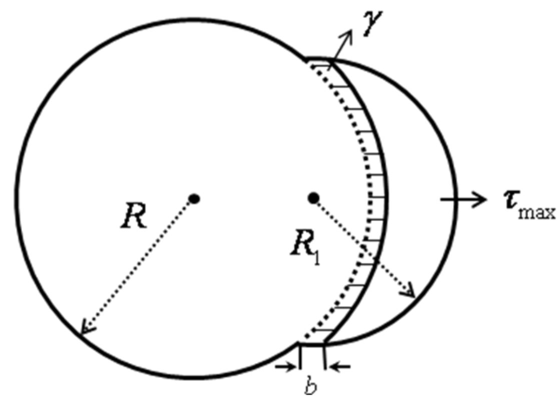

$$\tau = \frac{2\gamma}{\pi\rho b} + \frac{Gb(2-\nu)}{4\pi(1-\nu)R_1}\ln\frac{8mR_1}{e^2\rho b}$$

$$\frac{\sigma_{vM}}{G_{<111>}} = \frac{0.448\tau_{max}}{G_{<111>}} = 0.448\left[\frac{2\gamma}{G_{<111>}\pi\rho b} + \frac{b(2-\nu_{<111>})}{4\pi(1-\nu_{<111>})R_1}\ln\frac{8mR_1}{e^2\rho b}\right]$$ BCC

$$\frac{\sigma_{vM}}{G_{<112>}} = \frac{0.33\tau_{max}}{G_{<112>}} = 0.33\left[\frac{2\gamma}{G_{<112>}\pi\rho b_p} + \frac{b_p(2-\nu_{<112>})}{4\pi(1-\nu_{<112>})R_1}\ln\frac{8mR_1}{e^2\rho b_p} + \frac{\gamma_{SF}}{G_{<112>}b_p}\right]$$ FCC

Rice and Thomson , Phil Mag 1974

Stress vs. Void Size: MD and Analytical Prediction

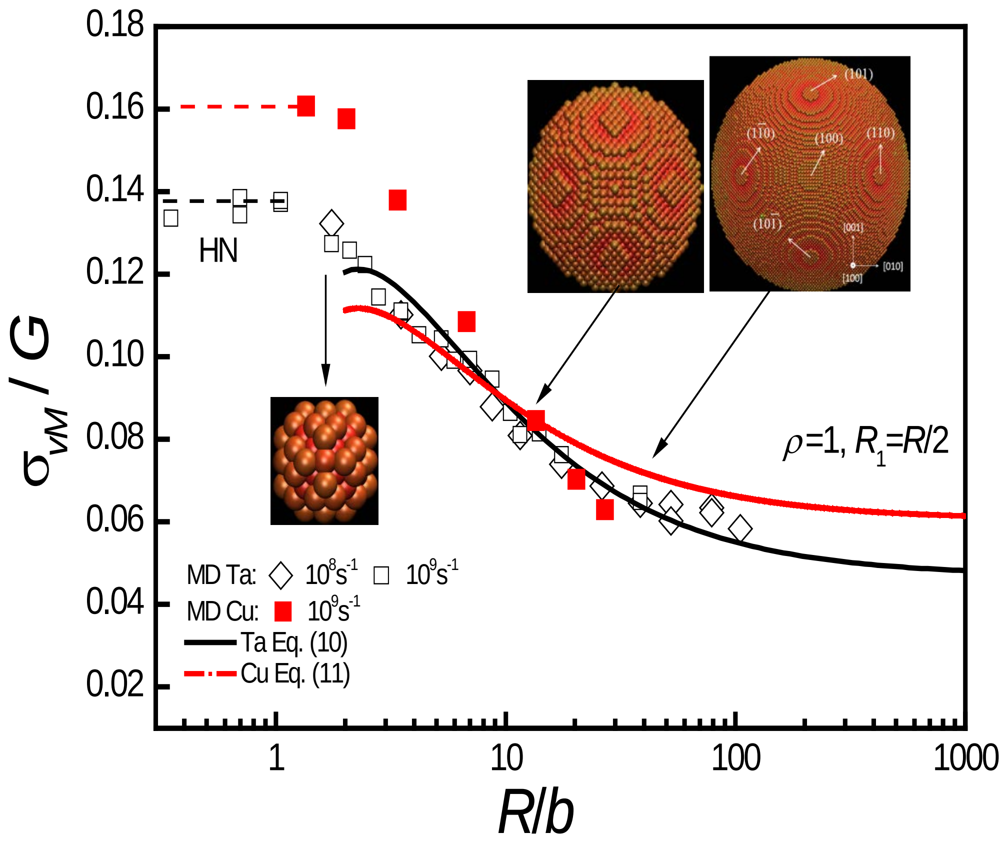

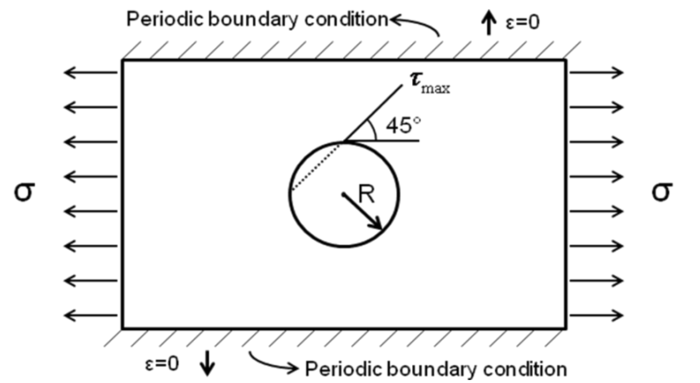

Tang et al., Acta Mat 2012

Void Initiation at Tri-Vacancy: BCC Ta

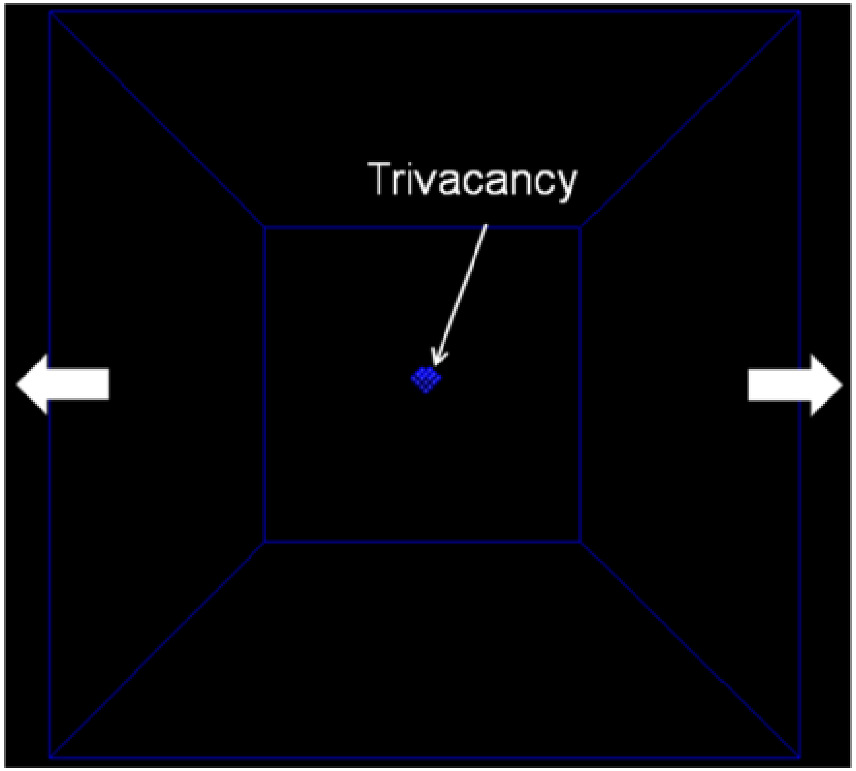

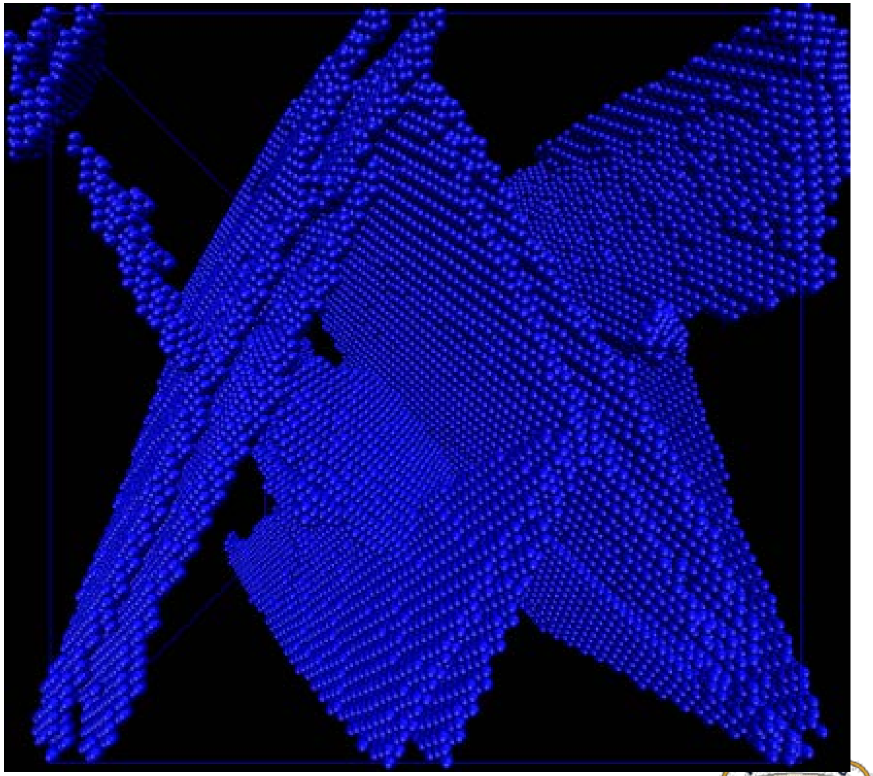

ε =11%

Tang et al. Acta Mat 2011

Experimental Evidence

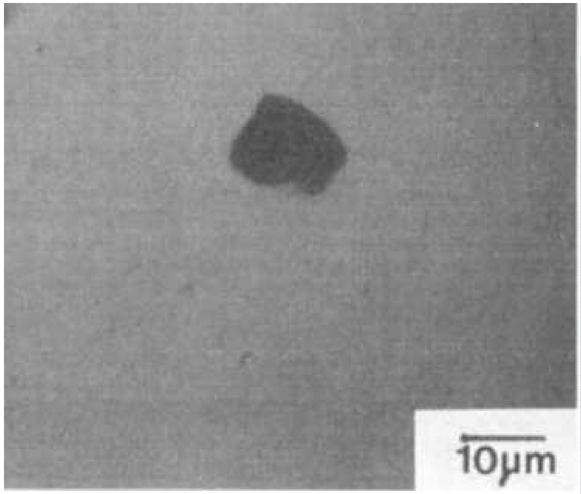

Meyers and Aimone, PMS

Christy et al.

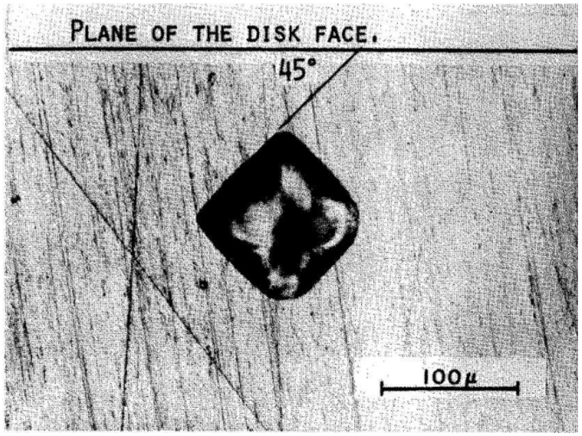

Stevens and Davison

Void Shape Development

[001] Strain in z

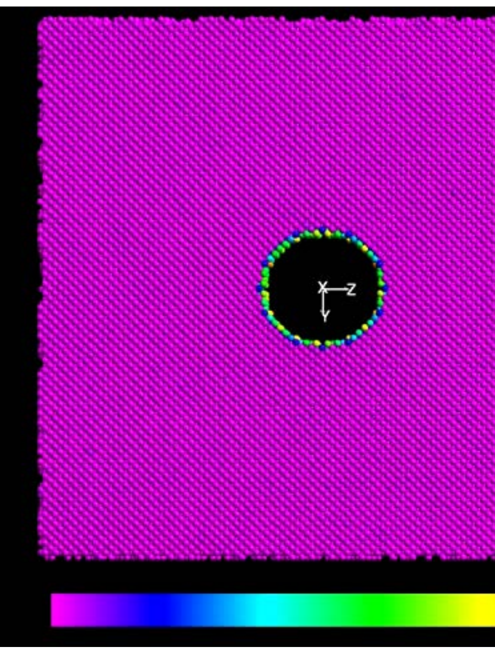

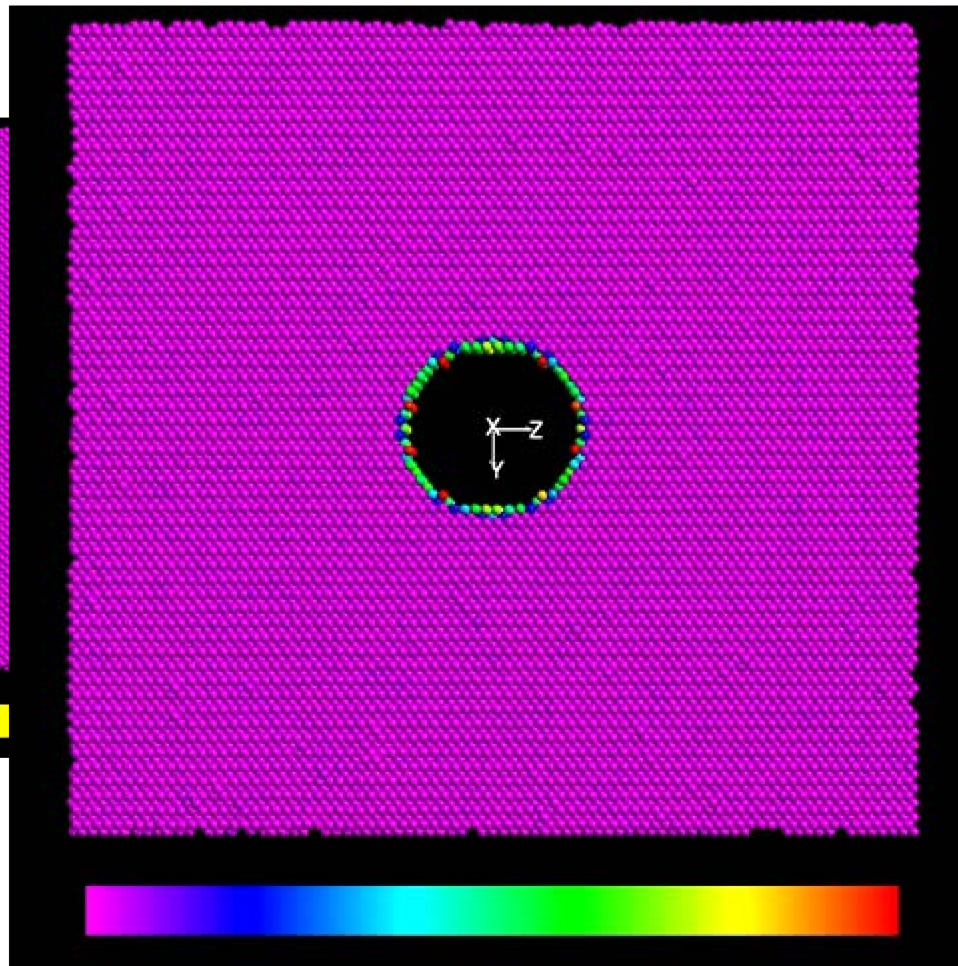

[111] Strain in z

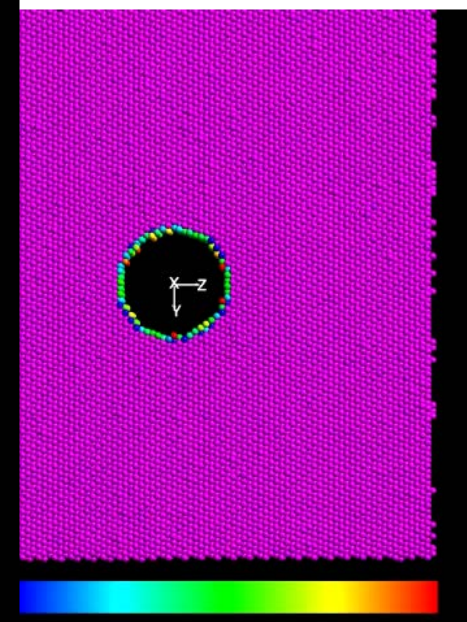

Traiviratana et al. Acta Mater 2008

Nanocrystalline Copper: Tension

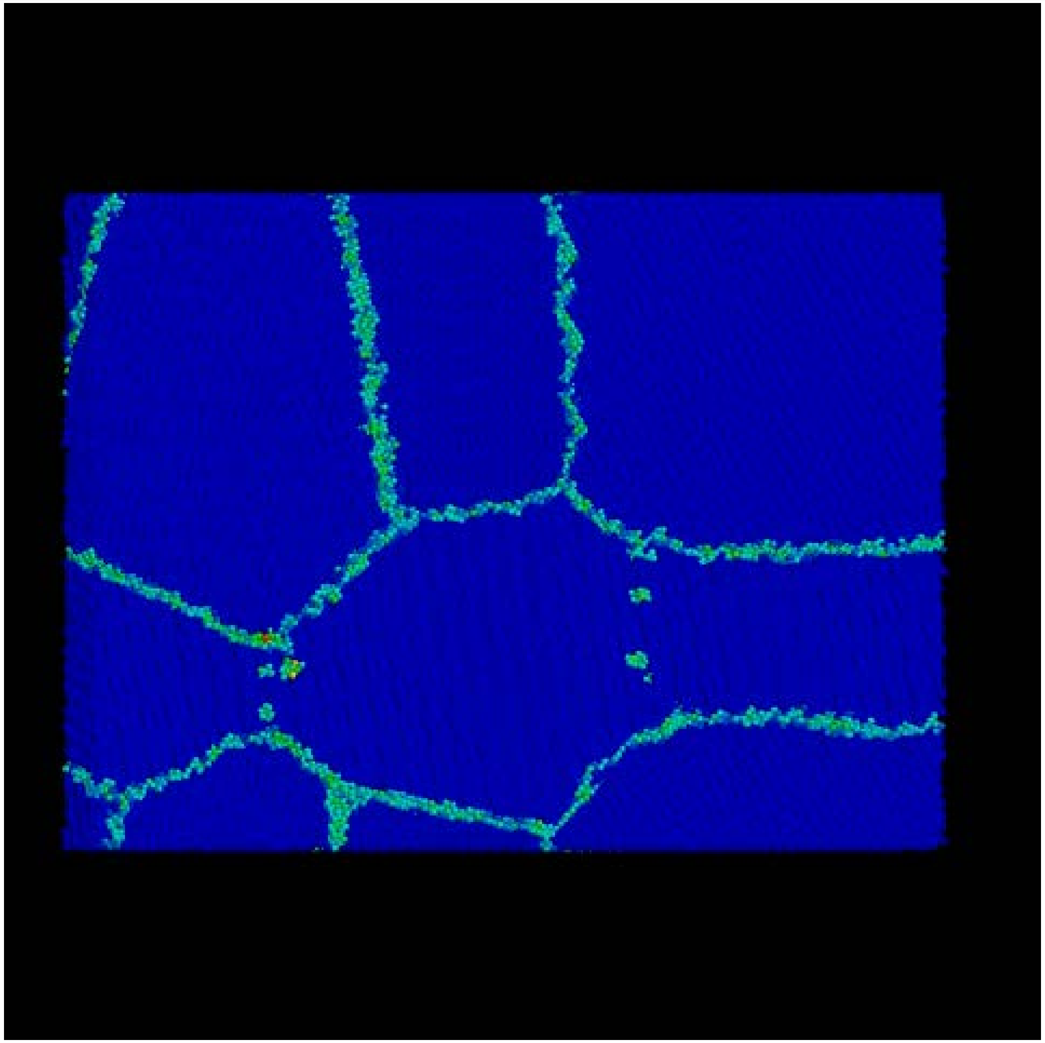

4 grains (D ~ 20nm)
1.3 million atoms
Hydrostatic expansion
Strain rate 10^9 /s

Bringa et al. Acta Mat. 2010

Tension of nanocrystalline Ta

d=27.3 nm

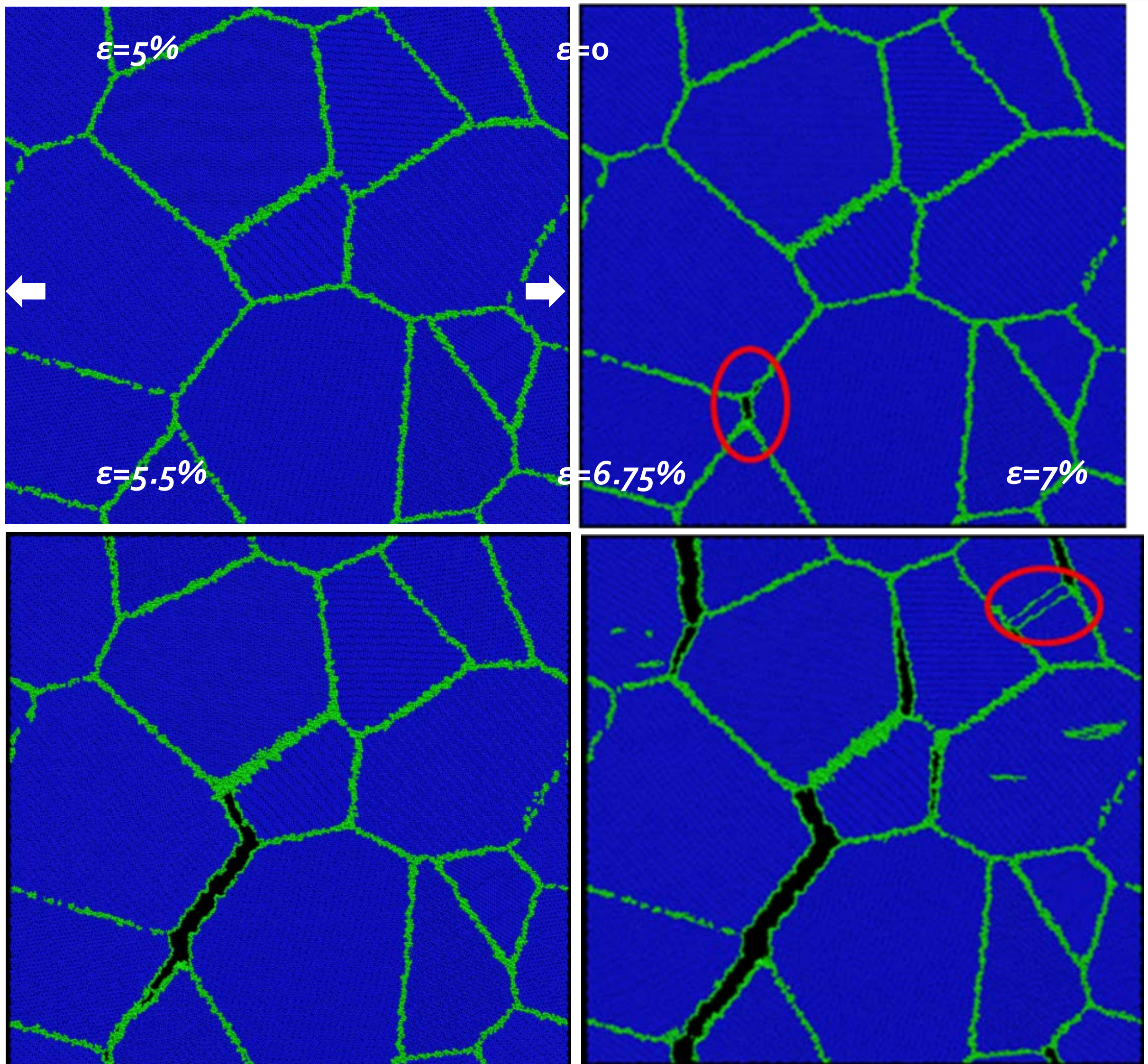

Tensile failure of nanocrystalline Ta

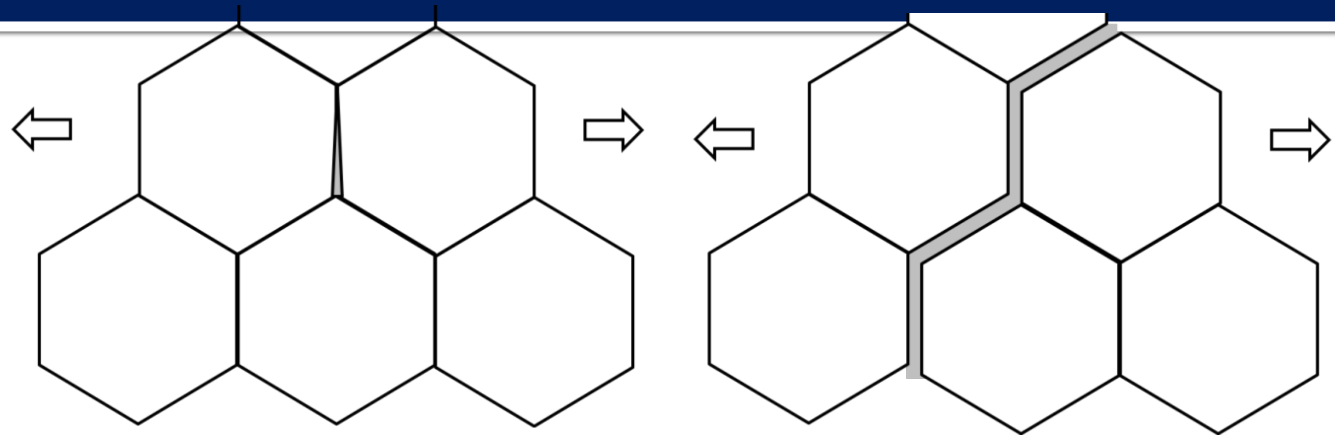

Grain-boundary separation

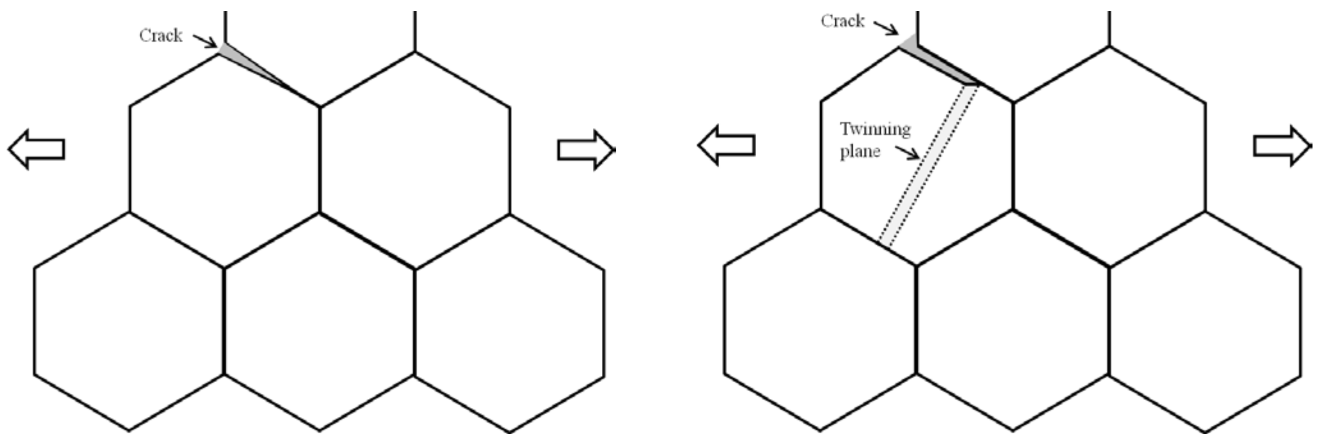

Crack induced twinning

High Velocity Dislocations: Nanoindentation as a Dislocation Source:Ta

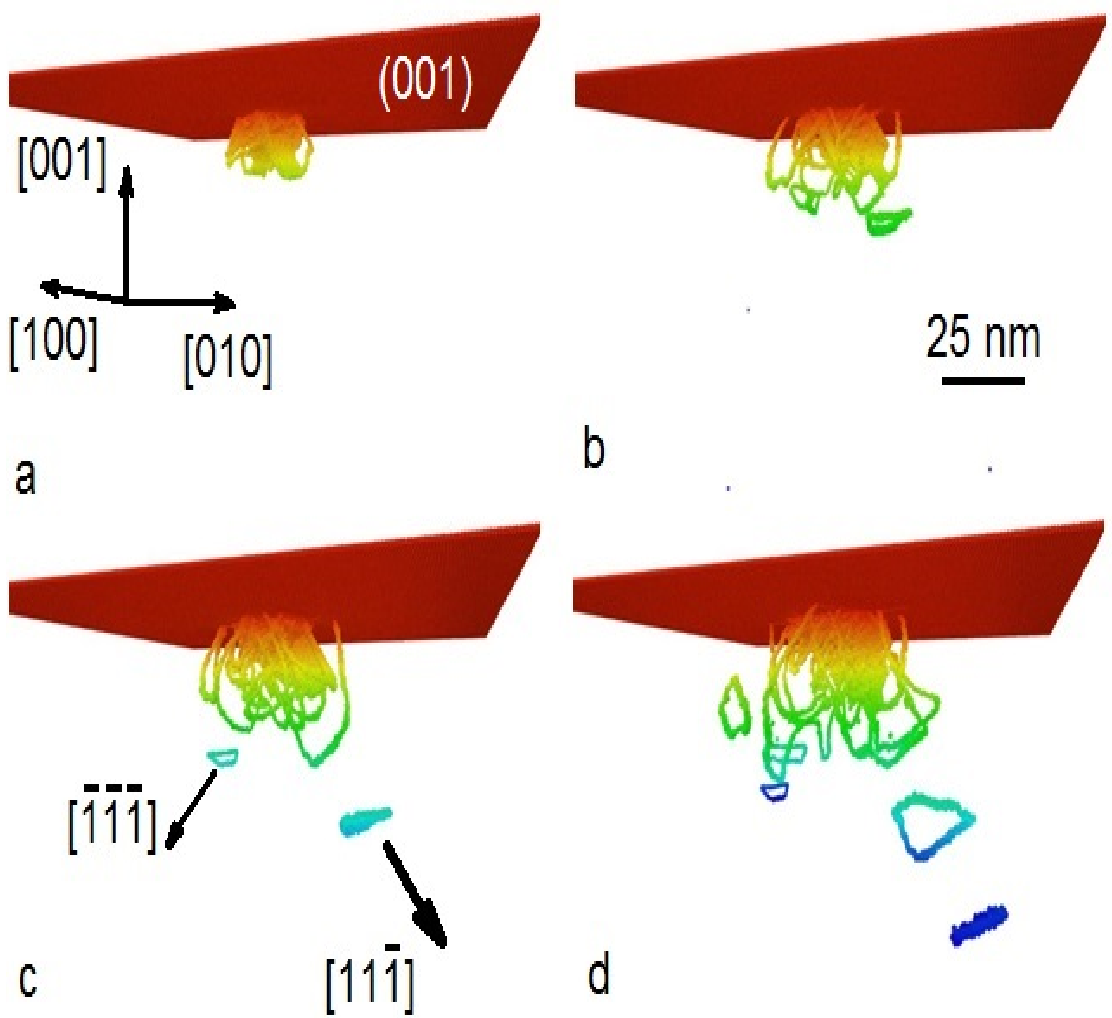

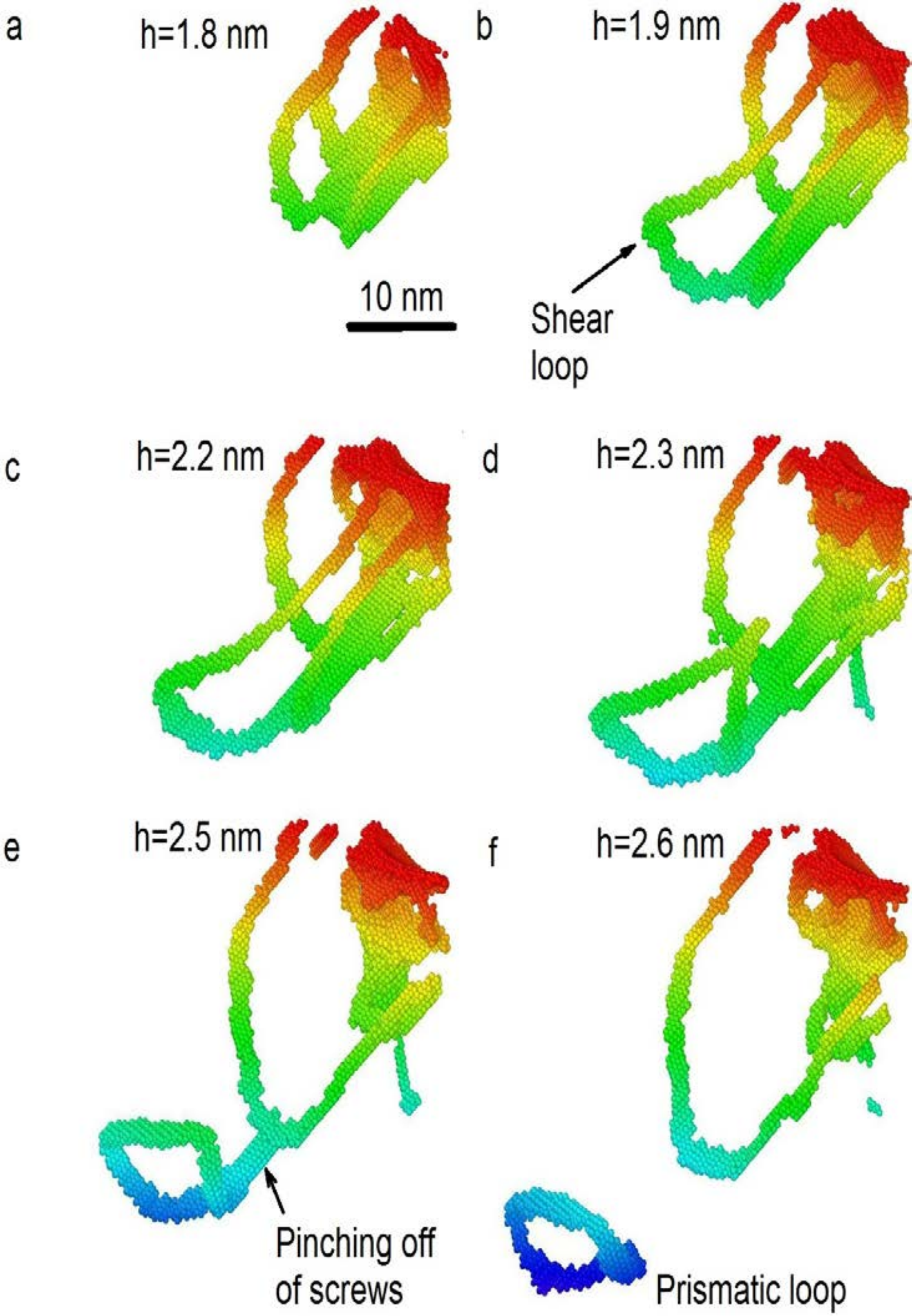
a
h=1.8 nm
10 nm
b
h=1.9 nm
Shear loop
c
h=2.2 nm
d
h=2.3 nm
e
h=2.5 nm
Pinching off of screws
f
h=2.6 nm
Prismatic loop

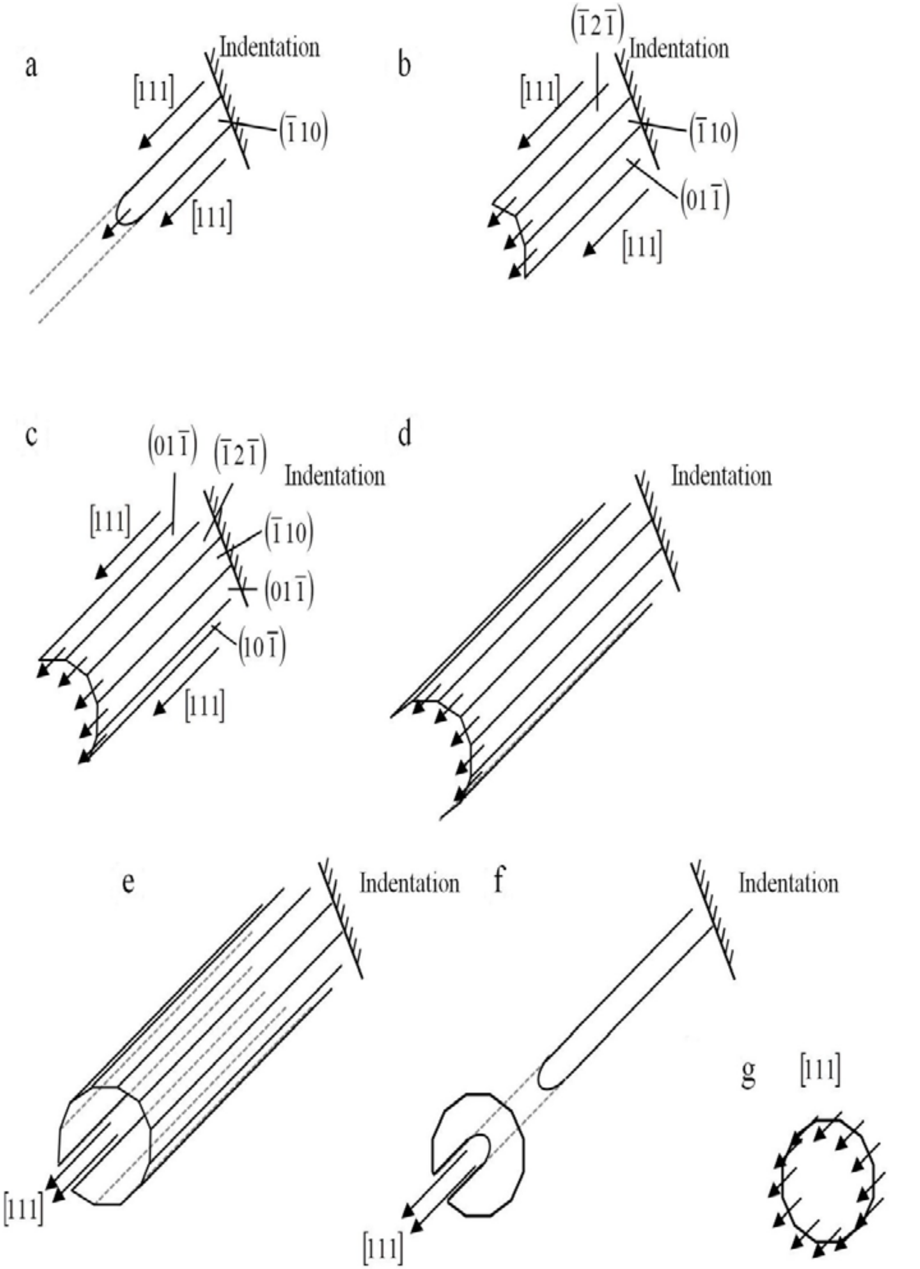
a
Indentation
[111]
$(\bar{1}10)$
[111]
b
$(\bar{1}2\bar{1})$
Indentation
[111]
$(\bar{1}10)$
$(01\bar{1})$
[111]
c
$(01\bar{1})$
$(\bar{1}2\bar{1})$
Indentation
[111]
$(\bar{1}10)$
$(01\bar{1})$
$(10\bar{1})$
[111]
d
Indentation
e
Indentation
[111]
f
Indentation
[111]
g
[111]

Removal of Surface Layer and Shock Compression of Prismatic Loops

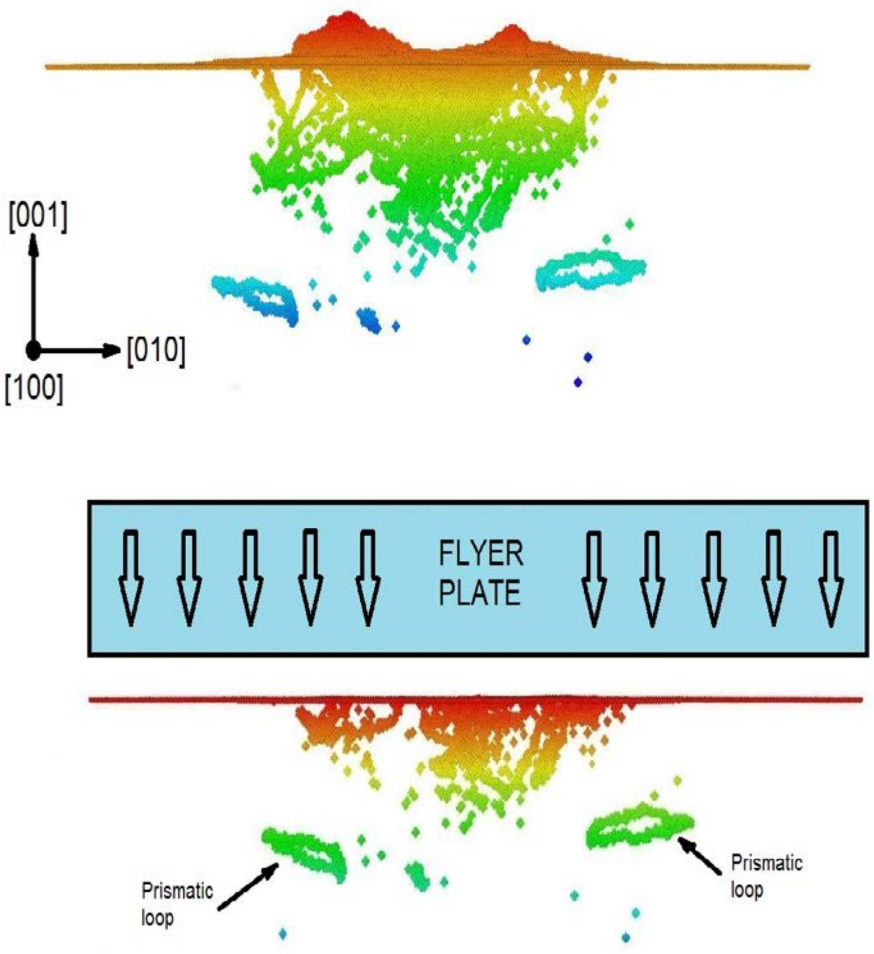

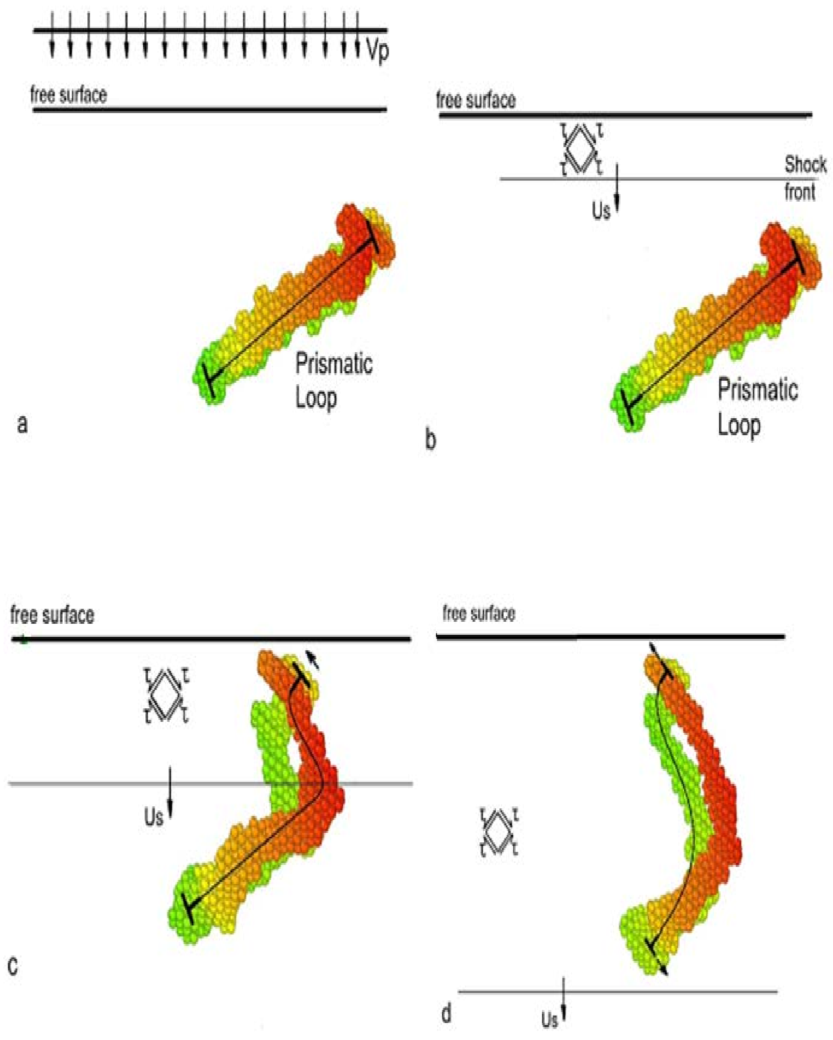

High Velocity Dislocations: Tantalum

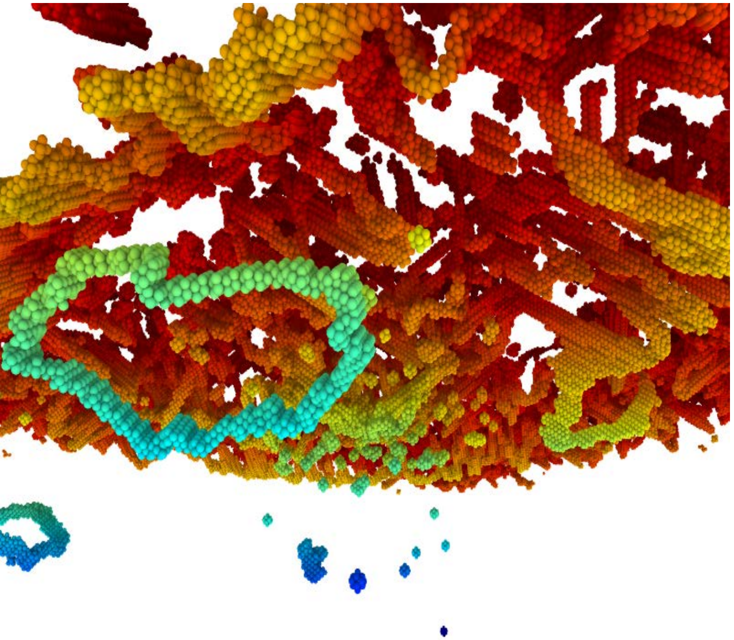

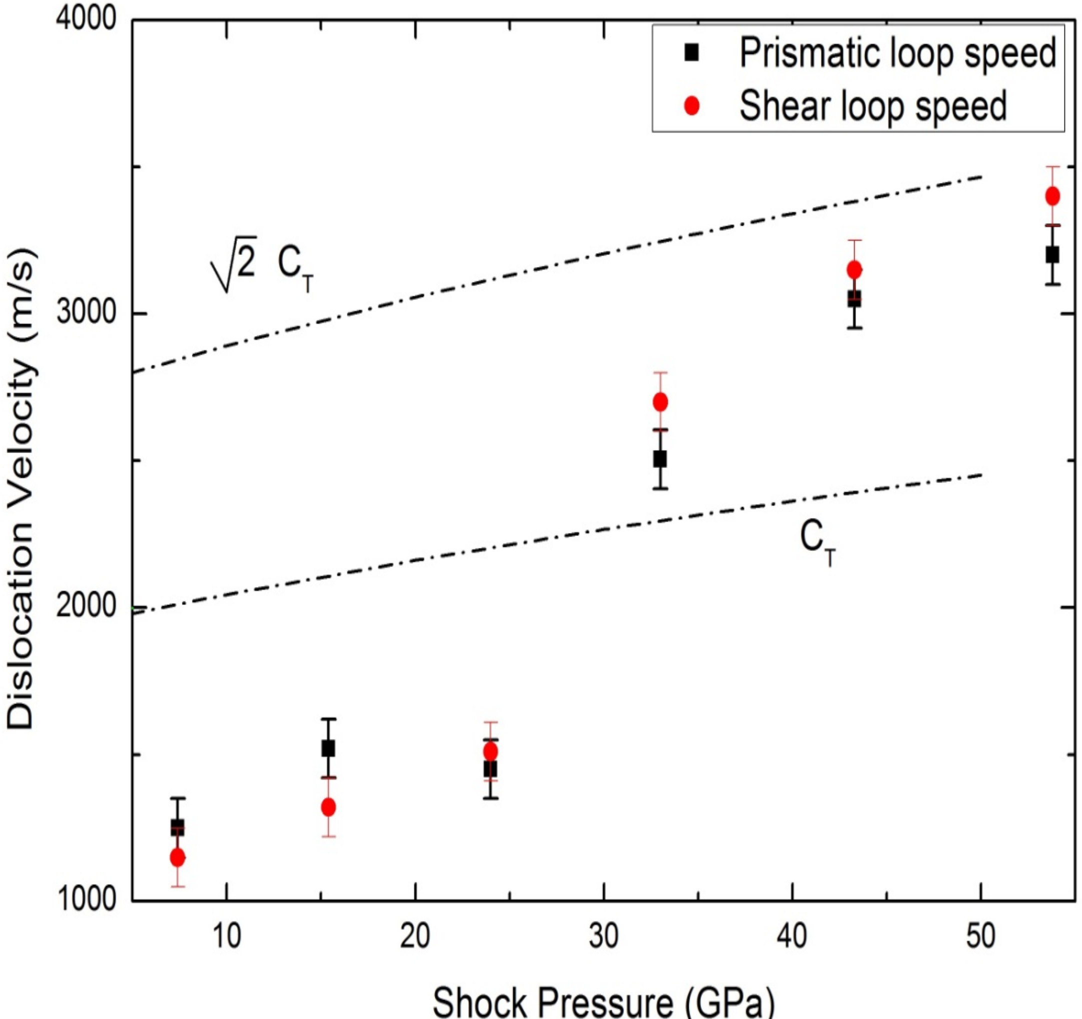

High Velocity Dislocation:Silicon

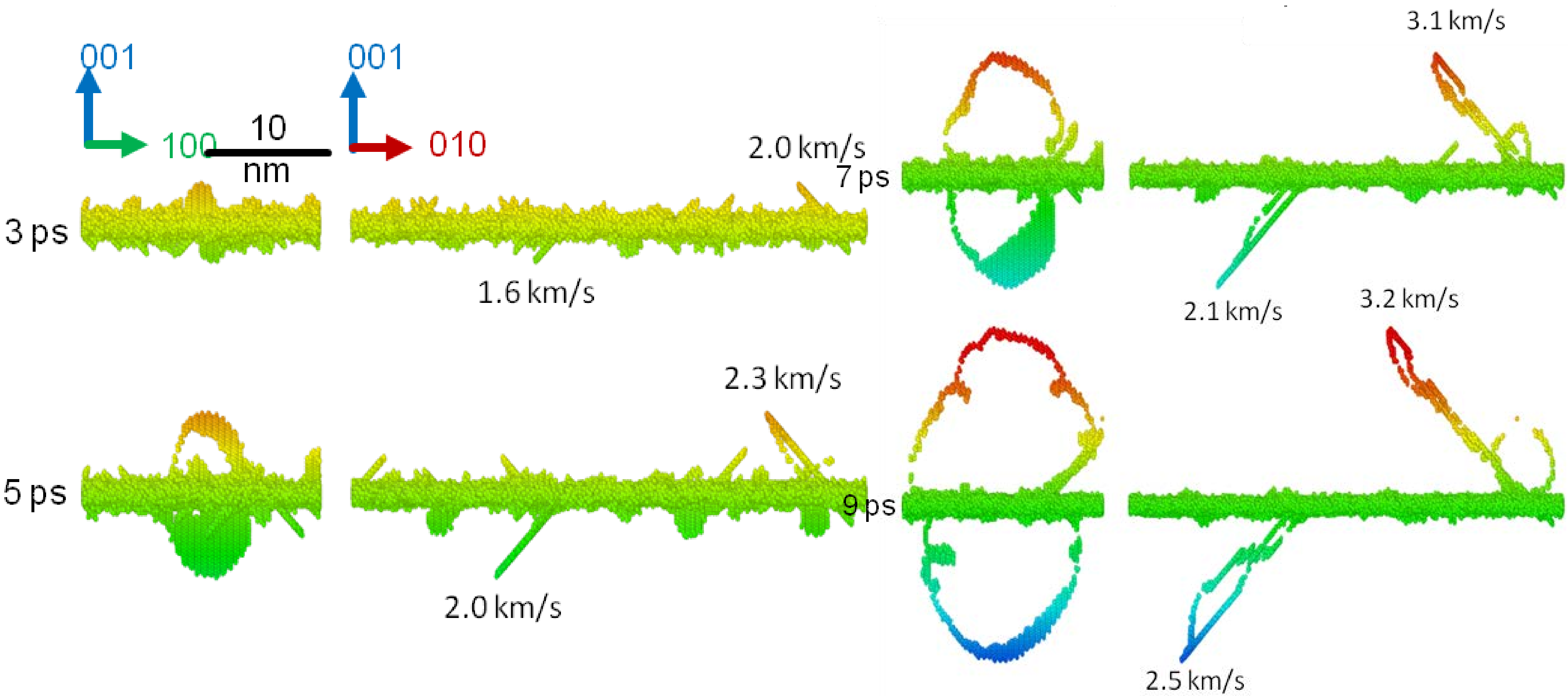

Shock of 001 silicon using the SW potential P=35 GPa; Particle vel. 1.75 km/s; flyer plate velocity of 3.5 km/s.

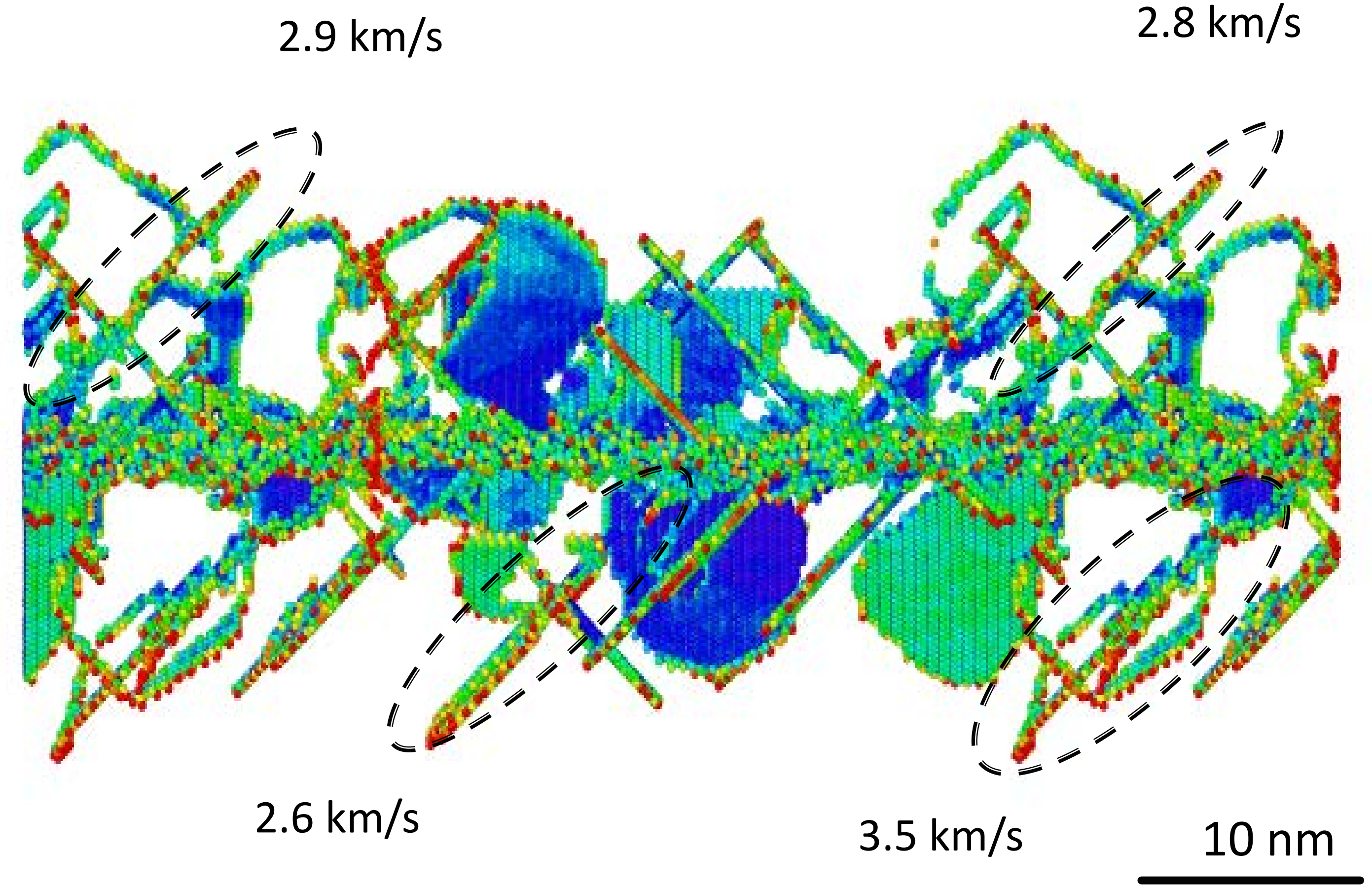

[001] Si: Pressure ~60 GPa

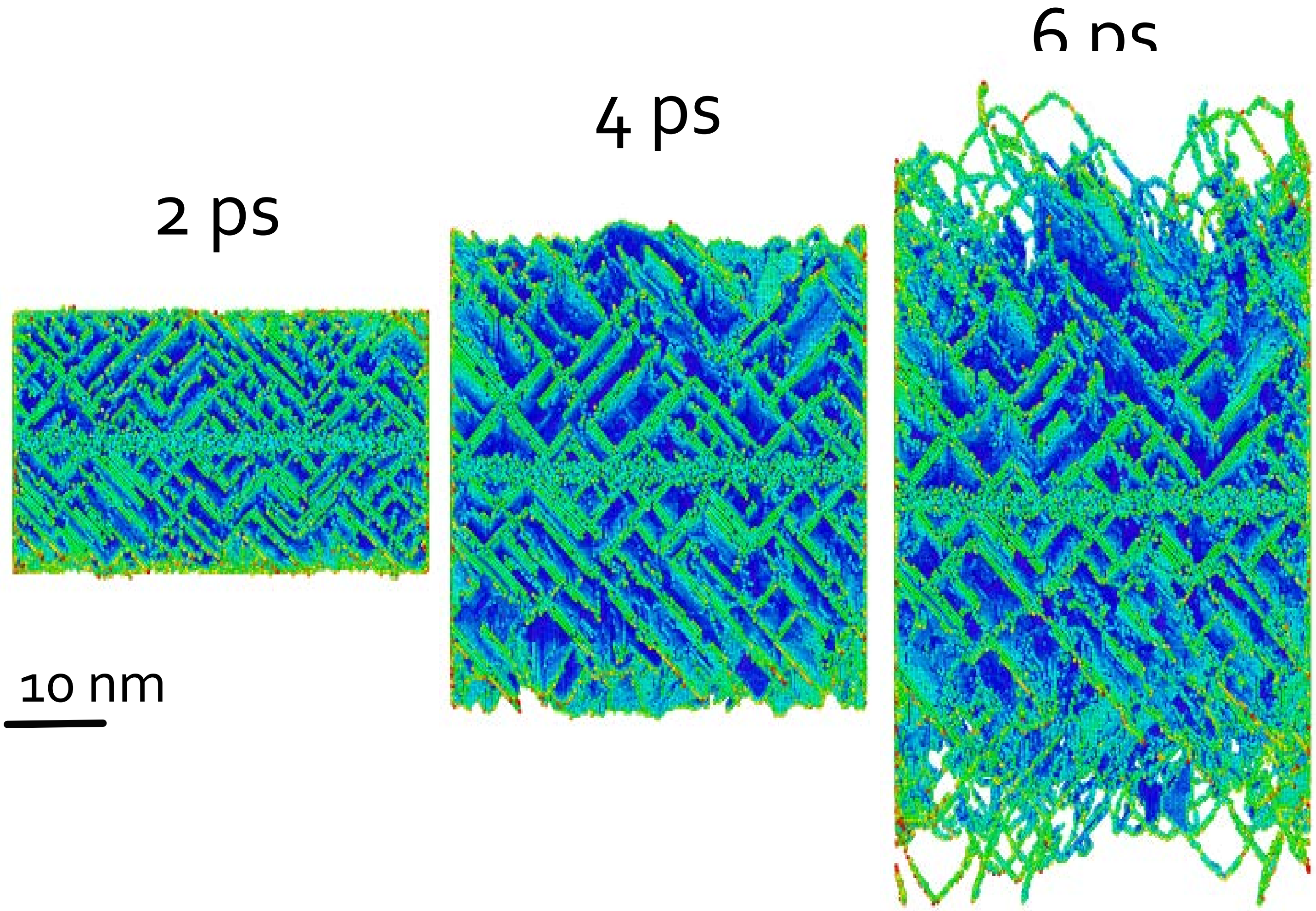

Fundamental Questions: Answers?

- Strength under extreme strain rates and pressures?

Great strides made up to 10 ^{10} s^{-1}

- Defect generation: dislocations

Homogeneous dislocation generation;FCC dislocation multiplication; BCC

- Twins in compression and tension?

Twinning threshold, pressure and shear induced transformations.

- Tensile failure
- Void formation explained.
- Dislocation velocities: transonic/supersonic?

Experiments January 30 in Omega

Conclusions Voids: I

- **‘Special’ Shear Loops – Primary Mechanism of Void Growth, as postulated by Lubarda et al. (2004)**

- **Model FCC Metal: Copper**
- New mechanisms for loop formation – Bi-Planar and Tri-Planar Loops – identified by MD.
- Dislocation reactions and energetics for mono-planar, and bi-planar loops analyzed.
- Growth Kinetics of void modeled and compared with Cocks-Ashby.
- Density of geometrically-necessary dislocation loops calculated; consistent with observations
- Partial dislocation velocities: sub and transonic

Conclusions Voids: II

Model BCC Metal: Tantalum

- Three mechanisms identified:
  - Shear loop formation
  - Twinning
  - Prismatic loop formation
- Dislocation velocities: subsonic
- Tension/Compression asymmetry
- Slip-twinning transition
- Void-size effect

Laser Shock Compression of Sandwich Micro-Nano-Micro Laminates

Marc A. Meyers , Vitali F Nesterenko, T. Weihs
Ph. D. student: Chung-Ting Wei
Collaboration: B. R. Maddox, B. A. Remington, LLNL

Materials Science and Engineering
University of California, San Diego

UCSD Jacobs | Mechanical and Aerospace Engineering

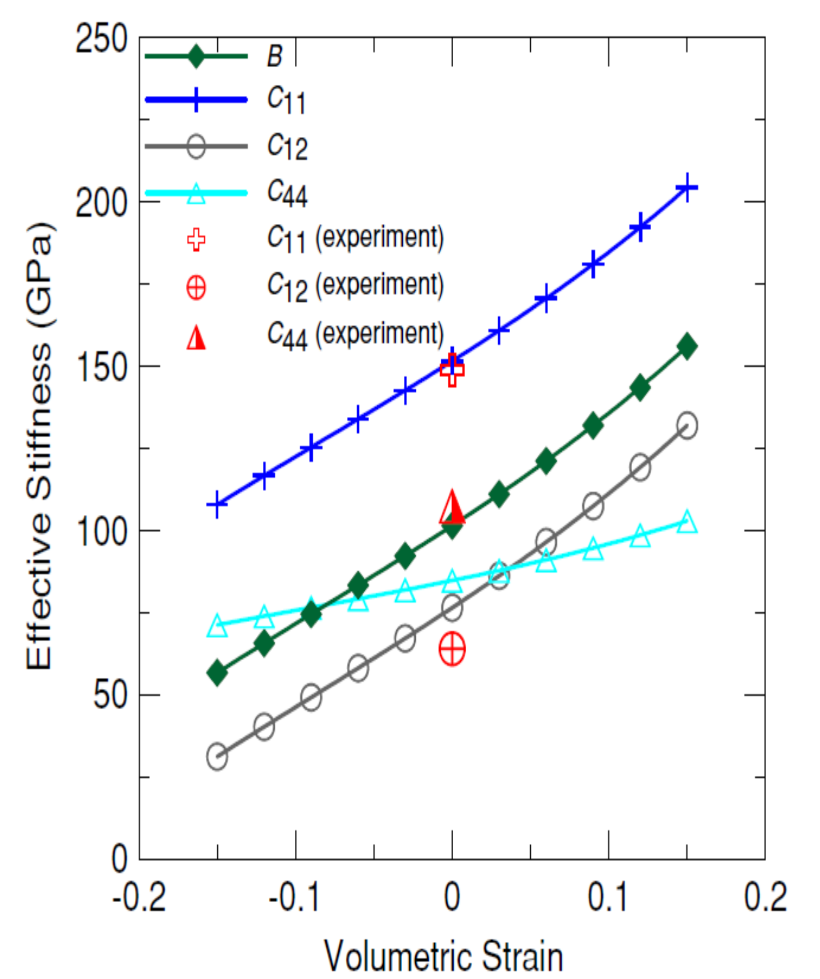

2D Sound velocity with (001) in the center

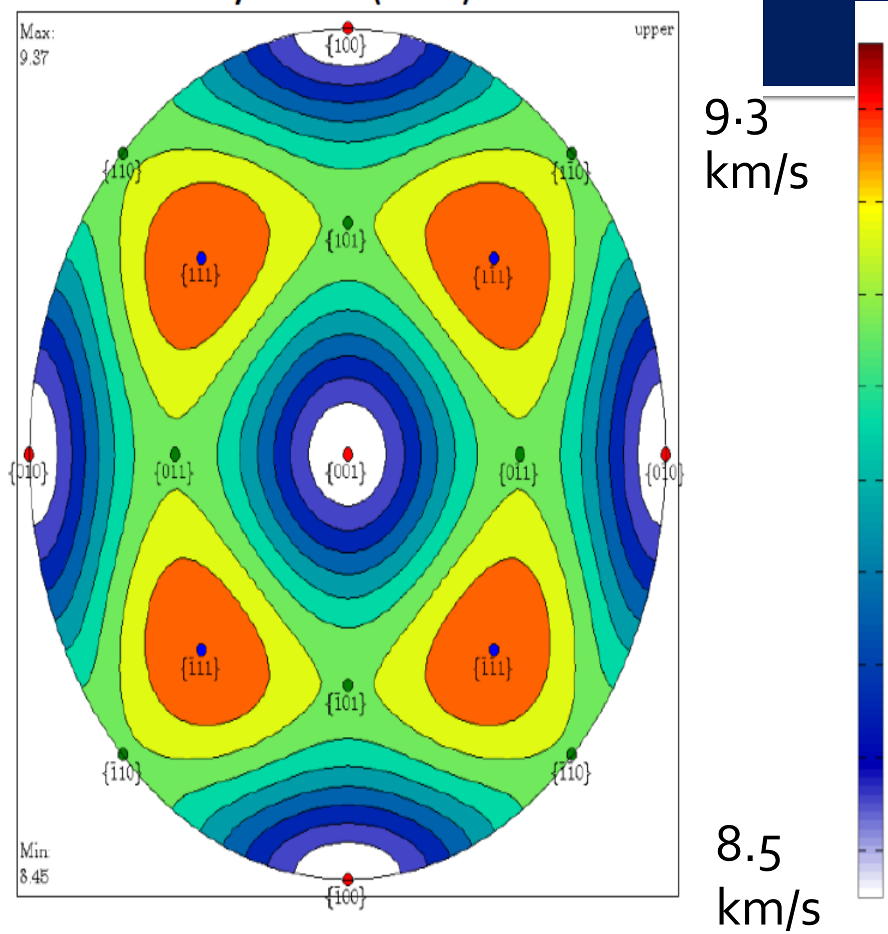

Based on statistical mechanics supplemented by the SW potential.

(Lovelady & Oleynik, 2005)

With compression the sound velocity will only decrease as C_{11}, C_{12} and C_{44} decrease.

Reactive Materials: Ni-Al Laminates

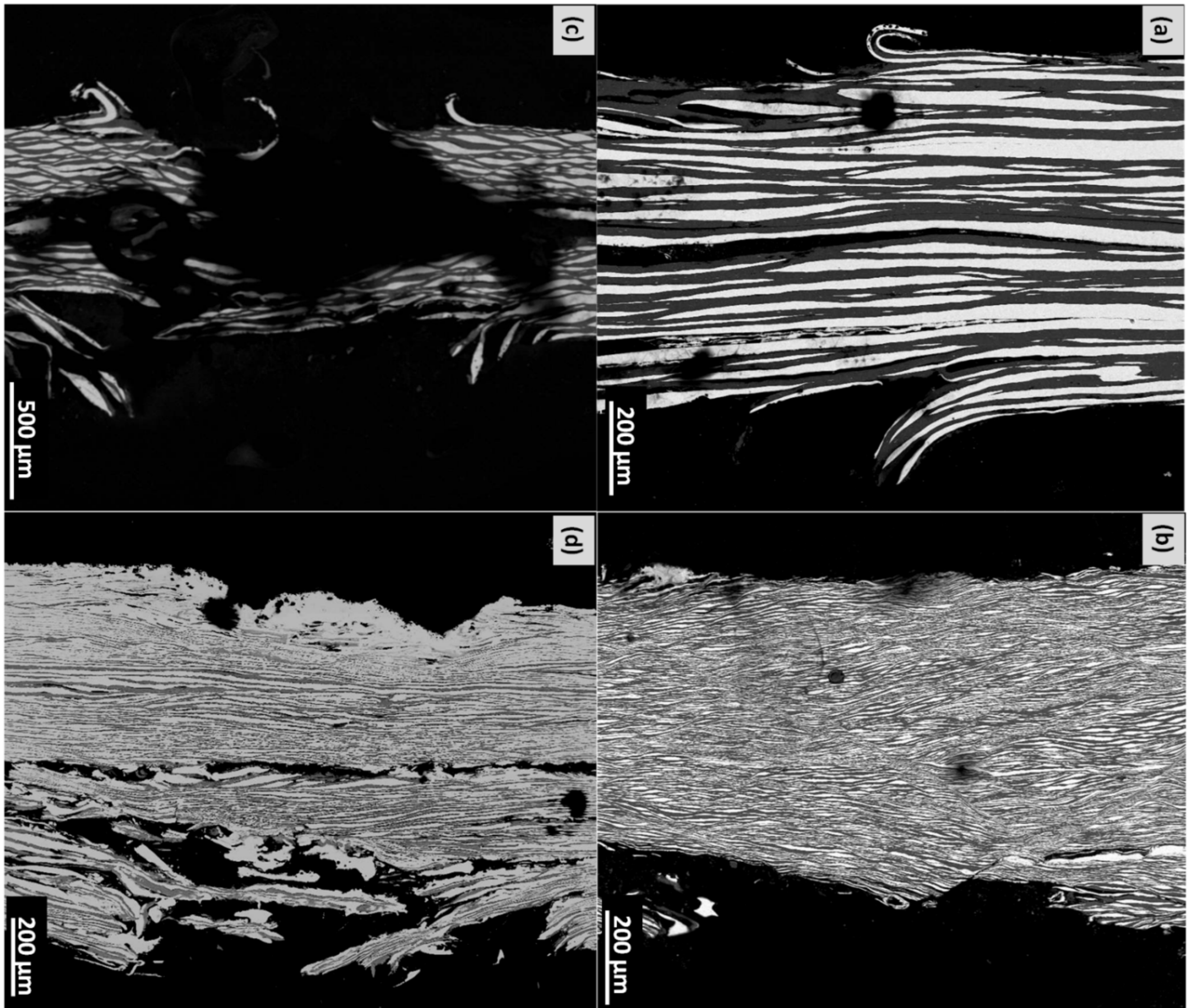

Sandwich Assembly

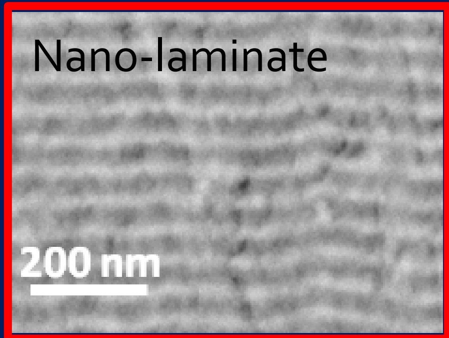

54 nm Bilayer Ni/Al laminates

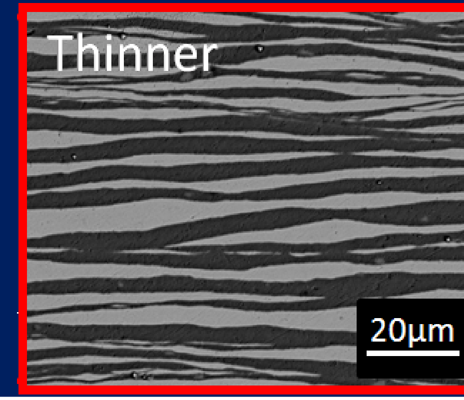

~5µm Bilayer Ni/Al laminates

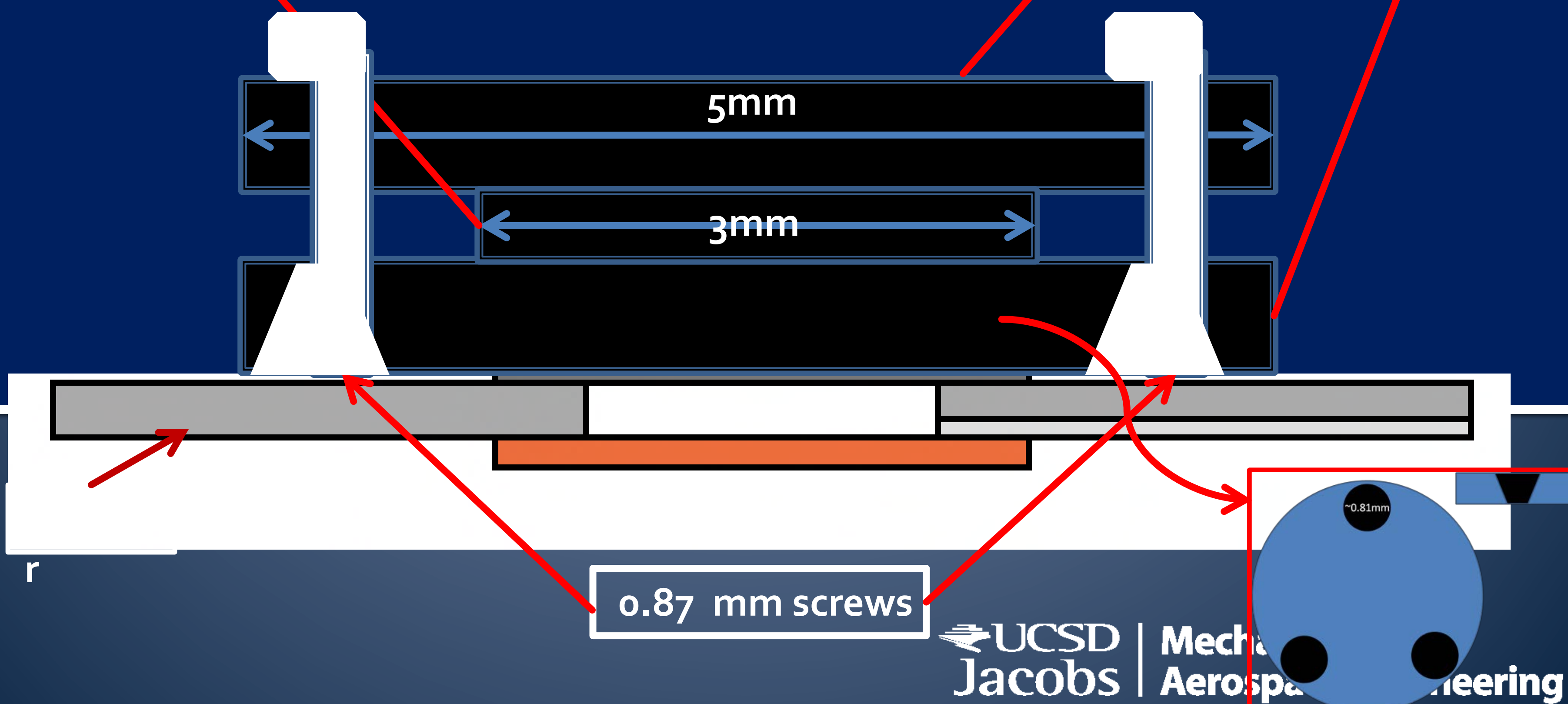

Schematic of Laser Experiment

Step 1. Laser irradiation of the ablator. → Step 2. Plasma explodes and conveys shock pressure. → Step 3. Crater, reacted nano-laminate and spall

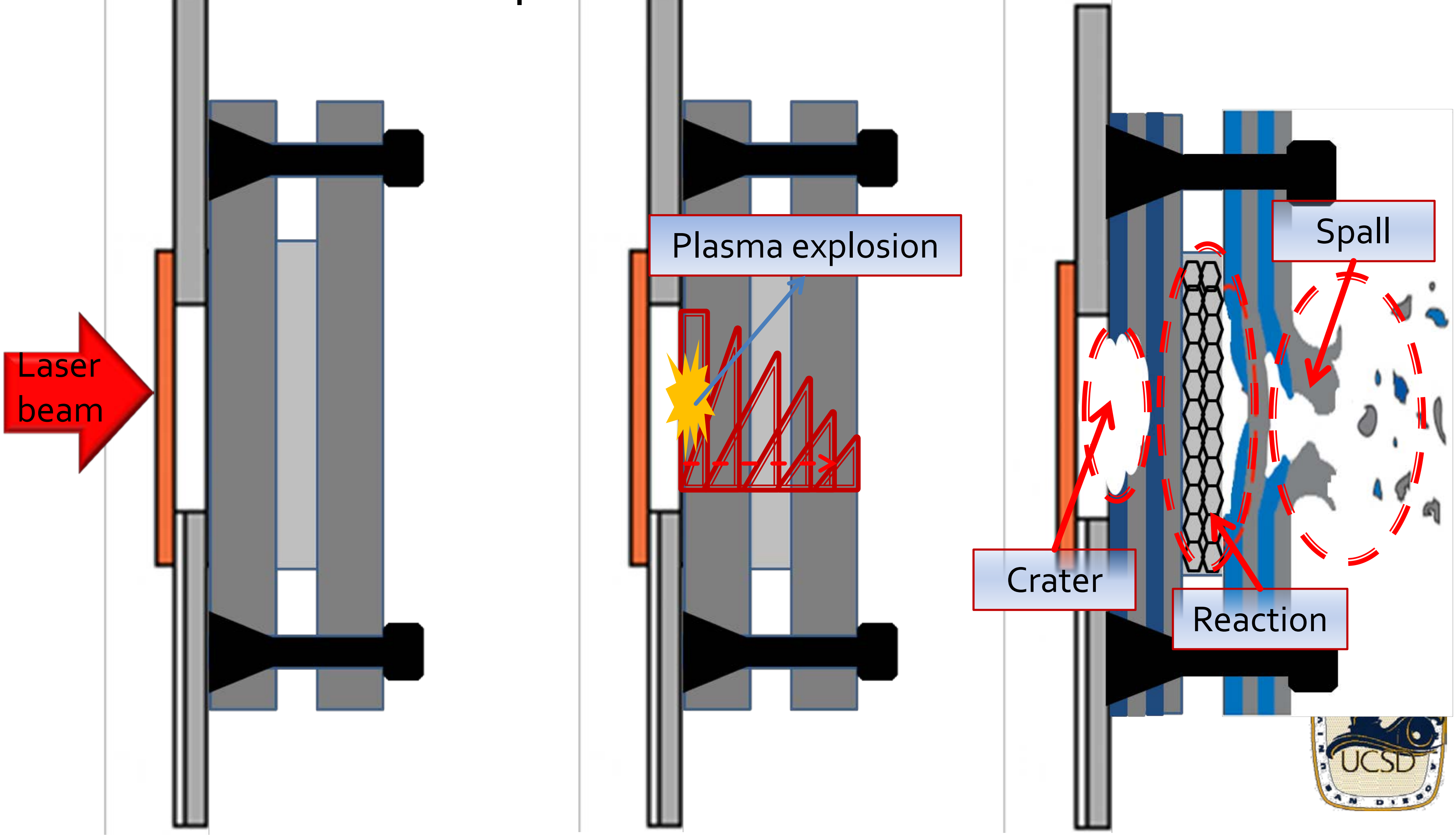

653 J Laser Energy

Capsule

Inside of the capsule

Fragments in the aero-gel

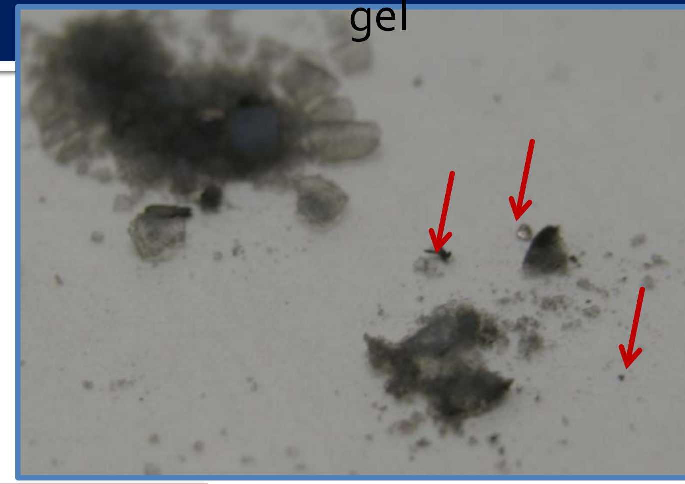

Sandwich structure

- ❖ After laser shock, the sandwich structure penetrated into the aero-gel in tube.
- ❖ Sandwich structure had fully developed irradiated crater and spall.
- ❖ Fragments were captured and stored in aero-gel,.

Dissembled Sandwich Structure

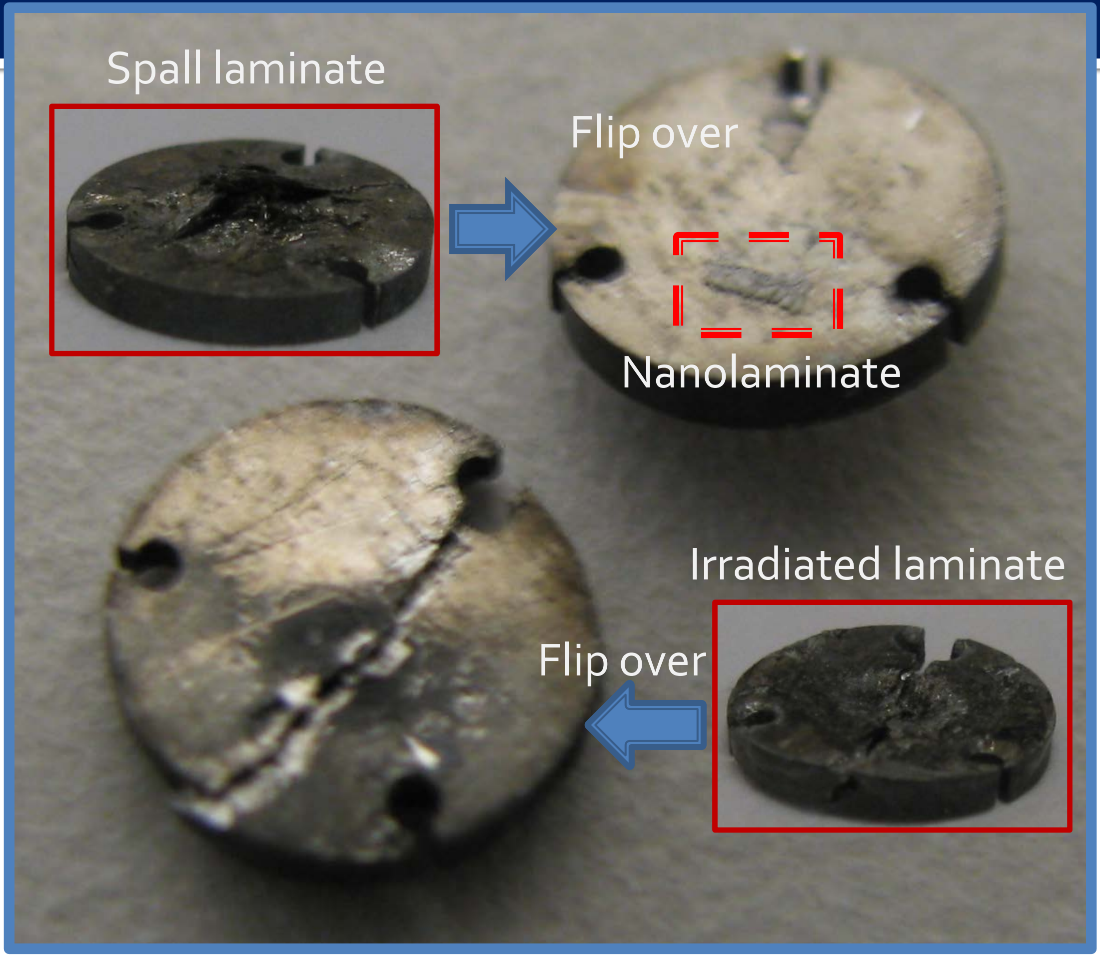

SEM Observation

Crater area (Irradiated surface)

Crater BSE image

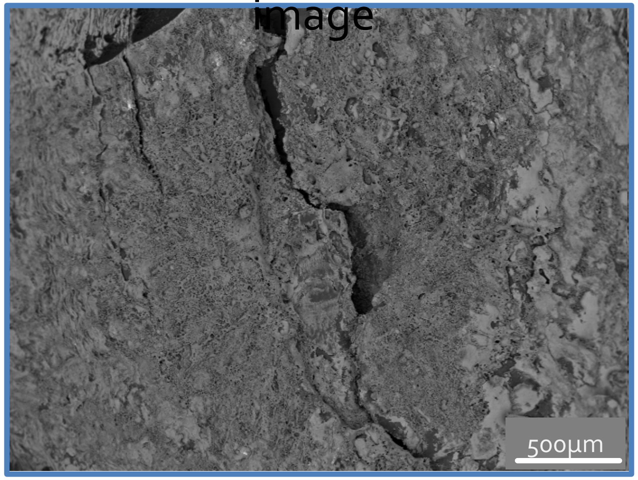

Crater SE image

Dendrites

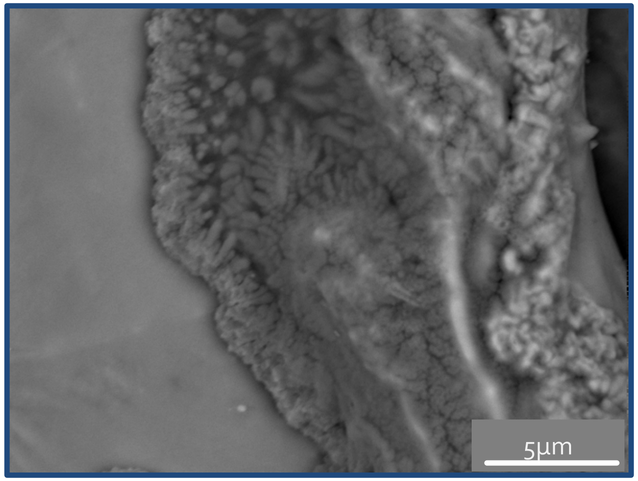

Molten Materials

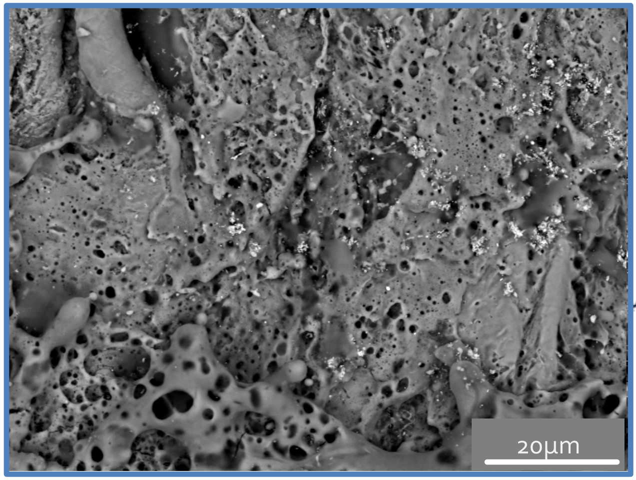

Spallation area (included rear surface)

Spall at the second micro-laminate

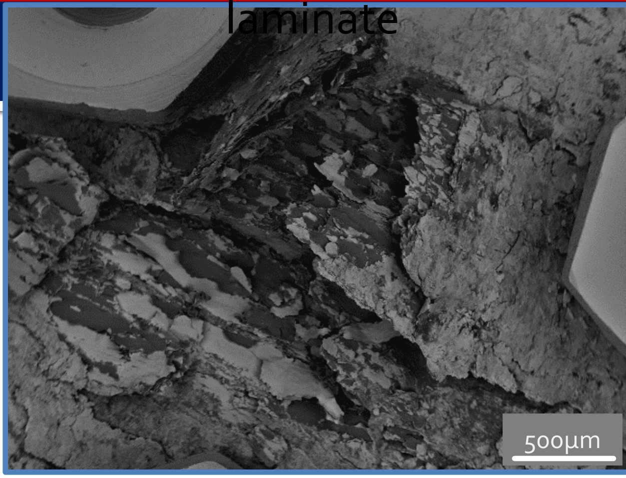

Ductile fracture edges of spall

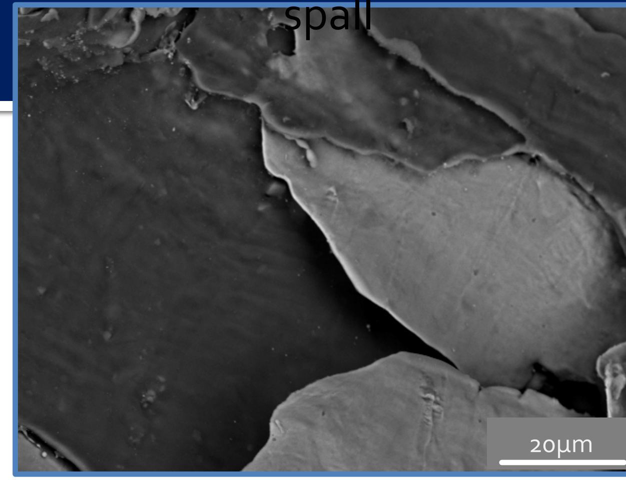

Reacted nano-laminate at the rear surface of spall

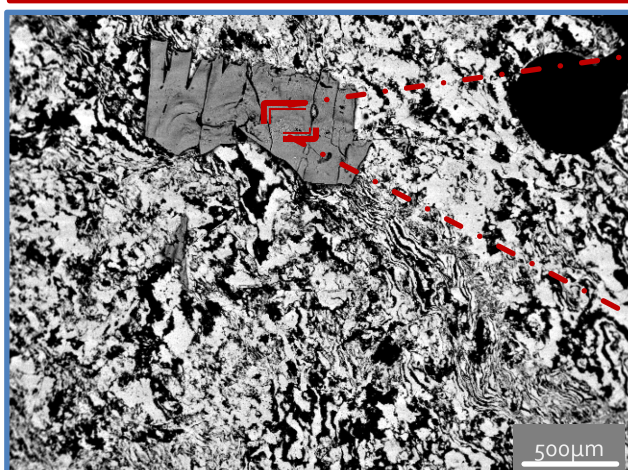

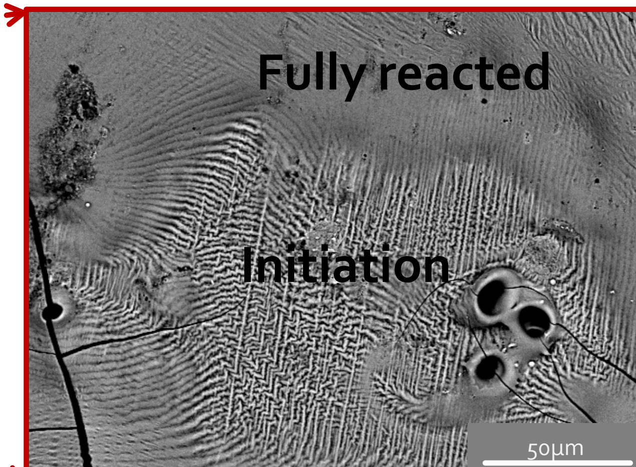

Reacted Nano-laminate (Rear surface of spall laminate)

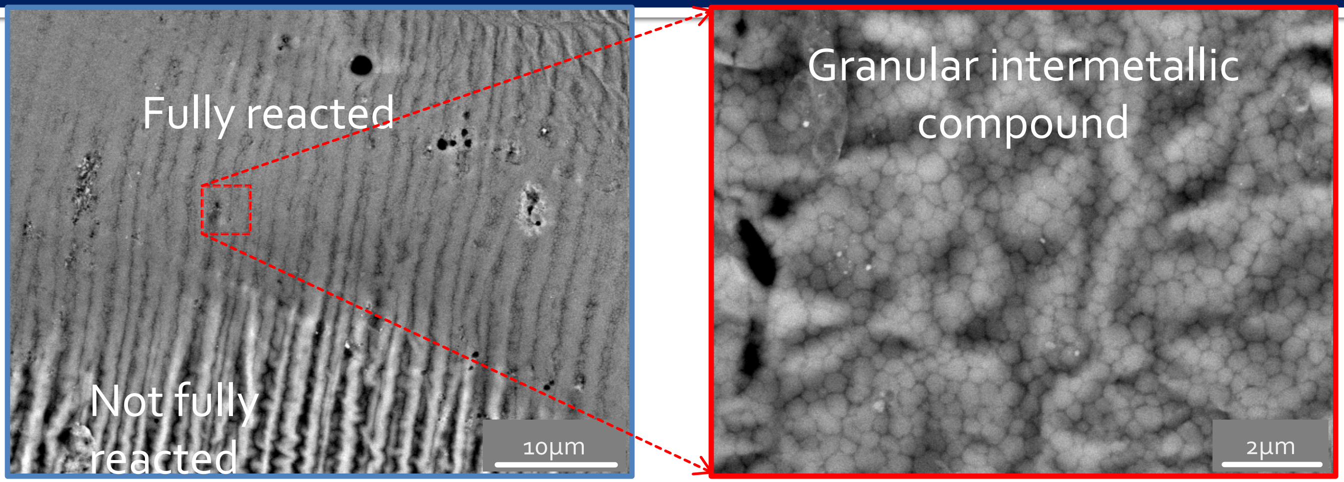

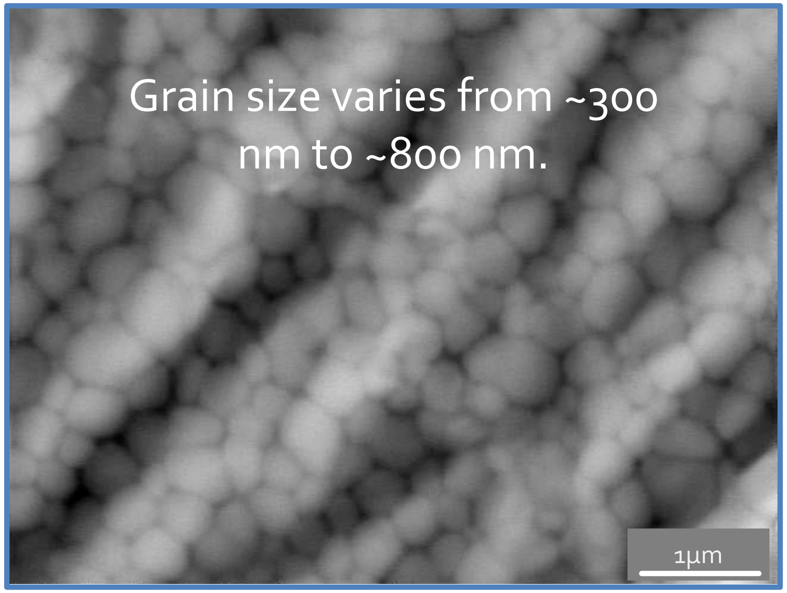

SEM Observation

Crater BSE image

Crater SE image

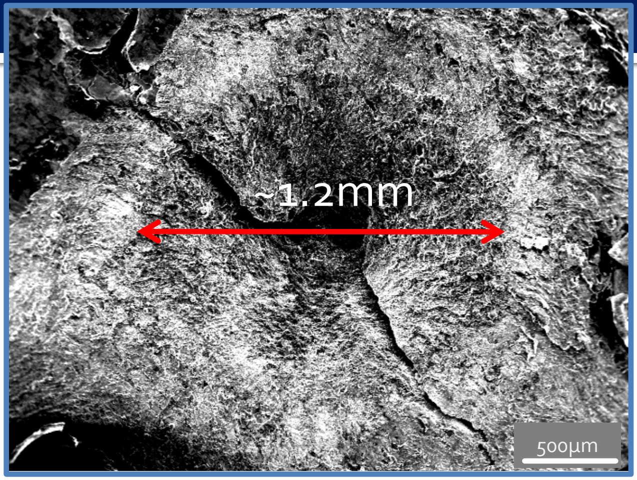

Edge of the crater

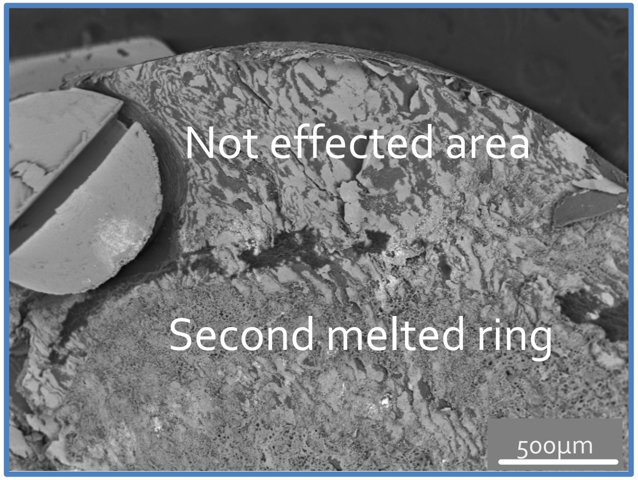

Molten materials on the crater

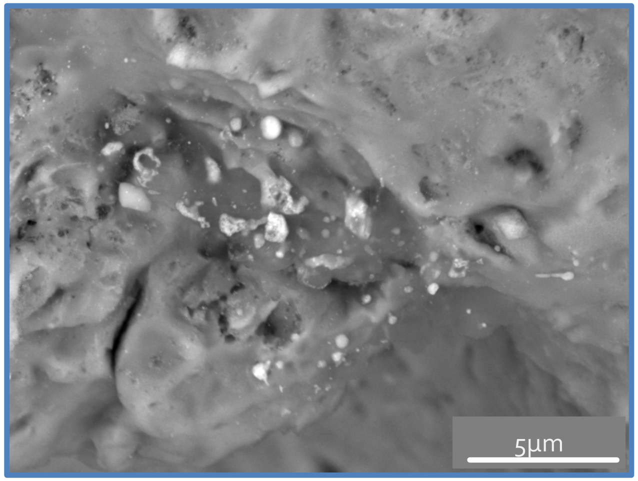

Rear Surface of The Crater

Rear surface

Reacted nano-laminate

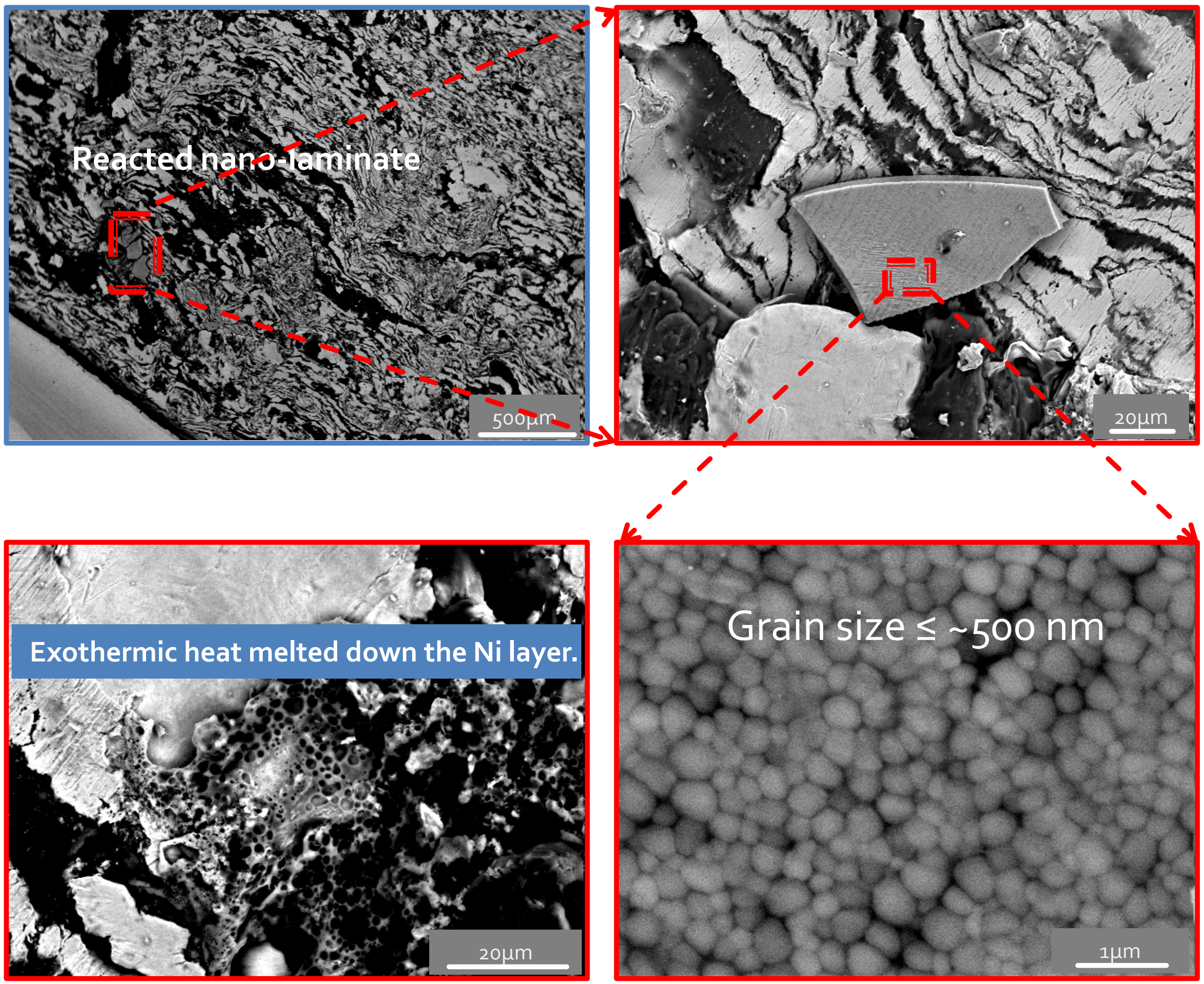

EDX Dot Mapping

Granular intermetallics

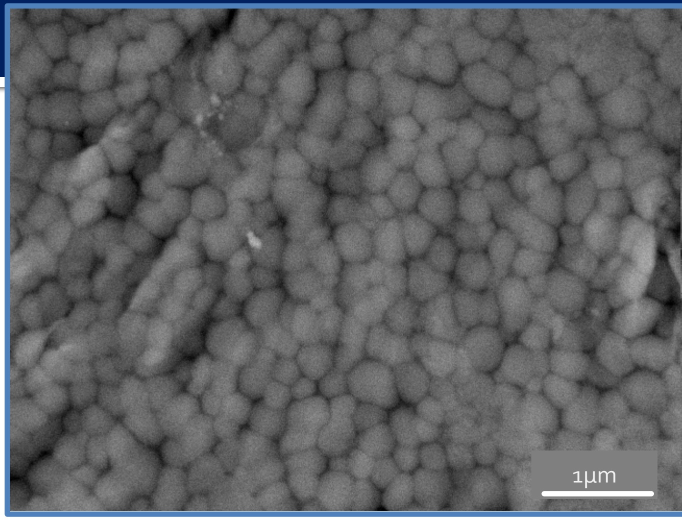

Al distribution

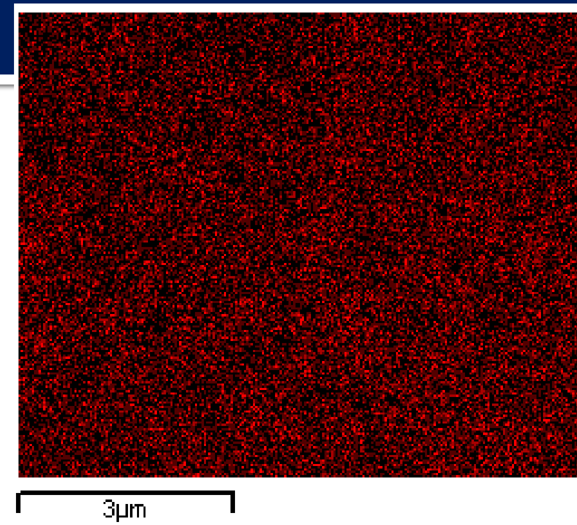

Ni distribution

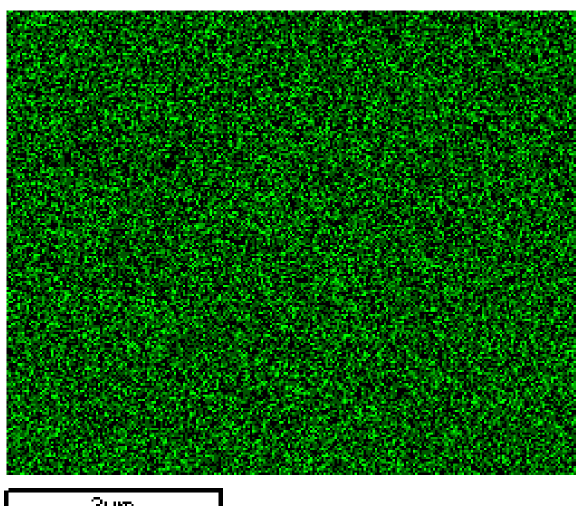

Ni+Al distribution

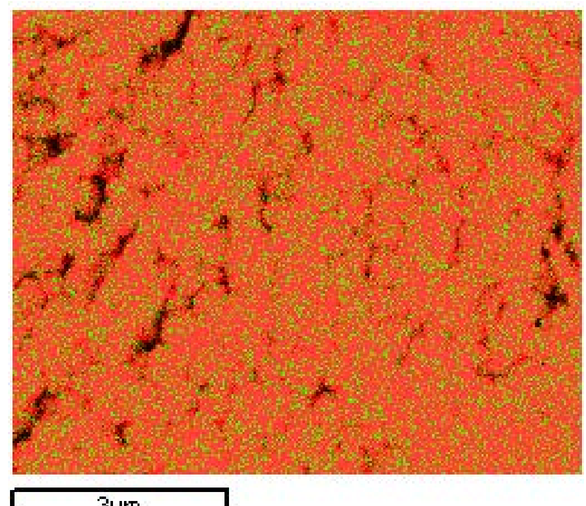

Spallation of 875 J Laser Irradiation

Spall surface

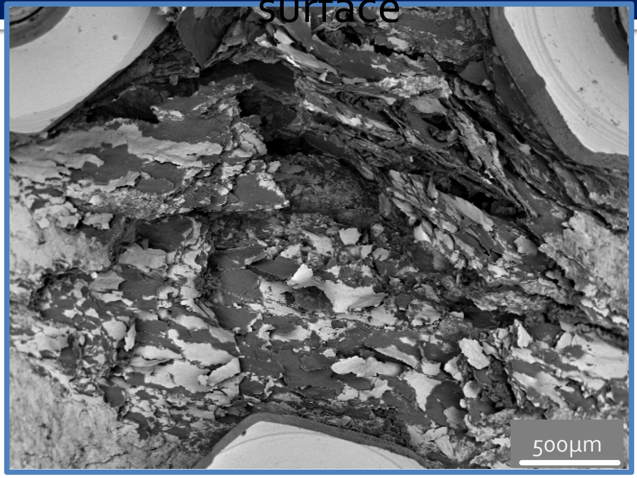

Ductile fracture

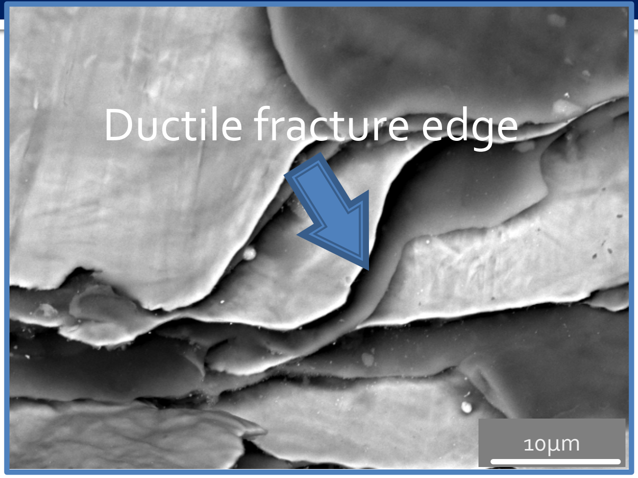

Rear surface of spall (BSE)

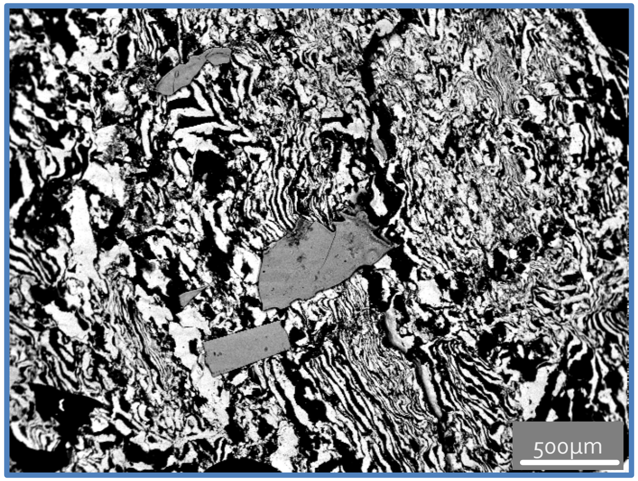

Rear surface of spall (SE)

Evidence of Intermetallic reaction

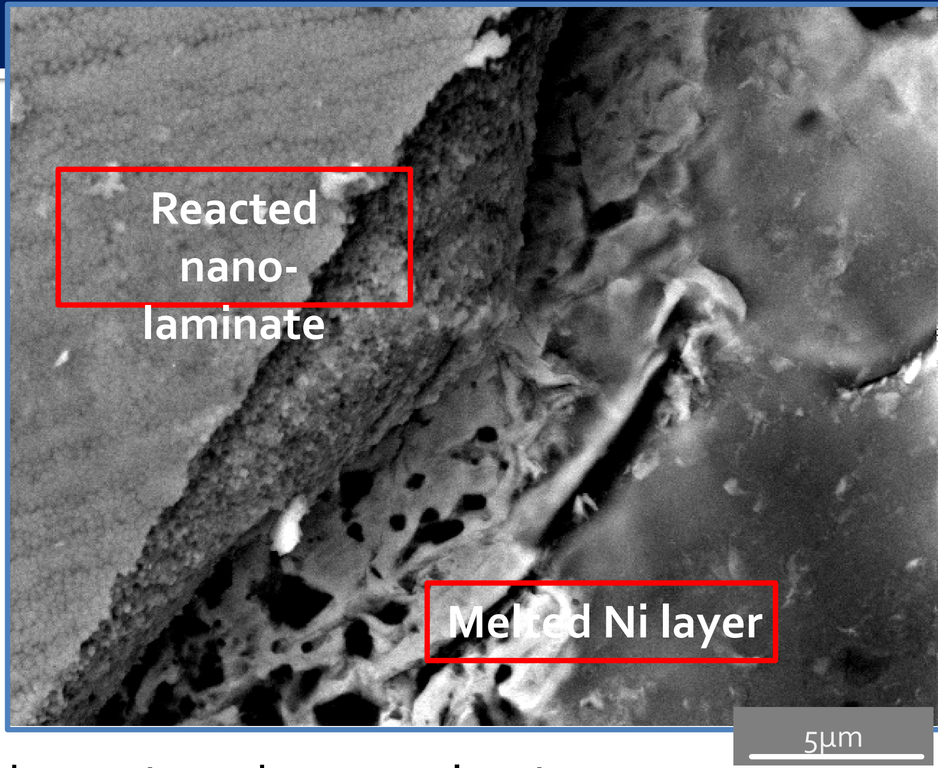

❖After shock induced reaction, the nano-laminate turns to a granular intermetallic structure

❖The strong exothermic heat melted micro-laminate (both Ni and Al layers)

❖Reaction did not propagate

SEM Observation

Irradiated micro-laminate

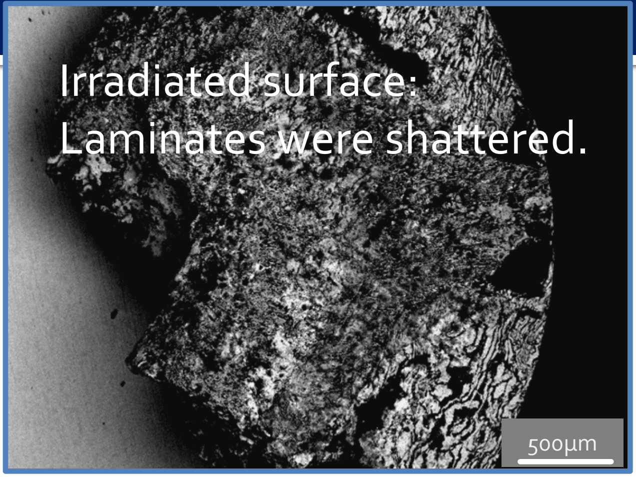

Intermetallic dendrites

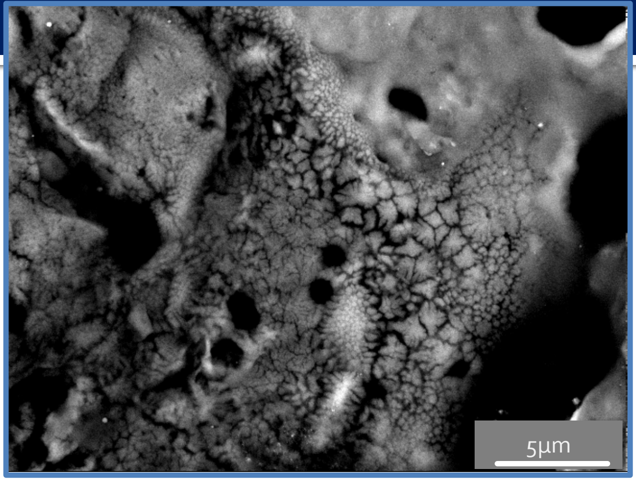

Molten Pool

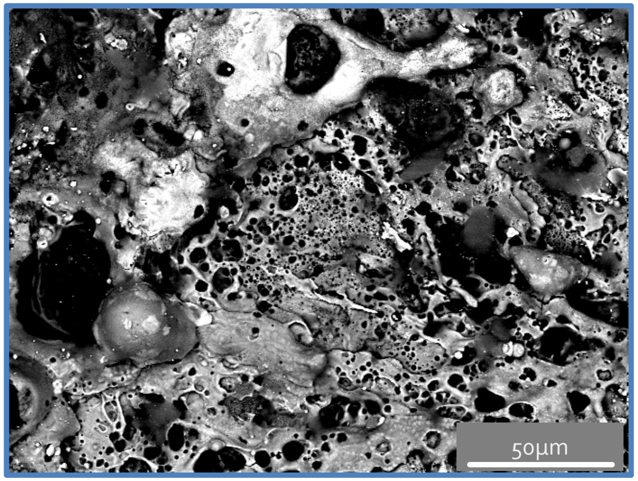

Intermetallic Compounds

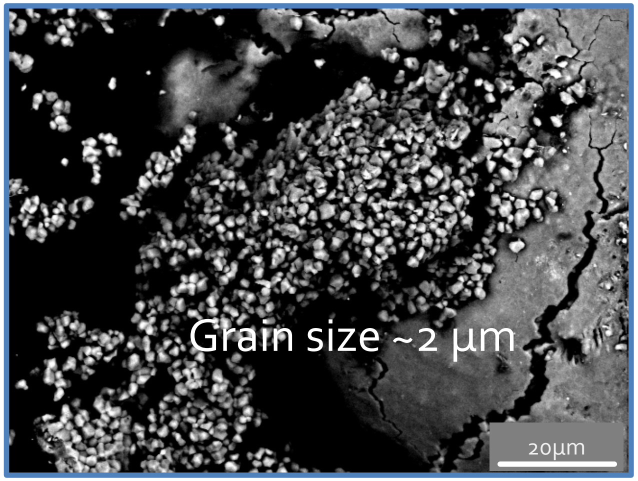

Rear Surface of Irradiated Laminate

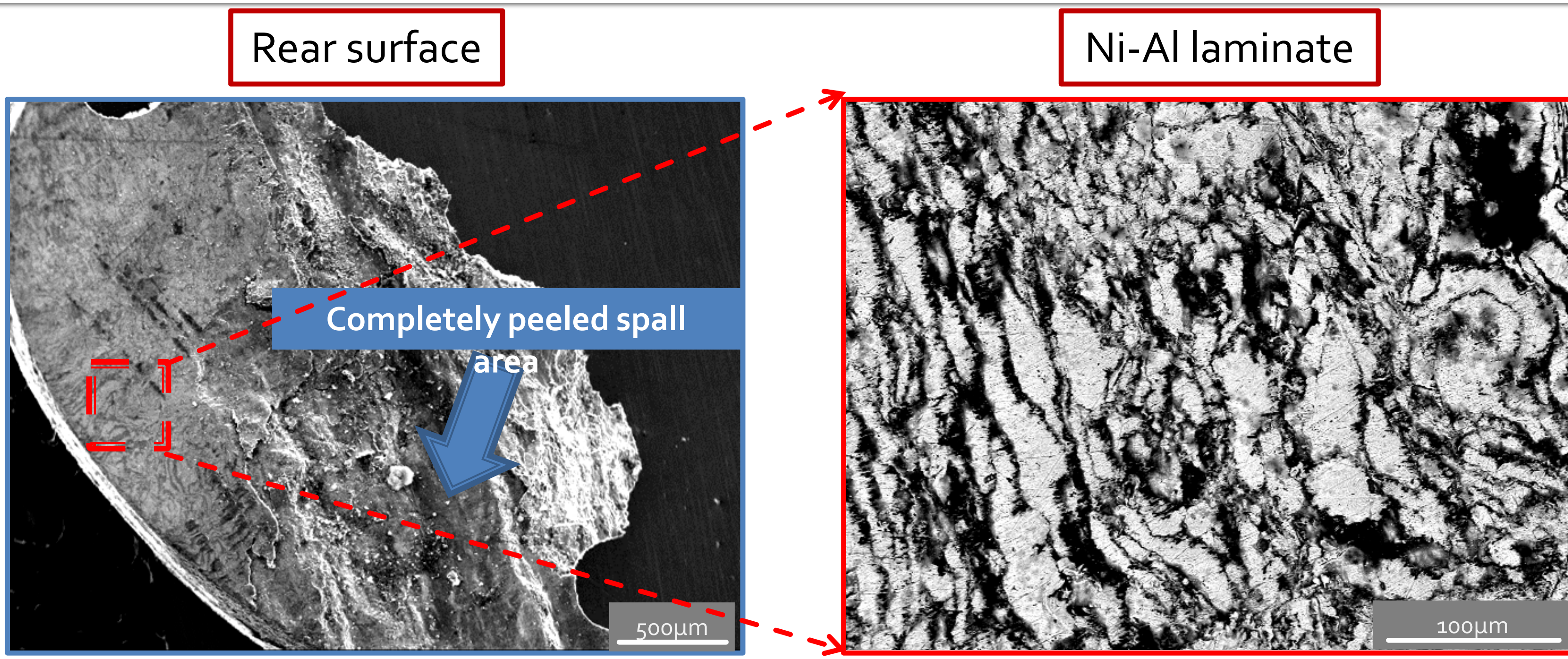

❖ The irradiated laminate was shattered by a intensive laser shock, over 1300 J.

❖The spall was completely developed and peeled out off the rear surface of the irradiated laminate.

Conclusions

- Laser shock did not generate reaction in microlaminate up to 1300 J.
- Nanolaminate fully reacted at 650 J
- Granular intermetallic compounds with size ~200 nm to ~800 nm.
- Grain size decreases with increasing laser energy
- Spall surface has no reaction and molten materials. The fracture edge showed a clear ductile fracture. It implies that the spallation process is controlled by plastic flow.
- The inner surfaces of the sandwich structure show that strong exothermic heat from the intermetallic reaction of the nano-laminate can melt down the micro-laminate.
- However the reaction did not proliferate to the adjacent mico-laminates.
- The irradiated surface shows molten pools, intermetallic dendrites, and possible intermetallic grains.

Laser Spalling and Fragmentation in Vanadium

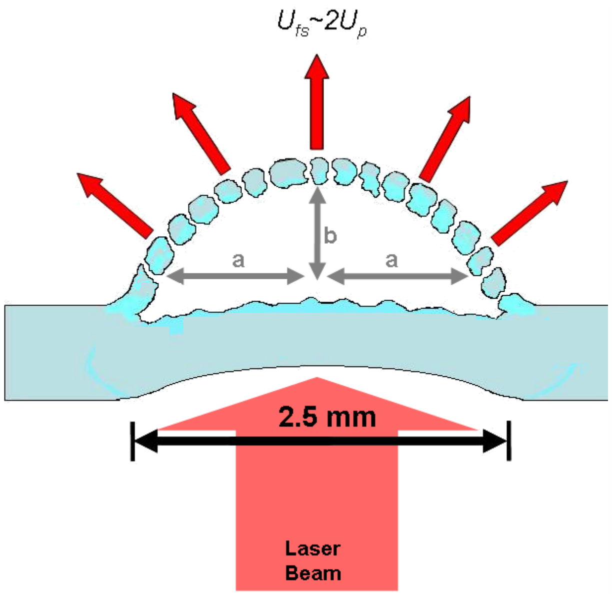

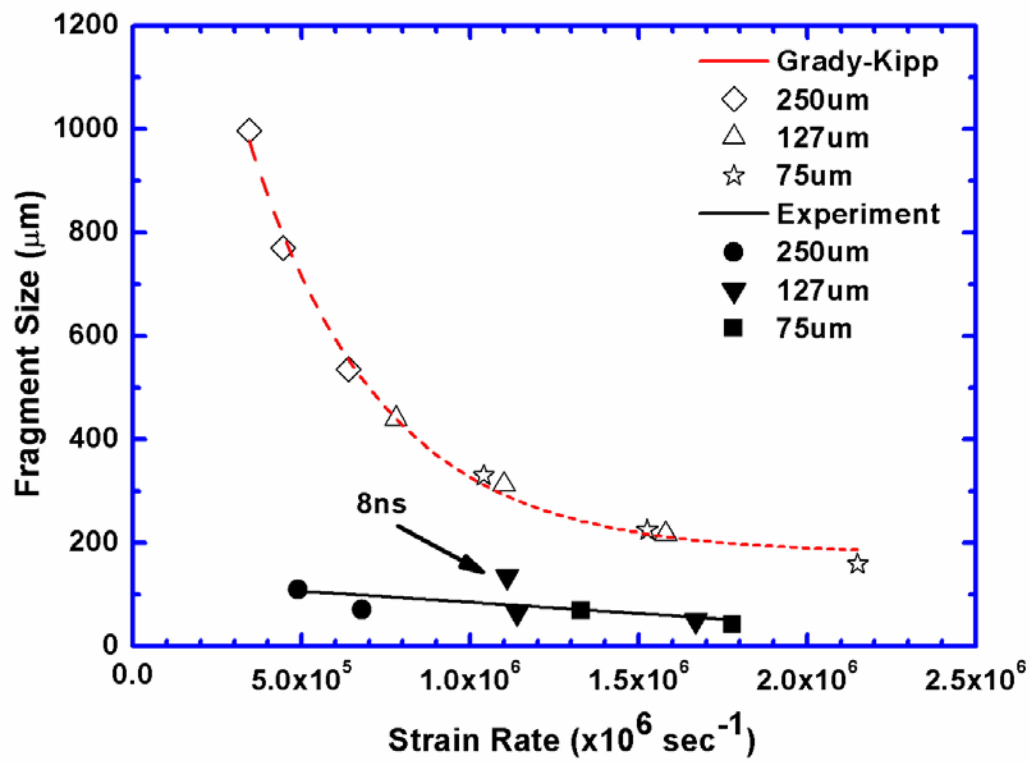

Dislocation Velocities: Ta

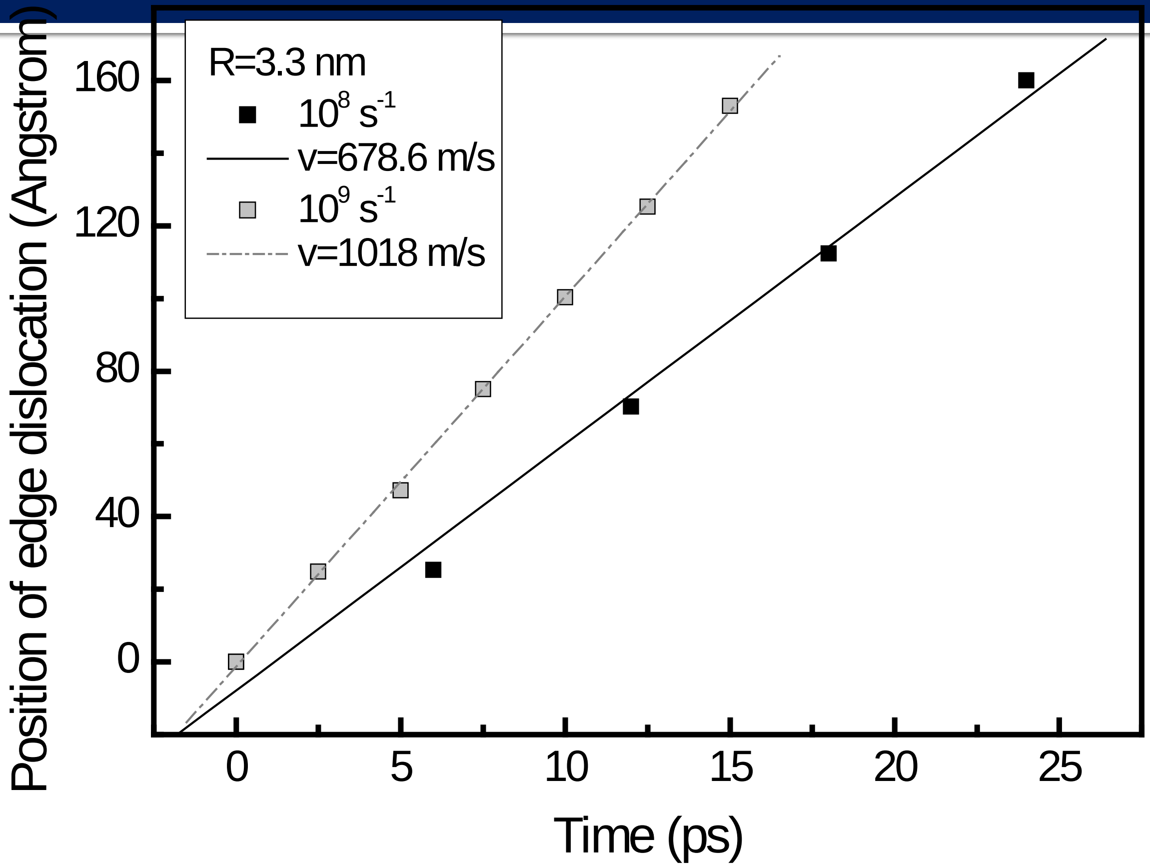

$$E = 186\,\mathrm{GPa} \quad \rho = 16.654\,\mathrm{g/cm^3} \quad \nu = 0.35$$

$$c_l = \sqrt{\frac{E}{\rho}} = 3.34\times10^3\ m/s \qquad c_t = \sqrt{\frac{E}{2\rho(1+\nu)}} = 2.03\times10^3\ m/s$$

Spall Strength: Gas Gun, Laser, Theoretical Maximum

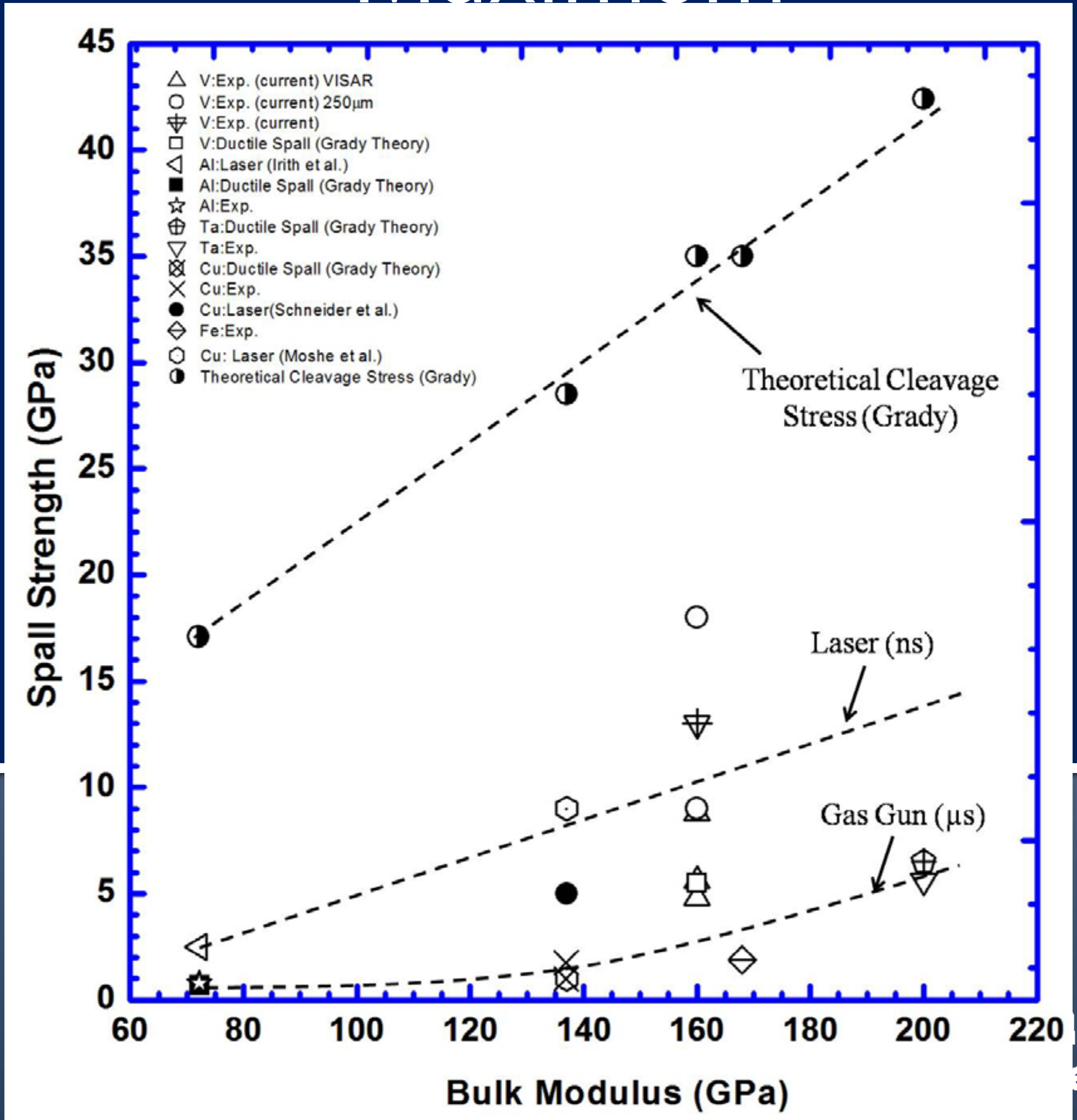

Mechanical and Aerospace Engineering

Future Work

- Laser spall and fragmentation experiments
- Continued collaboration with Cavendish: Jan. 2011 visit
- Quantitative analysis of reaction products: granular intermetallics.
- Shock pressure simulation and analysis
- X-ray diffraction analysis
- TEM analysis (By using FIB, we can slice out a specific area and make a TEM samples; UCLA has capability

Additonal Slides: Not Shown

Conclusions: Deformation in Compression

- **FCC Ni:** dislocation generation at grain boundaries and emission into grains, and annihilation in opposite GB. Partial separation.
- Grain boundary sliding: decreases with increasing GS.

- **BCC Ta:** In compression, plasticity, in the form of both GB sliding and dislocation activity, occurs.
- Inverse Hall-Petch from 2.5 to 30 nm , due to the decreasing role played by GB shear as GS increased.

Molecular Dynamics (MD): II BCC Metals (Ta)

- **Potential:** Extended Finnis-Sinclair Potential for Ta
- **Boundary Condition:** Periodic Boundary Conditions along three directions
- **Sample size:** 20 ~ 66 nm in length (0.4 M ~16 M atoms)
- **Strain rate:** 10^7 s^{-1} ~ 10^{10} s^{-1} , Loading along [100] orientation
- **Void:** Pre-existing, spherical, with radii between 0.15 and 30 nm
- **Simulator:** LAMMPS, Common Neighbor Analysis (CNA) as defect filter

Sequence of Shear Loop Emission in Ta

3.3 nm radius void, uniaxial compressive strain, strain rate $10^9 s^{-1}$

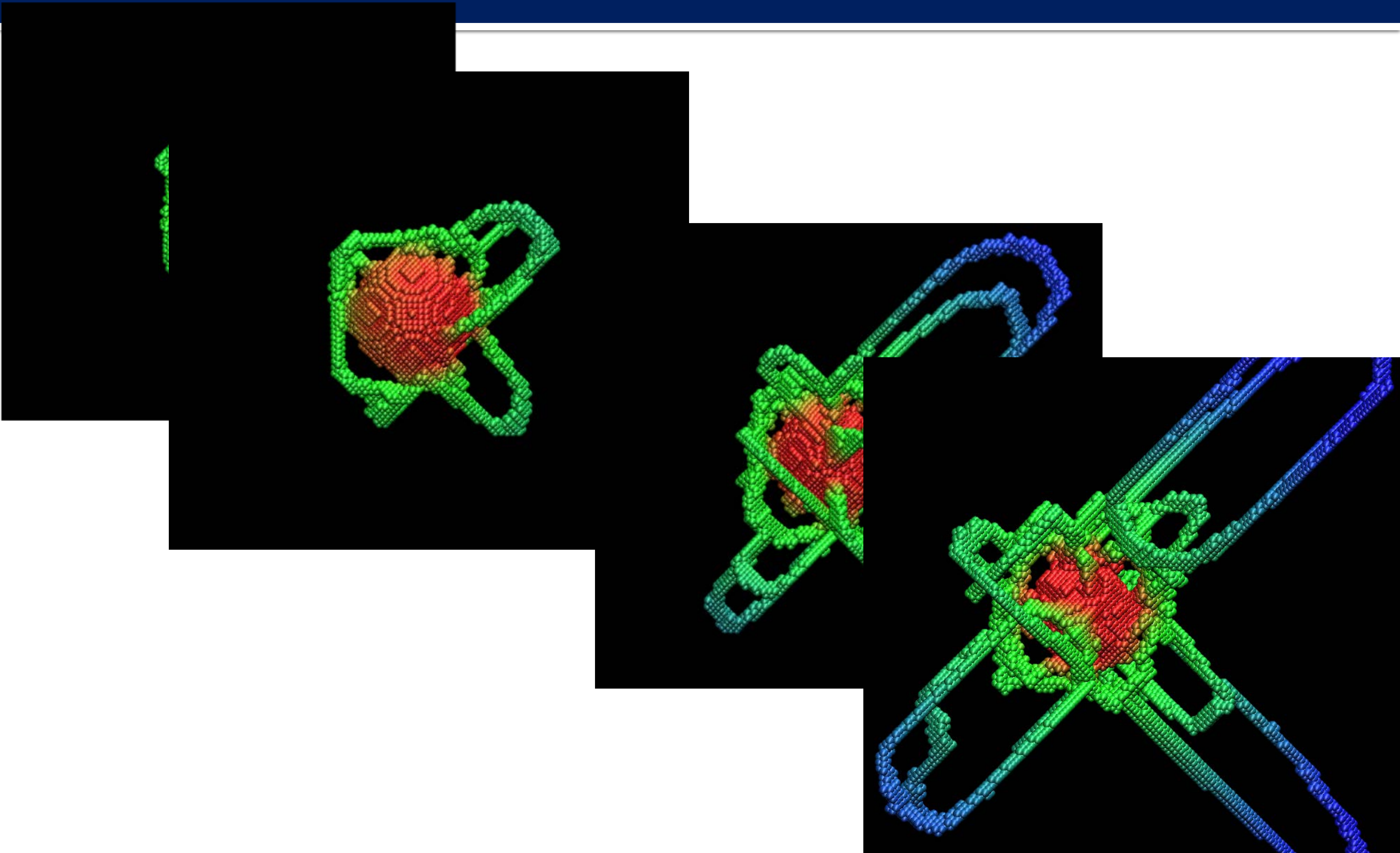

Twinning planes and directions

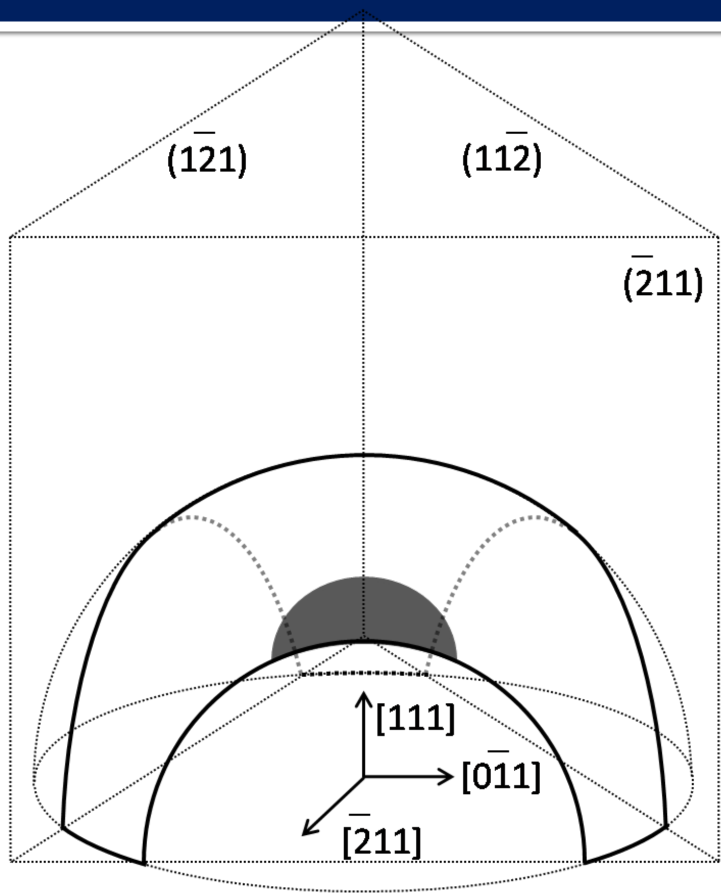

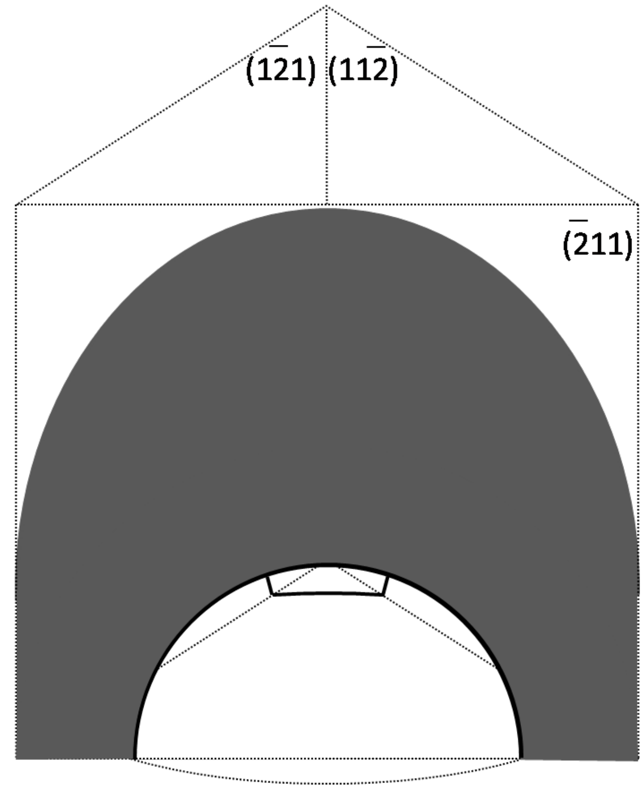

Dislocation Velocities: MD Predictions

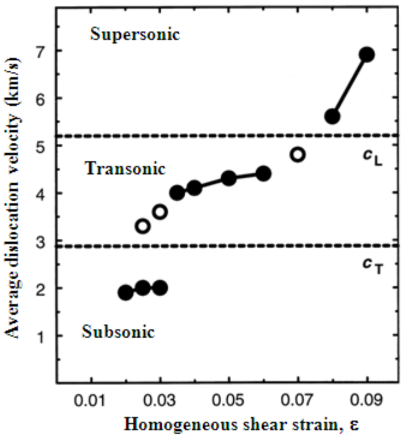

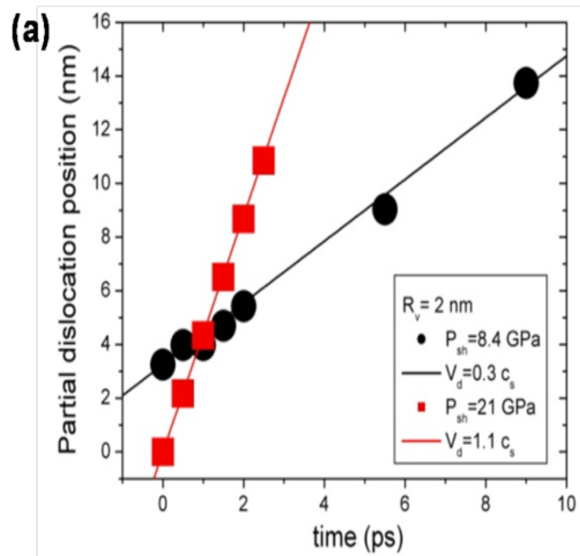

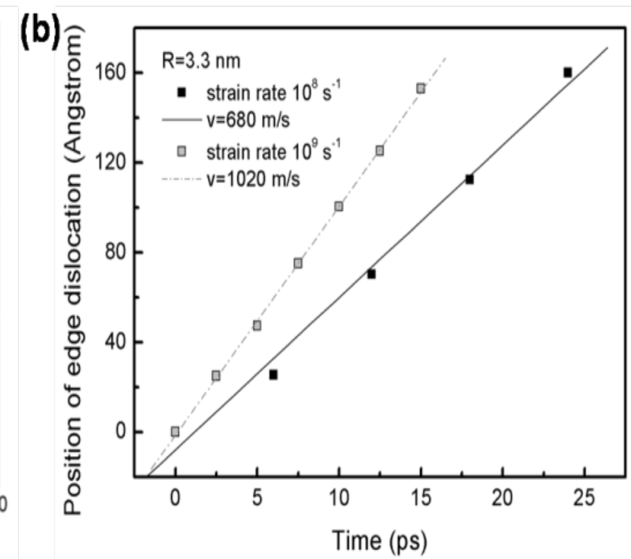

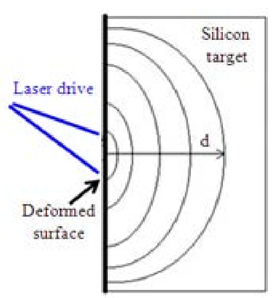

Ni G. S. = 10 nm
Uniaxial Compression to 23 GPa and Release

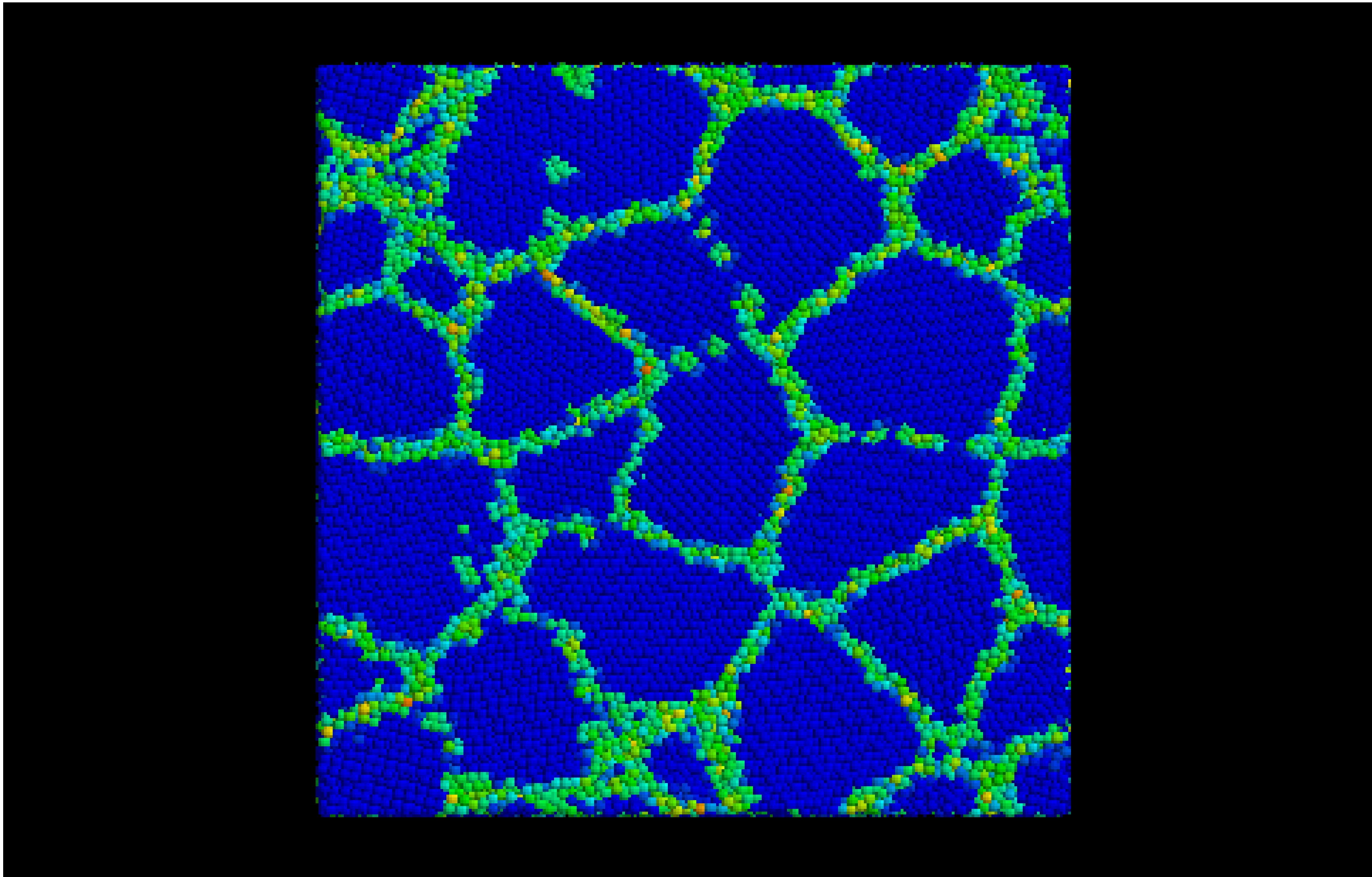

Tantalum Sample preparation: Voronoi Tesselation

Tension

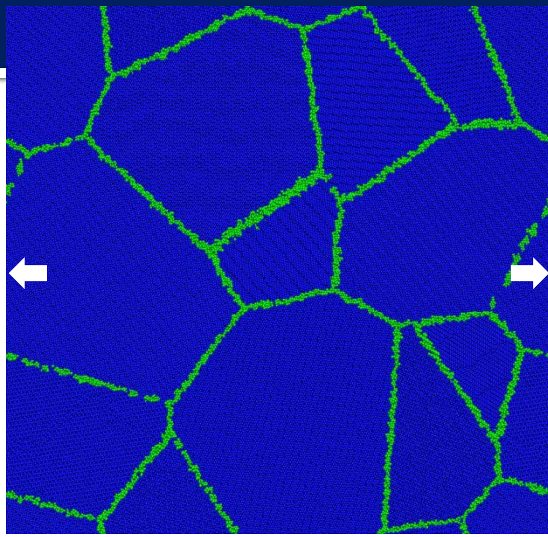

66*66*66 nm, *d*=27.3 nm

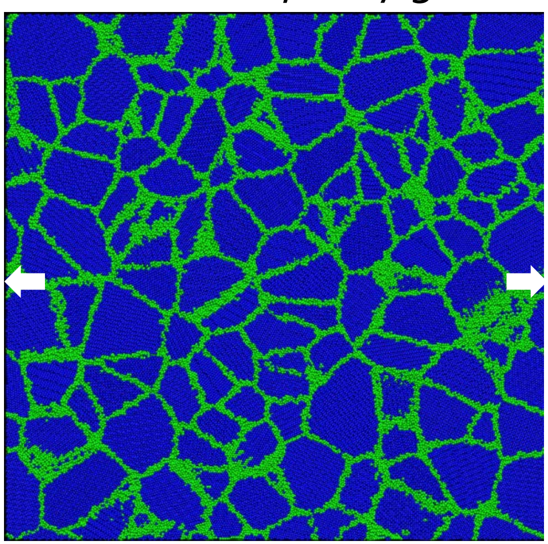

66*66*66 nm, *d*=8.2 nm

Compression

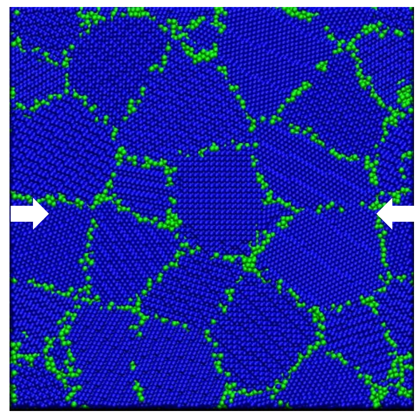

25*25*25 nm, *d*=7.5 nm

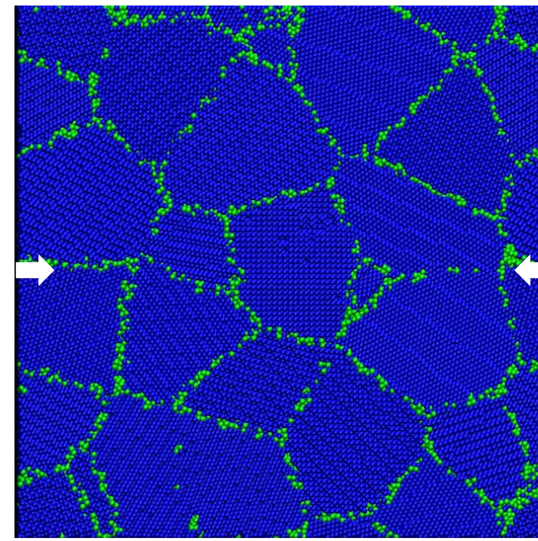

33*33*33 nm, *d*=10 nm

Same topological structures

Uniaxial tensile strain-Twnning

3.3 nm radius void, uniaxial tensile strain, strain rate $10^9 s^{-1}$

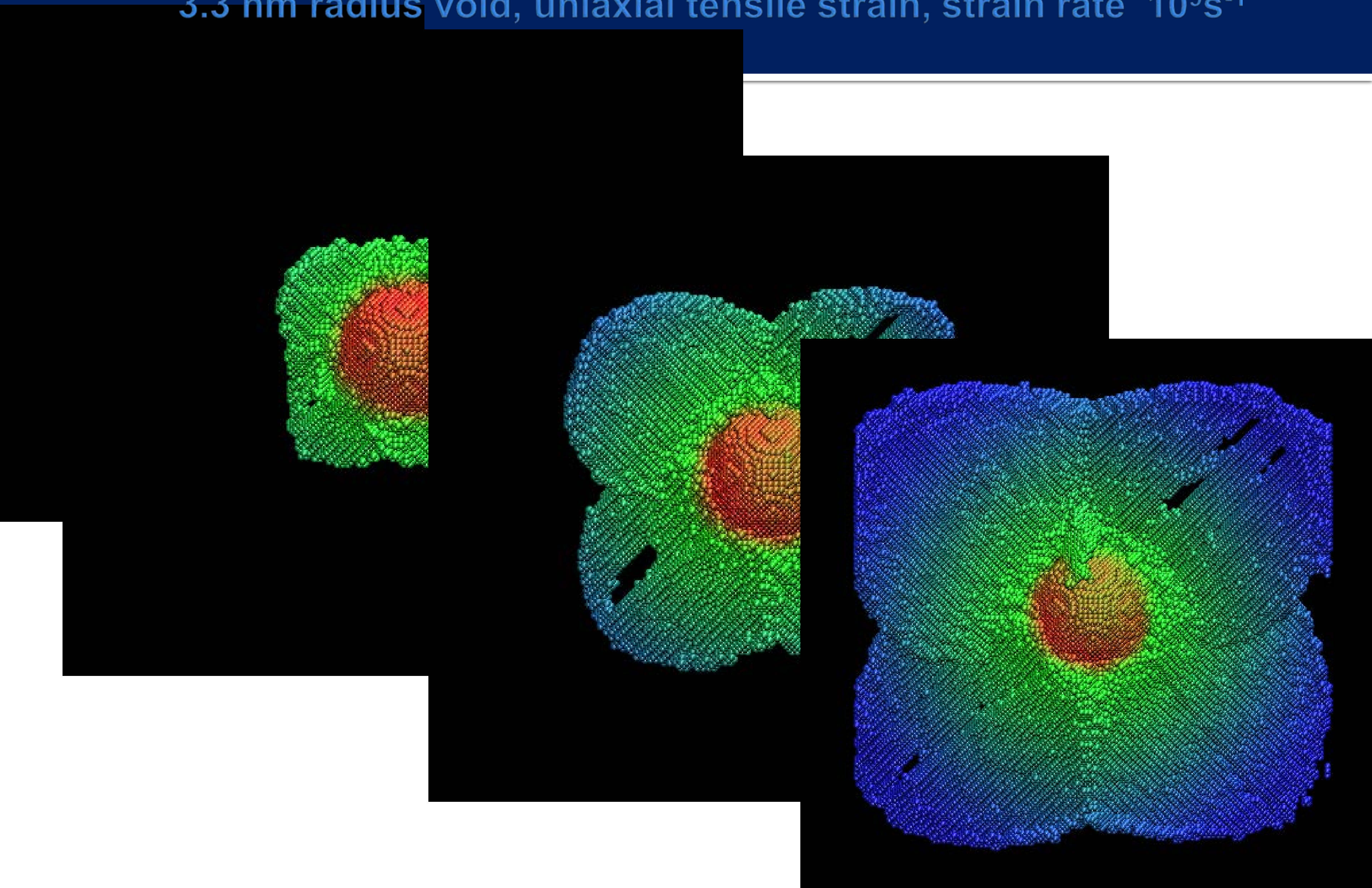

Compression of nanocrystalline Ta: GB shear

Grain rotation

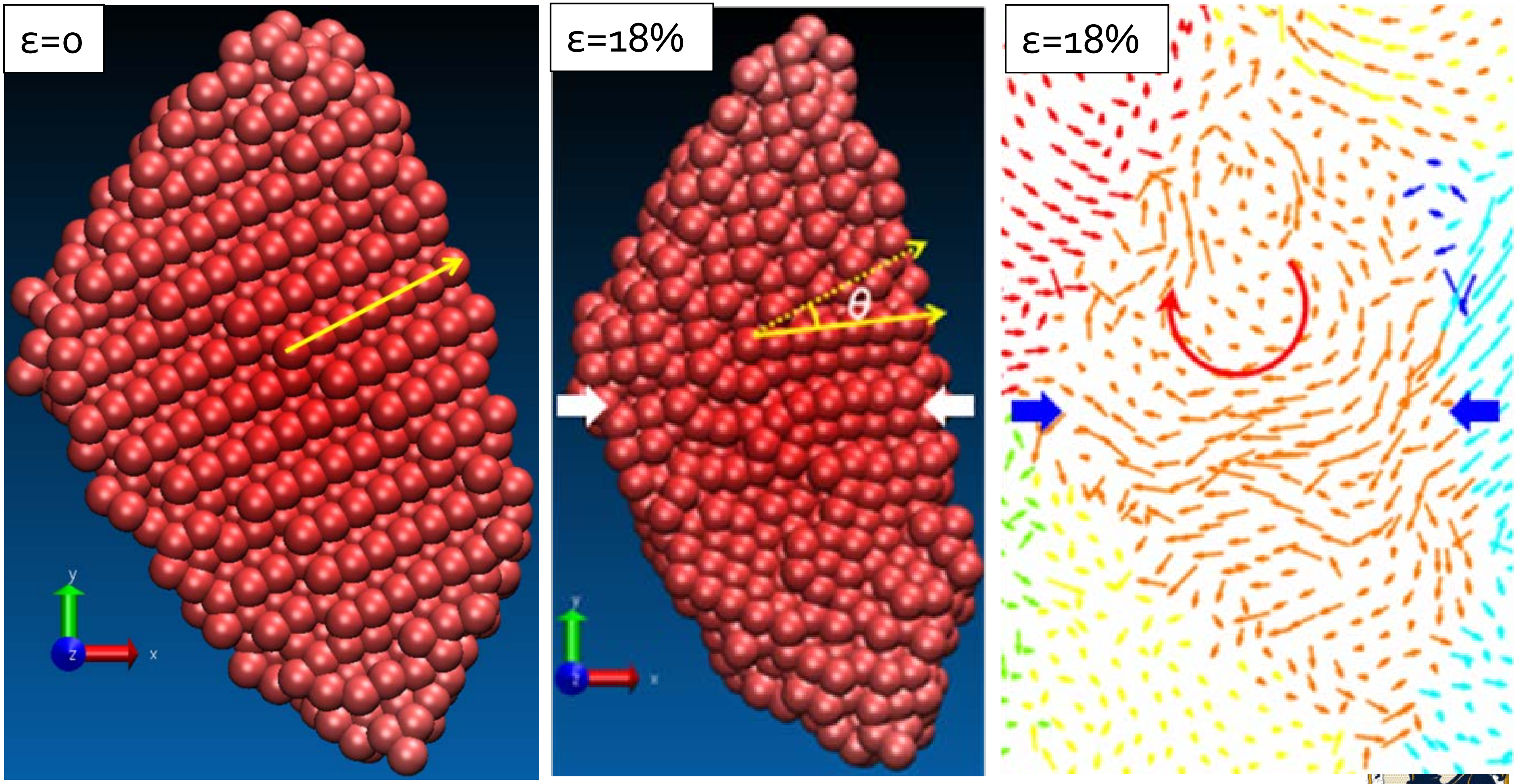

d=5 nm

Compression of nanocrystalline Ta: GB shear

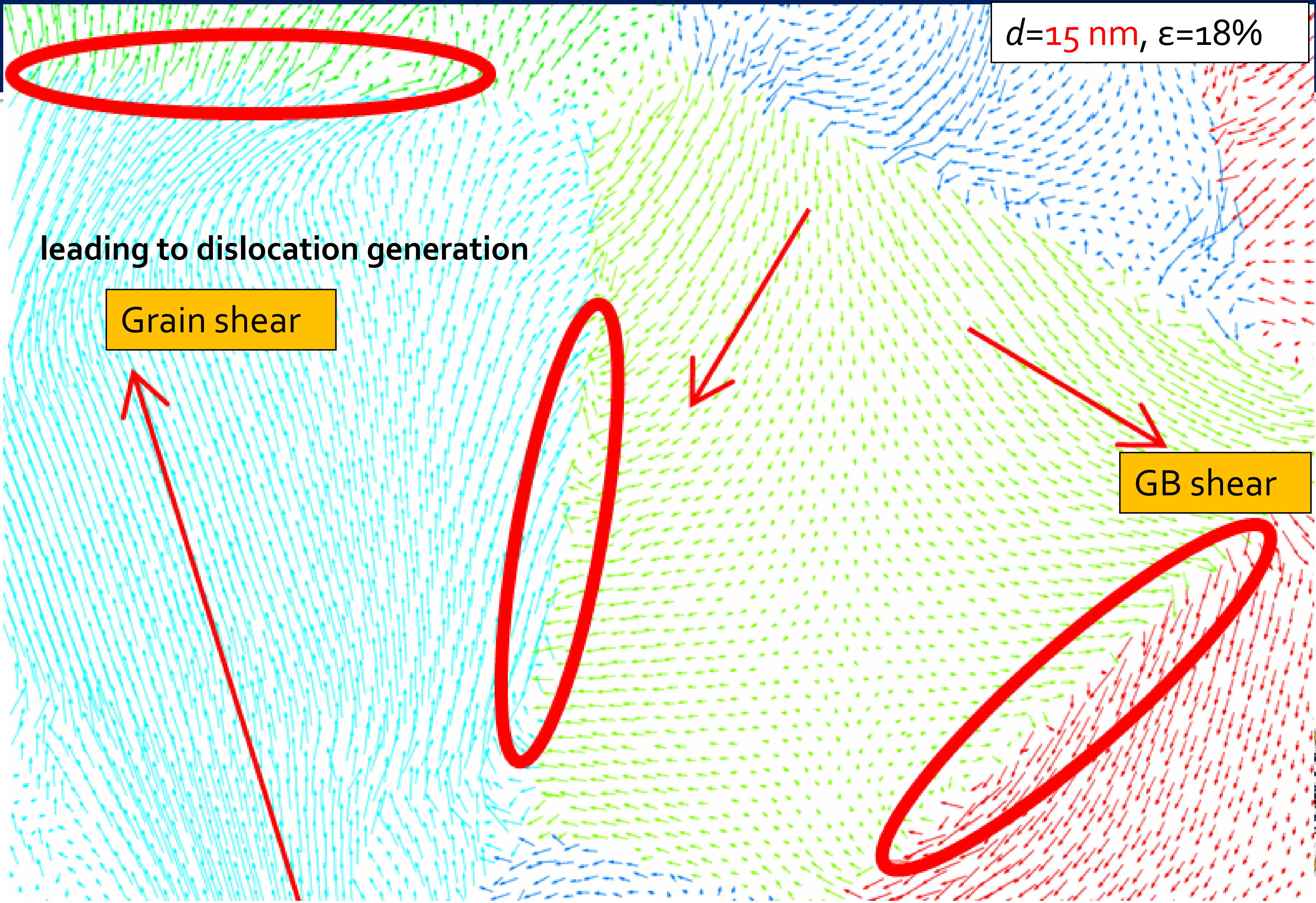

Stage I: Initiation by Vacancy Diffusion

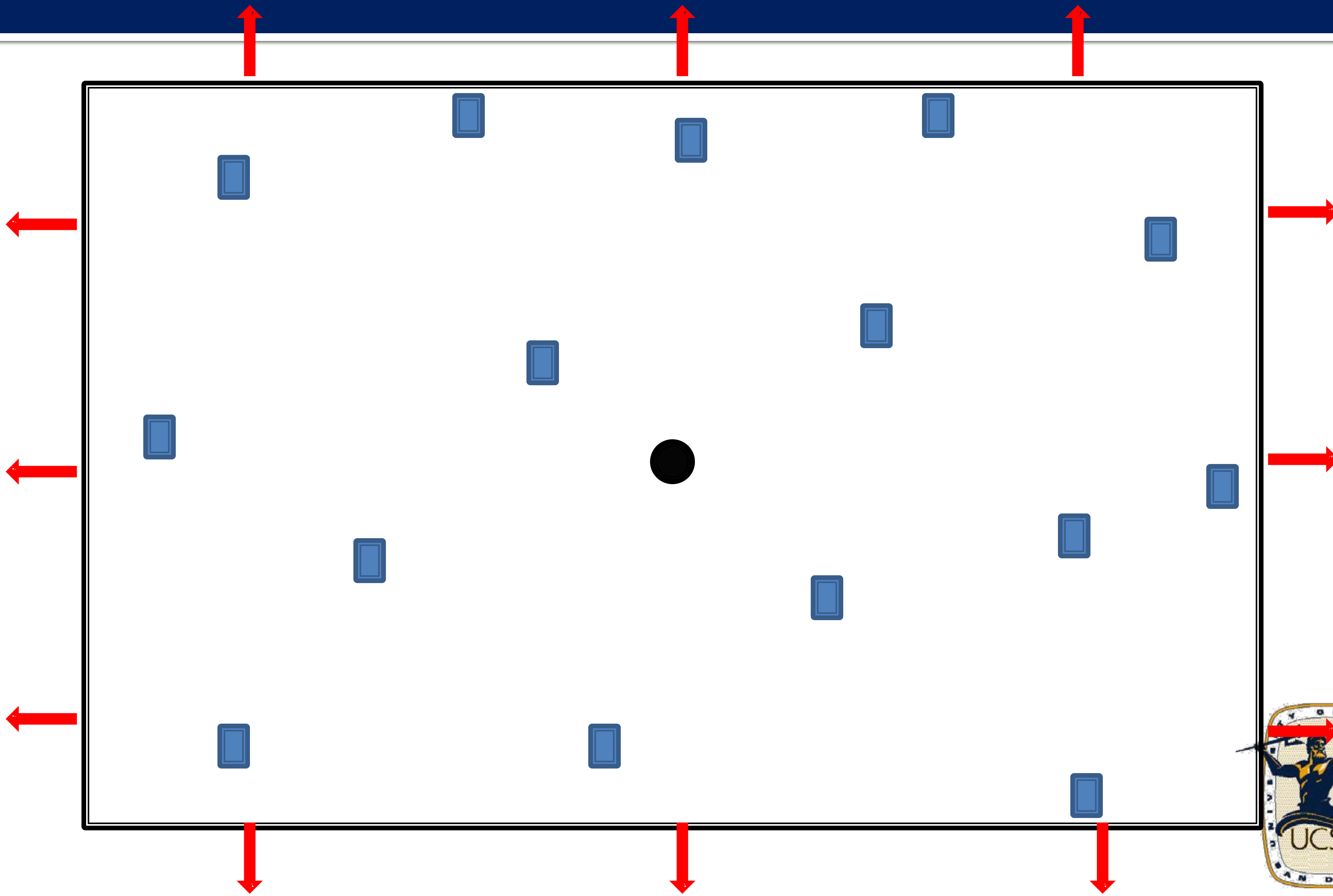

In-plane Dislocation loops

- Partial In-plane Dislocations

$$\vec{b}_1 = \frac{a}{2}[\bar{1}01] \Rightarrow \vec{b}_{p1} = \frac{a}{6}[\bar{1}\bar{1}2]\,;\vec{b}_{p2} = \frac{a}{6}[\bar{2}11]$$

$$\vec{b}_2 = \frac{a}{2}[\bar{1}10] \Rightarrow \vec{b}_{p3} = \frac{a}{6}[\bar{1}2\bar{1}]\,;\vec{b}_{p4} = \frac{a}{6}[\bar{2}11]$$

$$\vec{b}_{p1} + \vec{b}_{p3} = \frac{a}{6}[\bar{1}\bar{1}2] + (-)\frac{a}{6}[\bar{1}2\bar{1}] = \frac{a}{2}[0\bar{1}1]$$

$$\vec{b}_{p2} + \vec{b}_{p4} = \frac{a}{6}[\bar{2}11] + (-)\frac{a}{6}[\bar{2}11] = 0$$

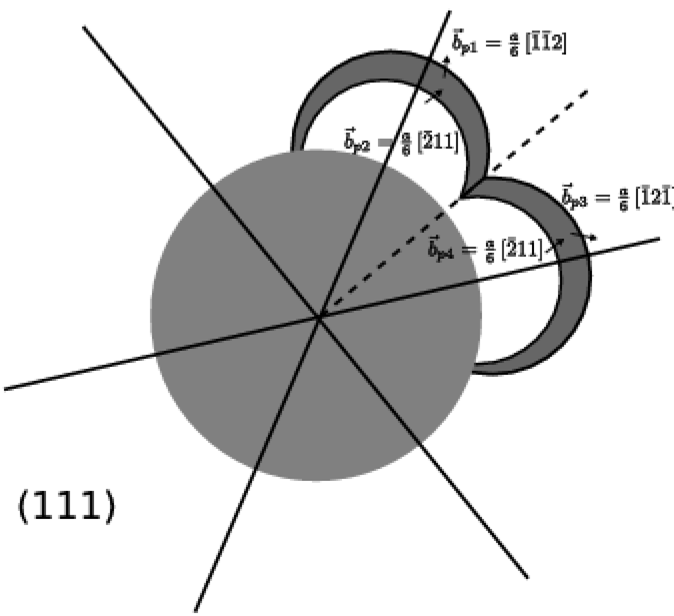

Traiviratana et al. Acta Mater 2008;56:3874

Void Growth Simulation-loading [001]

[001] strain direction
along z-axis

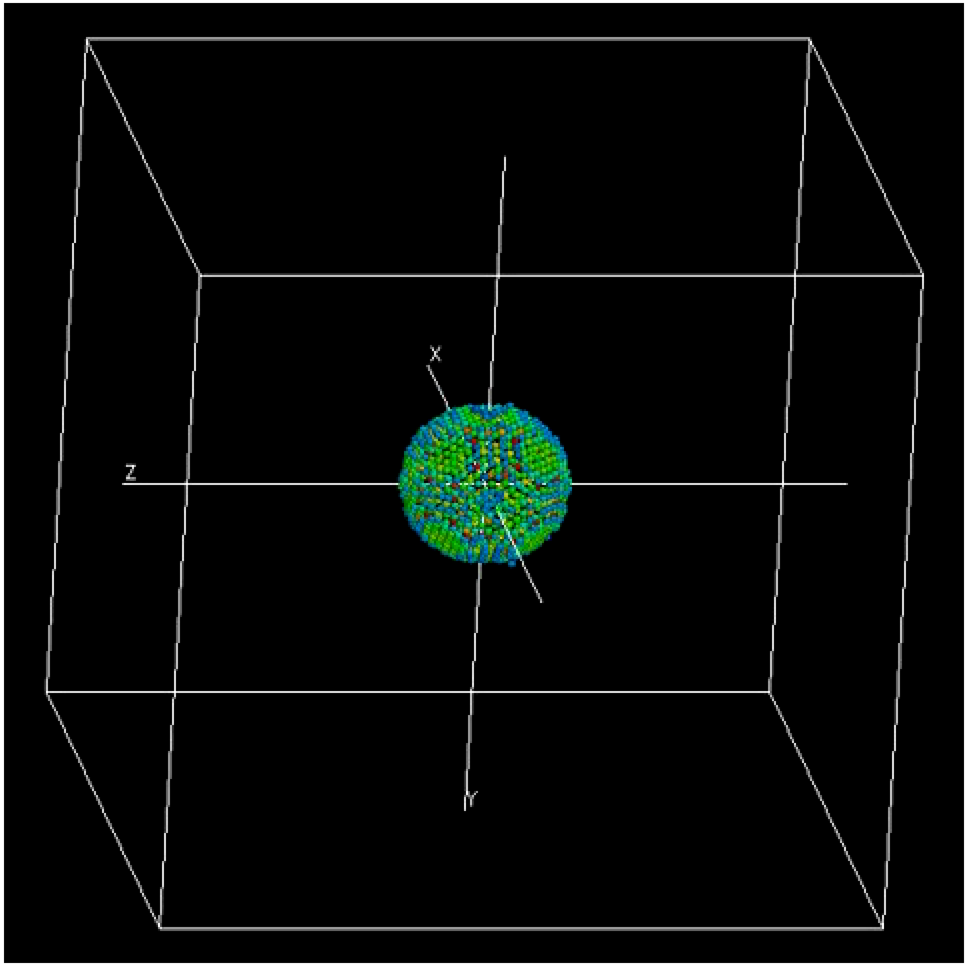

Traiviratana et al. Acta Mater 2008;56:3874

Bi-planar Dislocation loops

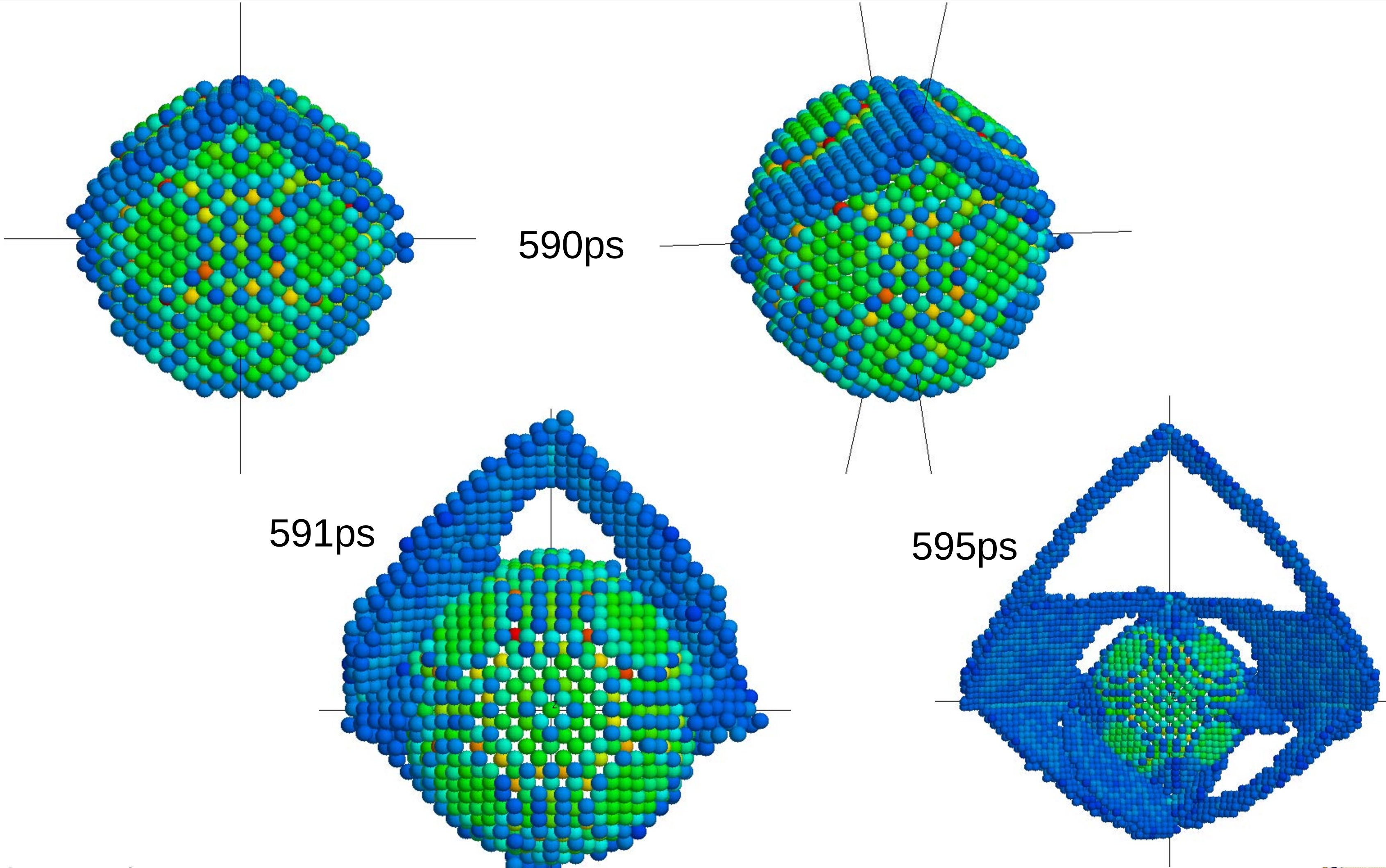

Traiviratana et al. Acta Mater 2008;56:3874

Bi-planar Dislocation loops

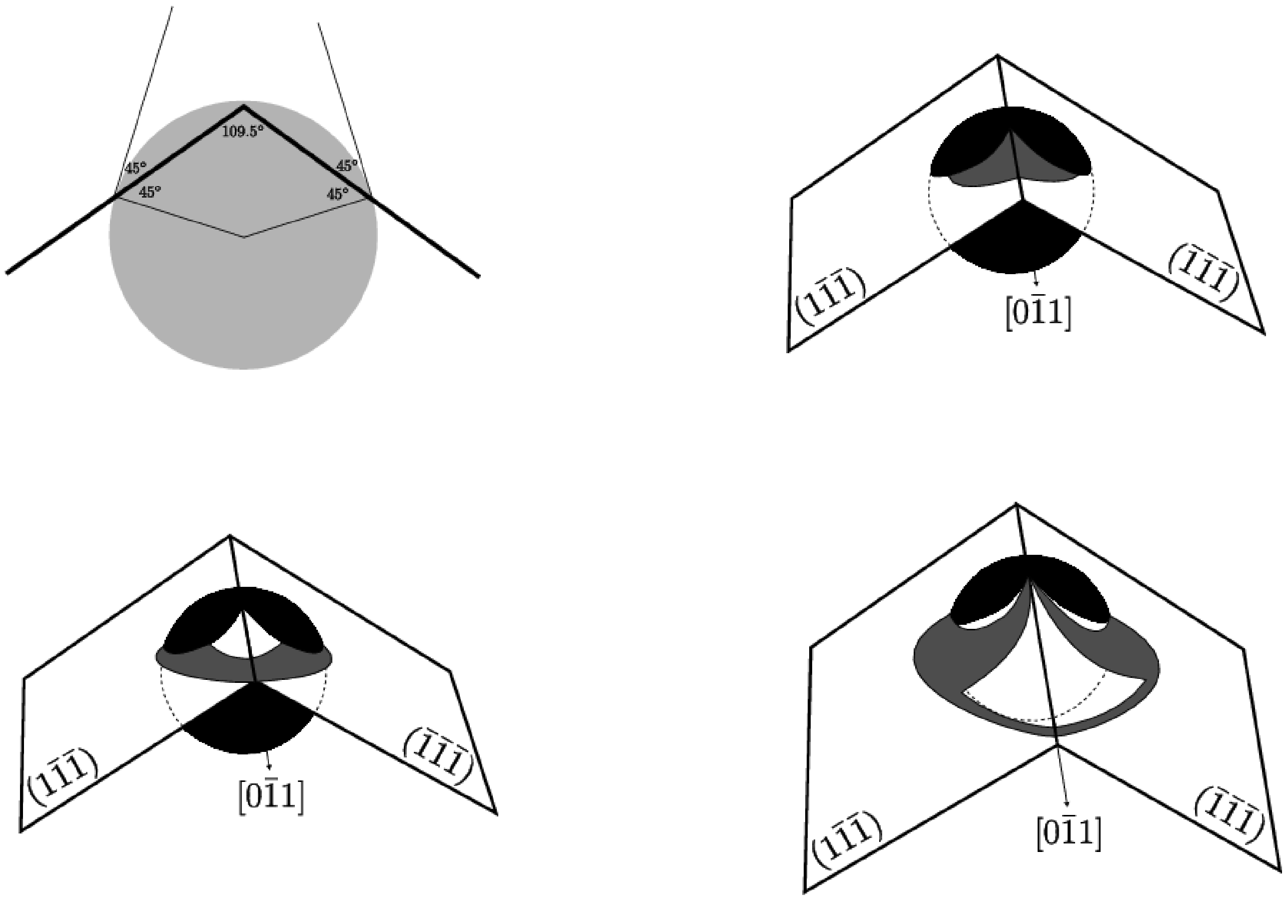

Traiviratana et al. Acta Mater 2008;56:3874

Loading on [110] (z-axis)

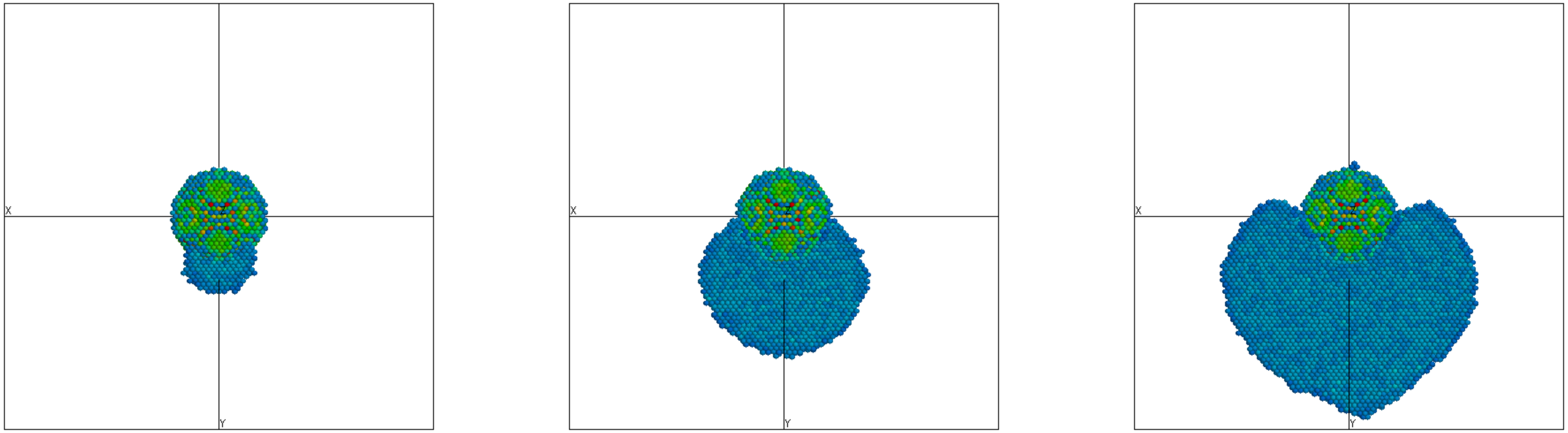

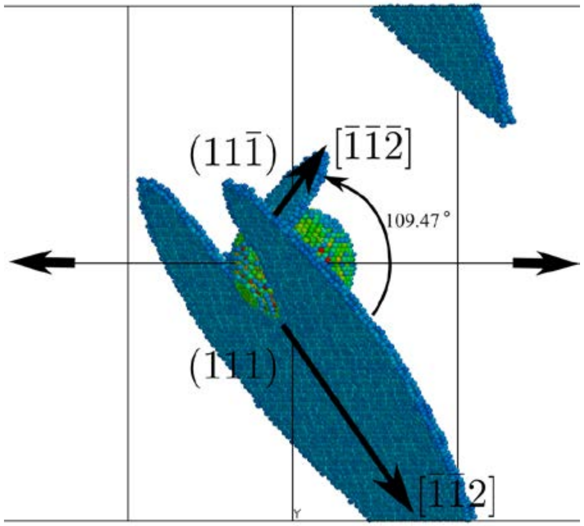

Bi-planar Dislocation loops

- Perfect Dislocation – Bi-Planar Interaction

$$\vec{b}_1 + \vec{b}_2 = \vec{b}_7$$

$$\frac{a}{2}[0\bar{1}1] + (-)\frac{a}{2}[0\bar{1}1] = 0$$

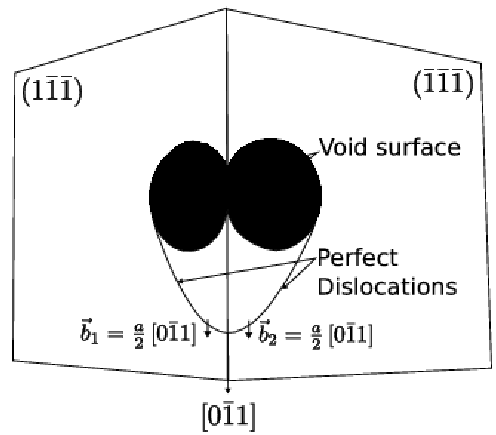

Traiviratana et al. Acta Mater 2008;56:3874

Modeling of Nanovoid Growth

Lubarda et l. Acta mat 2004.
Marian , Knap, Ortiz. Phys Rev Lett 2004; Acta Mat 2005
Traiviratana et al. Acta Mater 2008.
Meyers et al. J Mater 2009.
Bringa et al. Acta Mater 2010.

Bi-planar Dislocation loops

- Partial Dislocation – Bi-Planar Interaction

$$\vec{b}_1 = \frac{a}{2}[\bar{1}01] \Rightarrow \vec{b}_{p1} = \frac{a}{6}[\bar{1}\bar{1}2]\,;\vec{b}_{p2} = \frac{a}{6}[\bar{2}11]$$

$$\vec{b}_2 = \frac{a}{2}[\bar{1}10] \Rightarrow \vec{b}_{p3} = \frac{a}{6}[\bar{1}2\bar{1}]\,;\vec{b}_{p4} = \frac{a}{6}[\bar{2}11]$$

$$\frac{a^2}{2} > \frac{a^2}{6} + \frac{a^2}{6} = \frac{a^2}{3}$$

$$\vec{b}_{p1} + \vec{b}_{p3} = \frac{a}{6}[\bar{1}\bar{1}2] + (-)\frac{a}{6}[\bar{1}2\bar{1}] = \frac{a}{2}[0\bar{1}1]$$

$$\vec{b}_{p2} + \vec{b}_{p4} = \frac{a}{6}[\bar{2}11] + (-)\frac{a}{6}[\bar{2}11] = 0$$

$$\frac{a^2}{6} + \frac{a^2}{6} = \frac{a^2}{3} > \frac{a^2}{18}$$

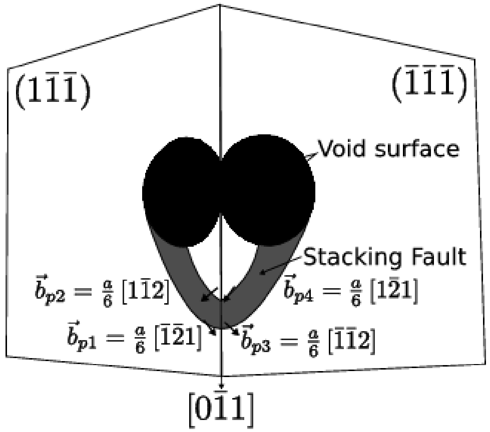

Traiviratana et al. Acta Mater 2008;56:3874

Loading on [111] (z-axis)

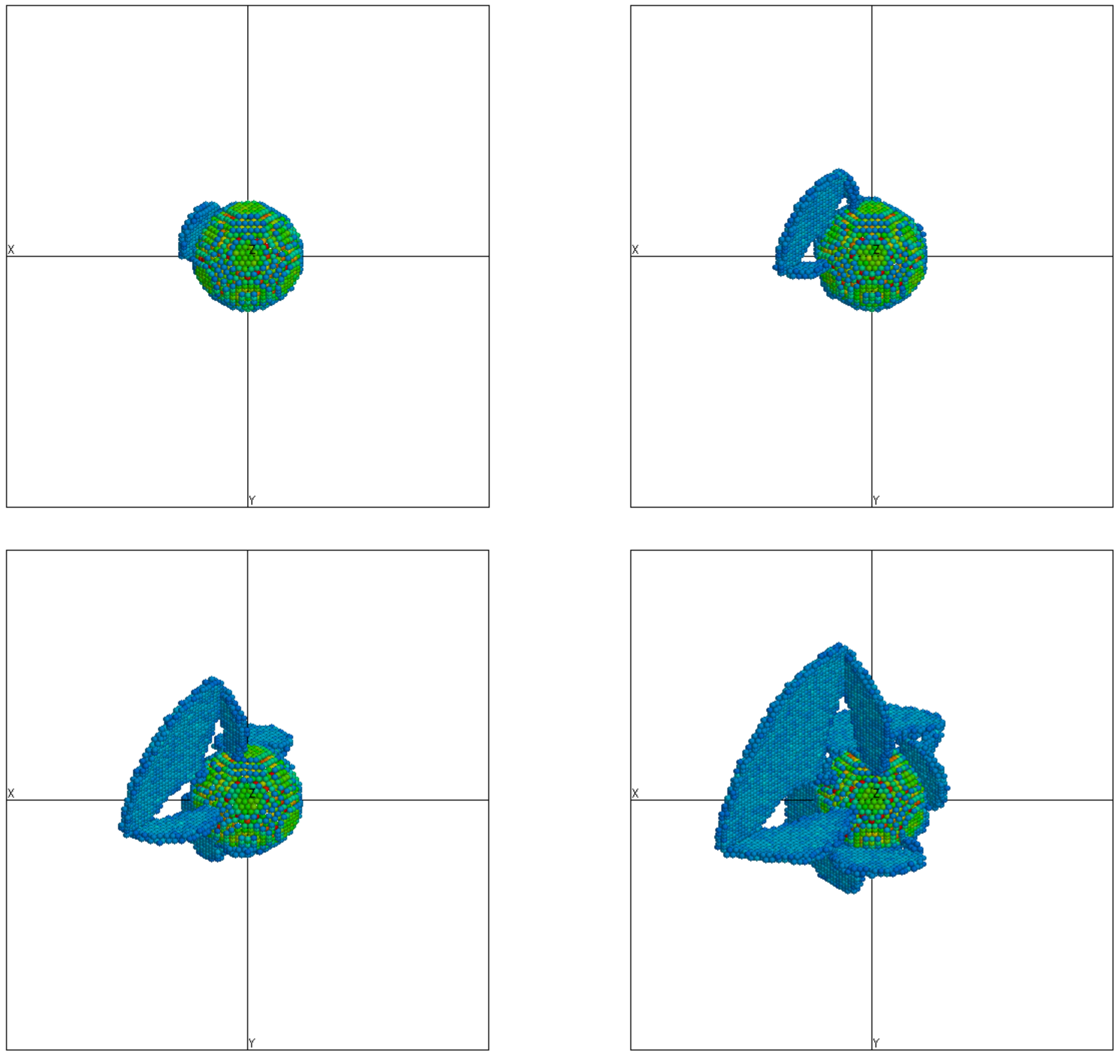

Conclusions: Deformation in Tension

- **FCC Cu:** dislocation generation at grain boundaries leads to void formation at GBs.

- **BCC Ta:** decohesion of GBs occurs before plasticity, due to flow stress exceeding grain-boundary cohesion strengh at the imposed strain rate (~10^8 s^{-1}).

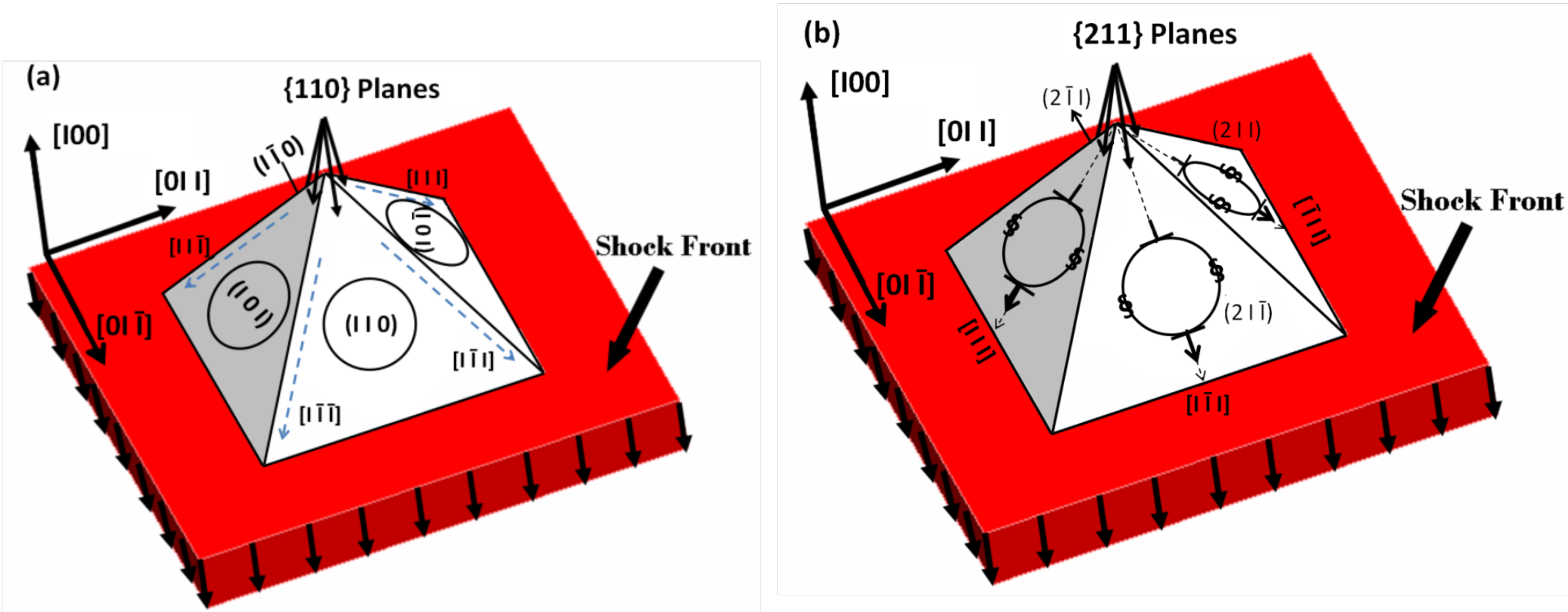
(a)
{110} Planes
[100]
[011]
[01 1̄]
(1 1̄ 0)
[111]
[11 1̄]
(1 0 1̄)
(1 0 1)
(1 1 0)
[1 1̄ 1]
[1 1̄ 1̄]
Shock Front
(b)
{211} Planes
[100]
[011]
[01 1̄]
(2 1̄ 1)
(2 1 1)
[1̄ 1 1]
[1 1 1]
(2 1 1̄)
[1 1̄ 1]
Shock Front

First Generation

Janus Laser facility in Lawrence Livermore National Lab

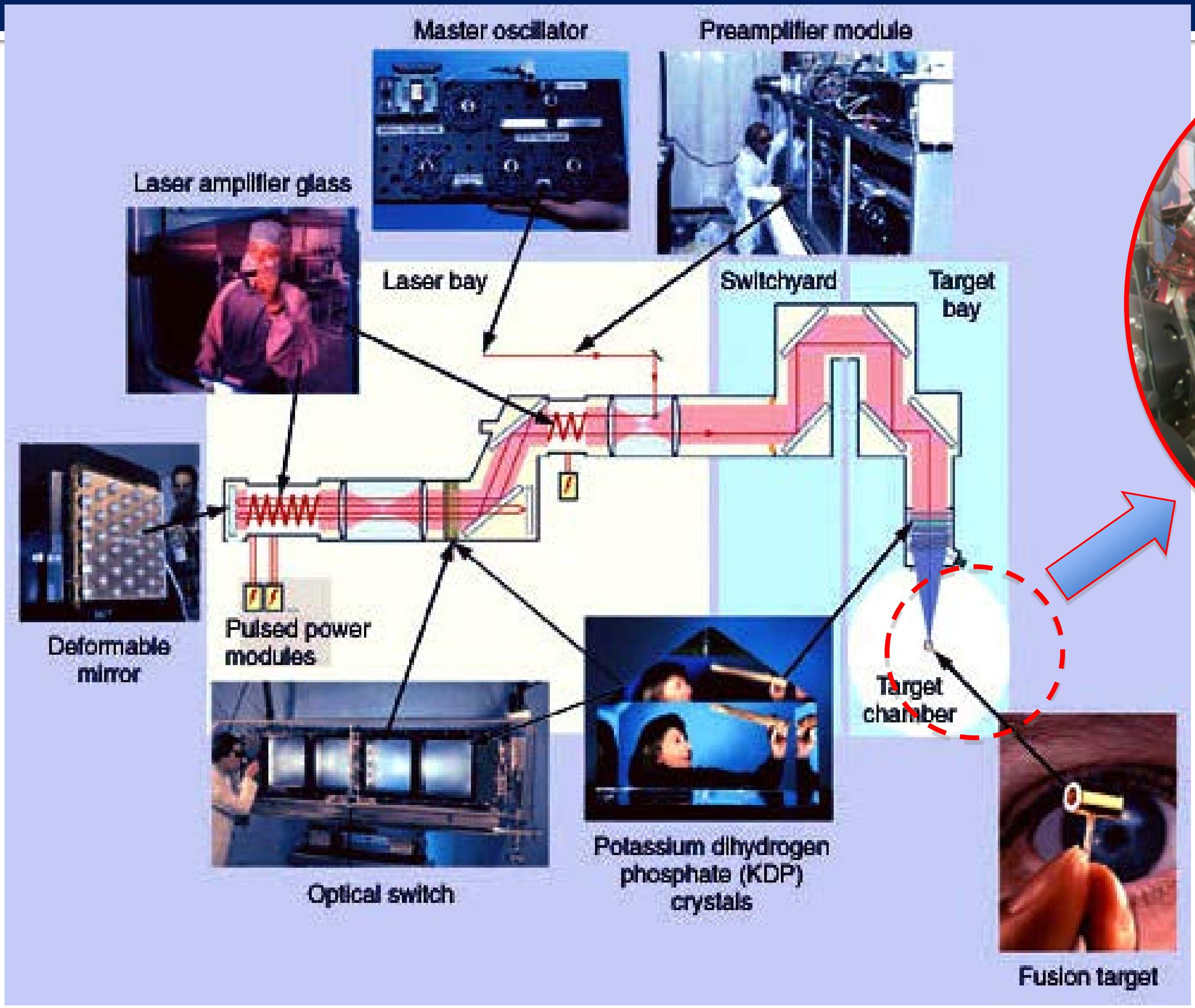

Target Chamber

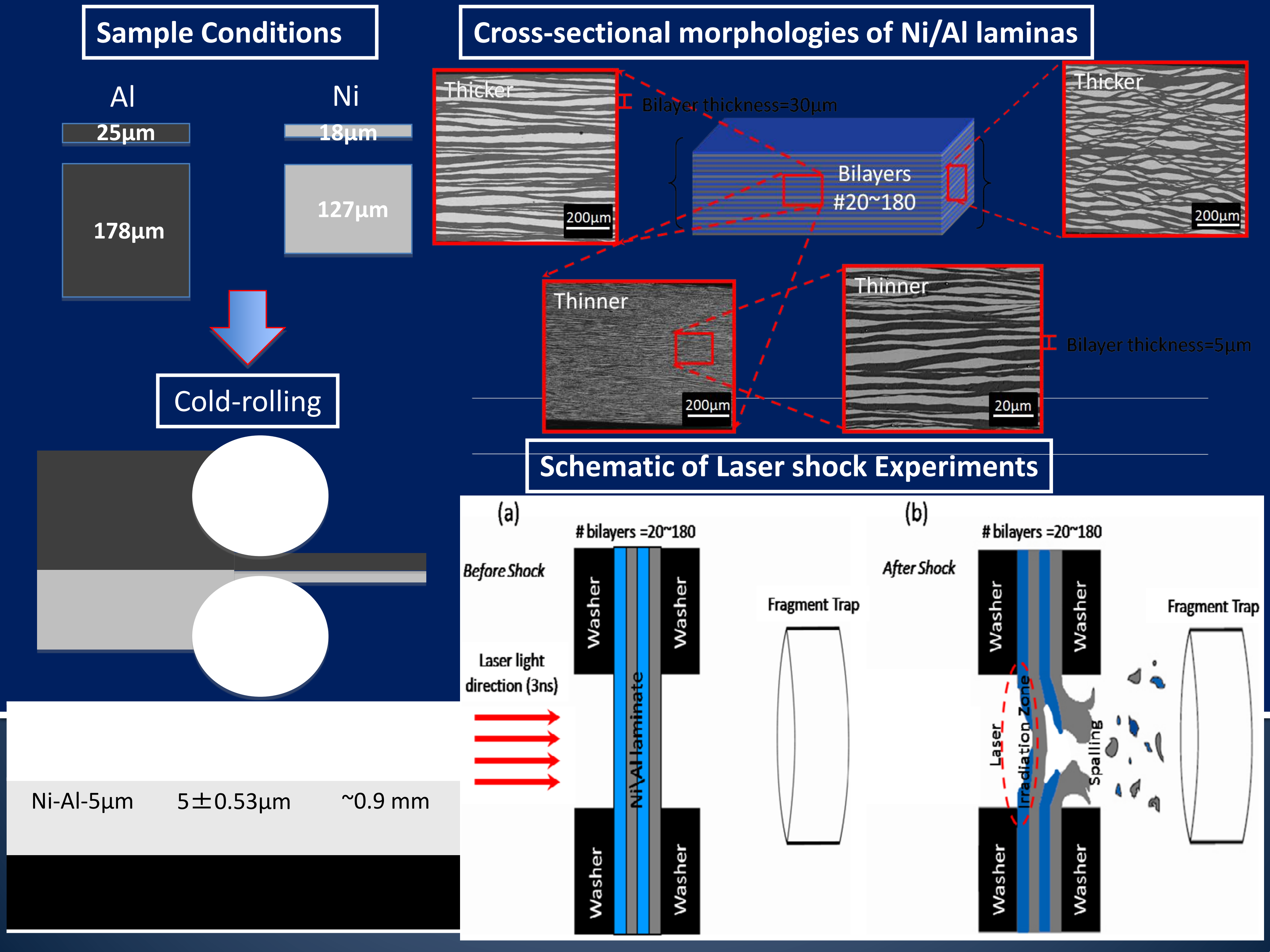

Sample Conditions
Al
Ni
25µm
18µm
178µm
127µm
Cold-rolling
Ni-Al-5µm
5±0.53µm
~0.9 mm
Cross-sectional morphologies of Ni/Al laminas
Thicker
Bilayer thickness=30µm
200µm
Bilayers
#20~180
Thinner
Bilayer thickness=5µm
20µm
Schematic of Laser shock Experiments
(a)
(b)
bilayers =20~180
Before Shock
After Shock
Washer
Ni\Al laminate
Fragment Trap
Laser light
direction (3ns)
Laser Irradiation Zone
Spalling

Laser Shock Eperiments: First Generation

Bilayer Thickness	8ns Laser Energy	Laser Intensity (8ns)	3ns Laser Energy	Laser Intensity (3ns)
5µm	229 J	2.56×10^{12} (W/cm^2)	107 J	3.18×10^{12} (W/cm^2)
5µm			430 J	1.28×10^{13} (W/cm^2)
30µm	24J	2.68×10^{11} (W/cm^2)	105 J	3.13×10^{12} (W/cm^2)
30µm	409J	4.56×10^{12} (W/cm^2)	421 J	1.25×10^{13} (W/cm^2)

Second Generation: OMEGA Laser Facility

OMEGA LLE

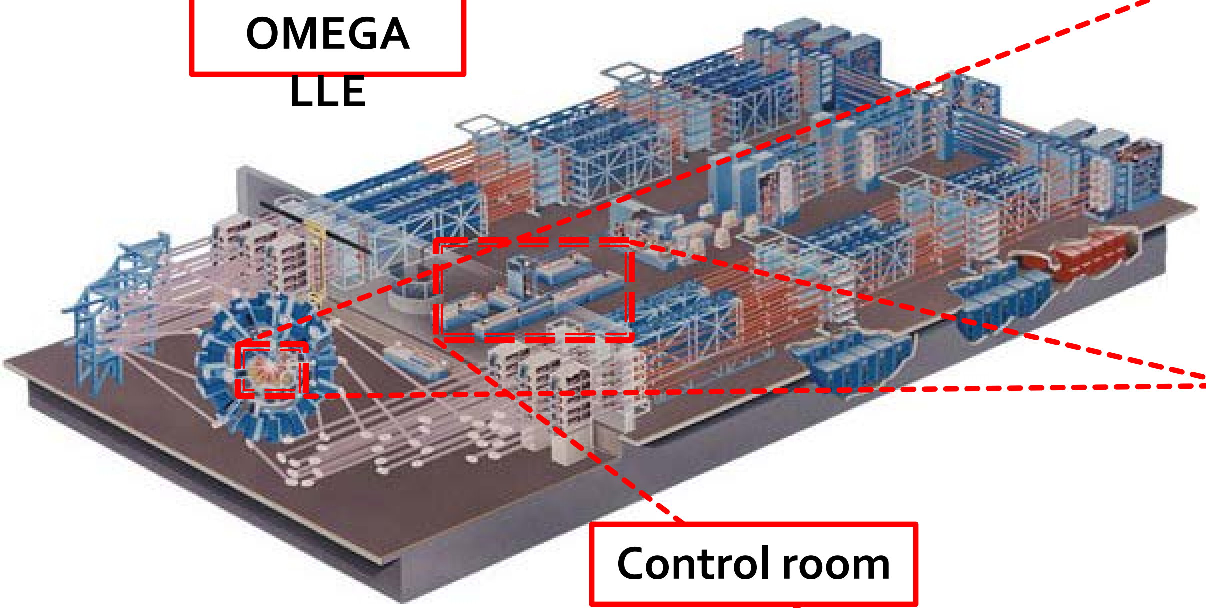

OMEGA target chamber

OMEGA laser drivers

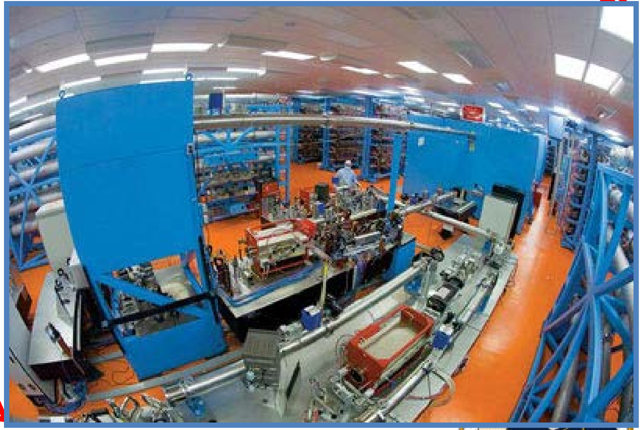

Control room

Shot #	SRF	shot ID	Configuration	Target IDs		On-target energy	
				H7-H14	H3-H18	H7-H14	H3-H18
1	32511	59039	Recovery/VISAR	19 VISAR	23 <110>	600.6	625.2
2	32745	59040	Recovery/VISAR	20 VISAR	24 <110>	351.8	352.5
3	32746	59041	Recovery/VISAR	21 VISAR	27 <100>	501.8	505.4
4	32747	59042	Recovery/VISAR	22 VISAR	30 <111>	682.7	525.2
5	32510	59043	Recovery/Recovery	25 <110>	28 <123>	476.9	489.0
6	32748	59044	Recovery/Recovery	29 <123>	$\boxed{40 \text{ <RL>}}$	633.0	$\boxed{653.0}$
7	32749	59045	Recovery/Recovery	32 <poly>	35 <nano>	509.3	495.0
8	32750	59046	Recovery/Recovery	33 <poly>	36 <nano>	362.2	351.9
9	32751	59047	Recovery/Recovery	31 <poly>	37 <nano>	657.2	650.7
10	32752	59049	Recovery/Recovery	34 <poly>	38 <nano>	837.4	662.9
11	32753	59050	Recovery/Recovery	26 <110>	39 <nano>	661.5	842.7
12	32754	59051	Recovery/Recovery	41 <RL>	42 <RL>	$\boxed{875.3}$	$\boxed{1305.3}$

Sample	Laser energy	Recovery
Tube-18	653J/3.7 ns	Complete Spall
Tube-19	875J/3.7 ns	Complete Spall
Tube-20	1305J/3.7 ns	Shattered

Capsule and Target Configuration

Laser arrangement

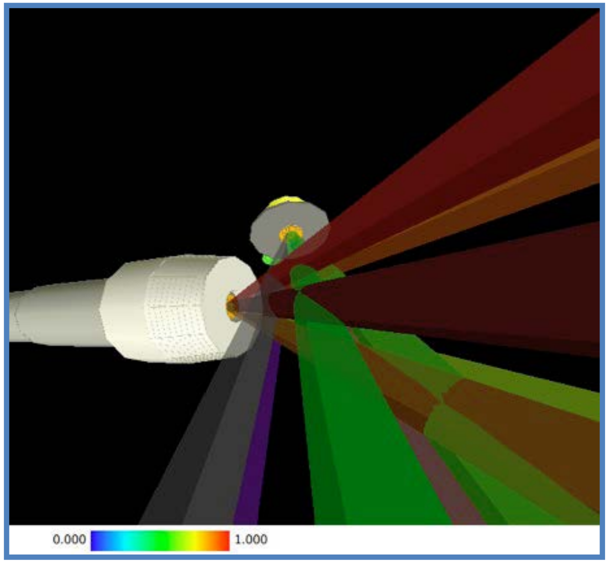

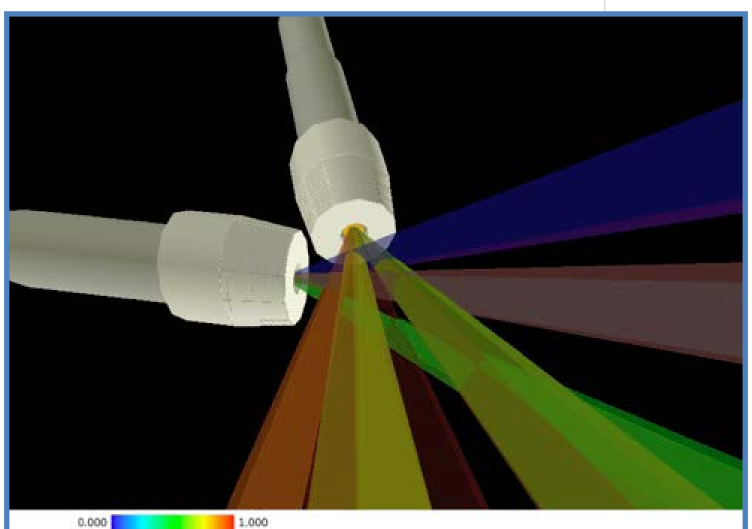

Vent Hole on this side

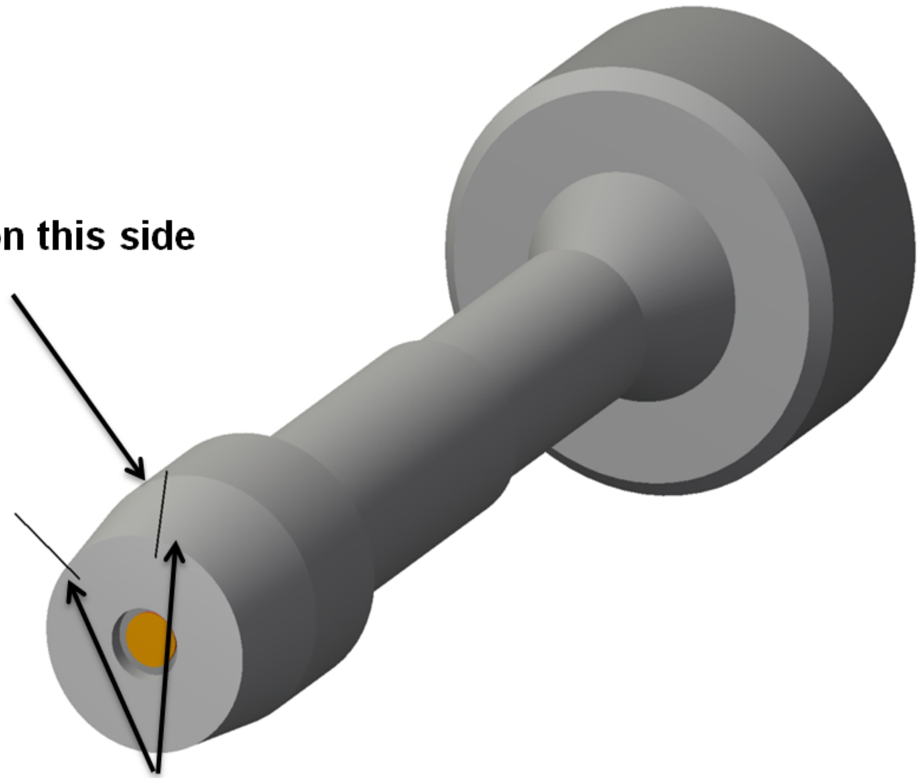

5 mm long Alignment Fibers (1 mm overlap with recovery tube)

*Only one fiber (drawing shows 2)

Second Generation

Sample Capsule

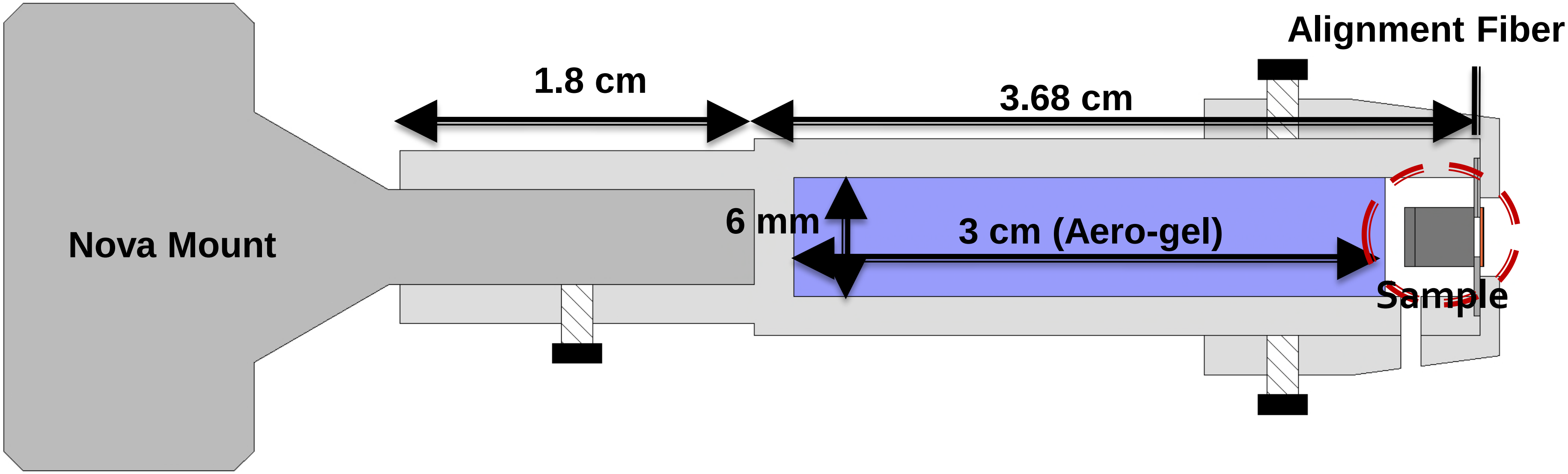

Collaboration with Cavendish lab, Cambridge U.

Monitoring of Fragment Velocity and Distribution